NMR
theory and experiments

http://www.cis.rit.edu/htbooks/nmr/inside.htm

NMR theory and experiments

Nano Science & Technology Program
TIGP, Academia Sinica

Instructor: Der-Lii M. Tzou Place: A207, IC, Academia Sinica

Hour: 9:00~12:00 pm May 27 and June 2, 2010

(02) 2789-8524
email:tzougate@gate.sinica.edu.tw

- **NMR basics and principle**
  (a) Rotation spectroscopy
  (b) Larmor frequency
  (c) Resonance, Fourier transfer

- **Applications of NMR to Biological Systems**
  (a) 1D NMR and chemical shifts
  (b) J-coupling
  (c) NOE and 2D NOE spectroscopy
  (d) 2D TOCSY spectroscopy
  (e) 2D COSY spectroscopy
  (f) ^{1}H, ^{13}C, ^{15}N NMR spectroscopy and high resolution multi-dimensional NMR
  (g) Other nuclear spin interactions

Structured approach bags chemistry prize

David Adam, London

Discerning the shape and structure of biomolecules is a sizeable problem — huge, complicated structures such as proteins are among the toughest molecules to analyse. Three researchers who developed key tools to study these giants have been rewarded with the Nobel Prize in Chemistry.

Half of the prize goes to Kurt Wüthrich of the Swiss Federal Institute of Technology in Zürich and the Scripps Research Institute in California, for finding ways to determine the three-dimensional structures of large biological molecules using nuclear magnetic resonance (NMR) spectroscopy.

John Fenn of the Virginia Commonwealth University in Richmond and Koichi Tanaka of the Shimadzu Corporation in Kyoto share the other half for inventing techniques to identify and analyse proteins and other large structures using mass spectrometry. At 43, Tanaka is the youngest chemistry laureate since 1967, and the second Japanese scientist to receive a Nobel this year, following physics winner Masatoshi Koshiba.

"The possibility of analysing proteins in detail has led to increased understanding of the processes of life," says the Nobel Foundation. "Researchers can now rapidly and simply reveal what different proteins a sample contains and also determine what protein molecules look like in solution."

Broad spectrum: techniques devised by (from left) Koichi Tanaka, John Fenn and Kurt Wüthrich have helped to reveal the secrets of protein structure.

Chemists have used NMR and mass spectrometry for decades to study small molecules. But the large size and complex structure of proteins posed problems for biologists wanting to do the same.

NMR analyses the way a molecule's atoms absorb radio waves in a powerful magnetic field. Proteins can contain thousands of atoms, so they give highly confusing NMR spectra. But in the 1980s, Wüthrich showed that NMR is possible for proteins. He invented 'sequential assignment' in which he determined the distance between any two hydrogen atoms in the molecule. He could then pair each peak of radio absorption with a hydrogen nucleus in the protein. This allowed the structure of proteins to be determined in the form in which they exist in the body — in solution — rather than as crystals.

Mass spectrometry is a highly sensitive analytical tool that separates molecules according to their size. Fenn and Tanaka found ways of turning proteins into a charged vapour, to be accelerated by an electric field and detected in a mass spectrometer.

Tanaka's technique — soft laser desorption — uses a laser pulse to blast material from solid or viscous biological samples. Fenn developed a different approach, electrospray ionization, which creates a fine spray from a protein solution using an electric field.

Fenn has "been in a total state of shock" since being given the news in a dawn phone call on 9 October. "It's like being struck by lightning," he says. "You know it happens to some people but the odds are so great you never believe it will happen to you."

Nobel Laureates related to NMR

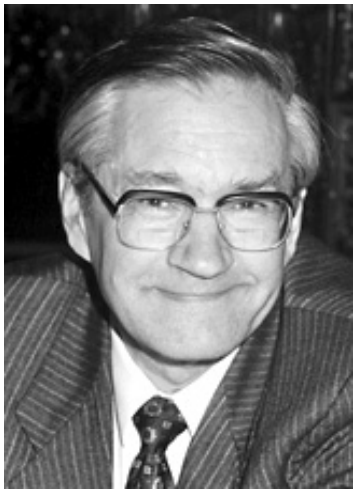

1991 Richard R. Ernst in Chemistry

Nobel Laureates related to NMR

2003 P. C. Lauterbur and P. Mansfield in Medicine

Nobel Laureates related to NMR

2003	P. C. Lauterbur and P. Mansfield in Medicine
2002	Kurt Wüthrich in Chemistry
1991	Richard R. Ernst in Chemistry
1952	Felix Block and E. M. Purcell in Physics

What is NMR ?

Nuclear Magnetic Resonance

N : Nuclear

M: Magnetic

R: Resonance


BRUKER
AVANCE 400

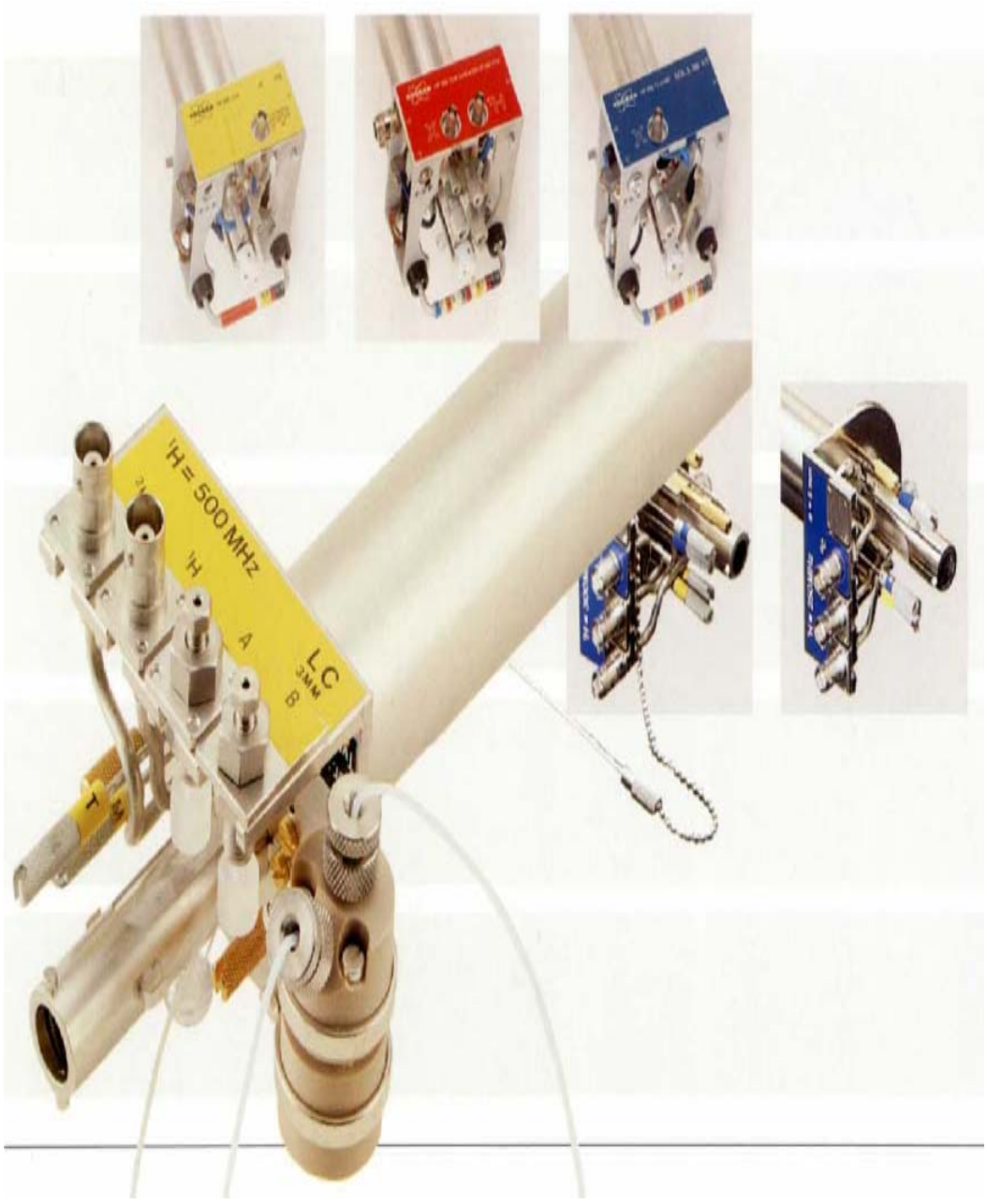
^{1}H = 500 MHz
^{1}H
A
LC
3MM
B

Without External Magnetic Field

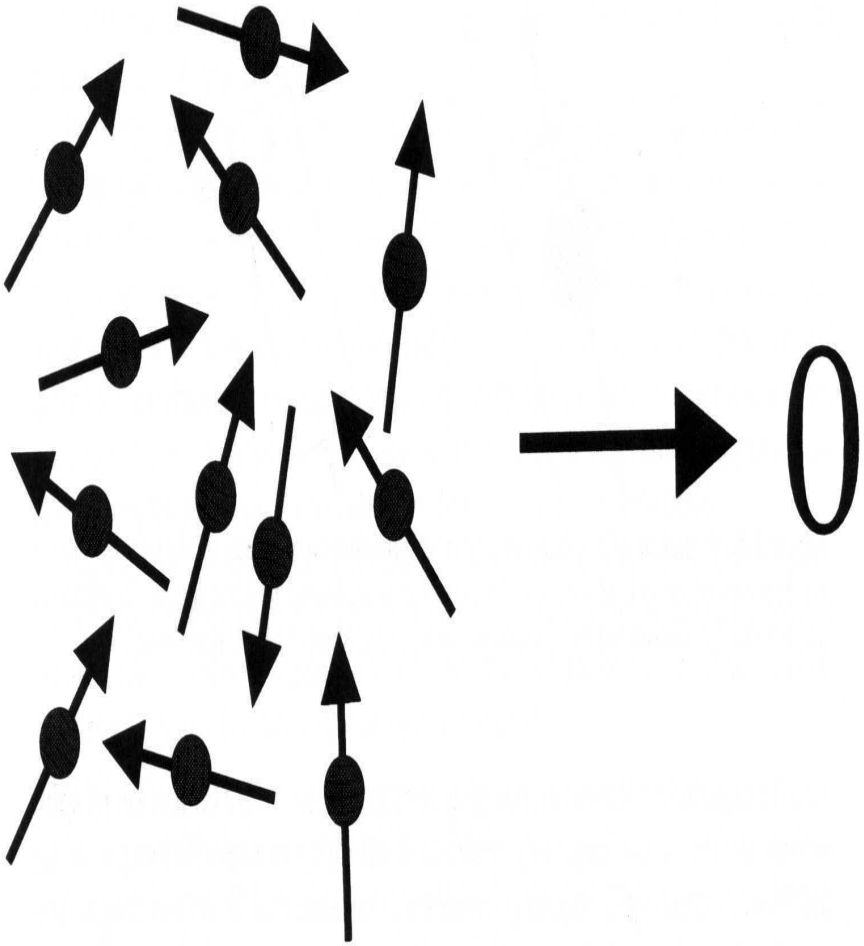

Figure 2.2. Microscopic picture and macroscopic picture of a collection of spins in the absence of an external magnetic field. In the absence of a magnetic field, the spins will have their spin vectors oriented randomly (microscopic picture). The vector sum of these spin vectors will be zero (macroscopic picture).

Number of spin states (2I +1) :

A nucleus with spin I can have 2I +1 spin states. Each of these states has its own spin quantum number m (m = −I, −I +1,…, I − 1, I). For nuclei with I =1/2, only two states are possible : m = +1/2 and m = −1/2.

Nuclear Zeeman effect :

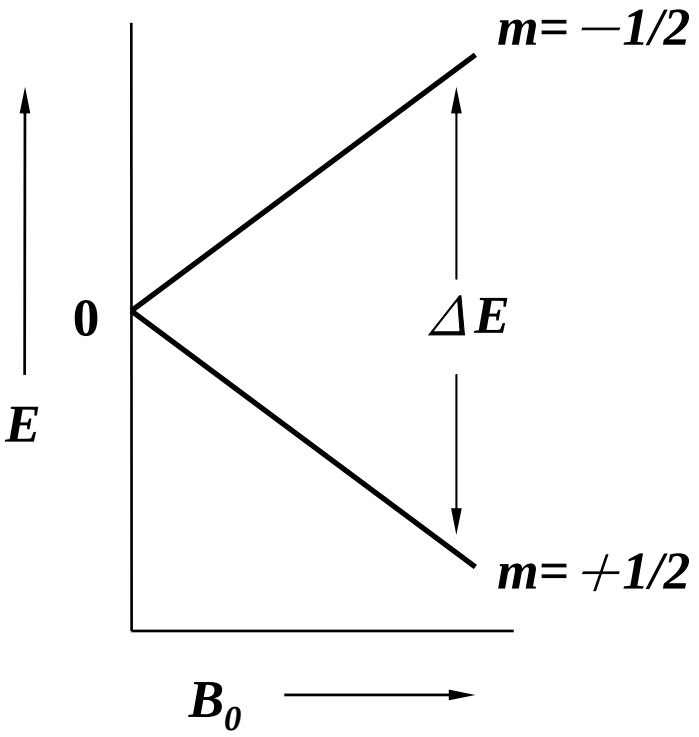

$$E = -mB_0(\gamma h/2\pi)$$

B_0 : magnetic field strength
h : Planck's constant
m : spin quantum number
γ : magnetogyric ratio

Larmor Frequency

$$\Delta E = \gamma \hbar B_0 = h\nu$$

$$\nu = \frac{\gamma}{2\pi} B_0$$

With External Magnetic Field

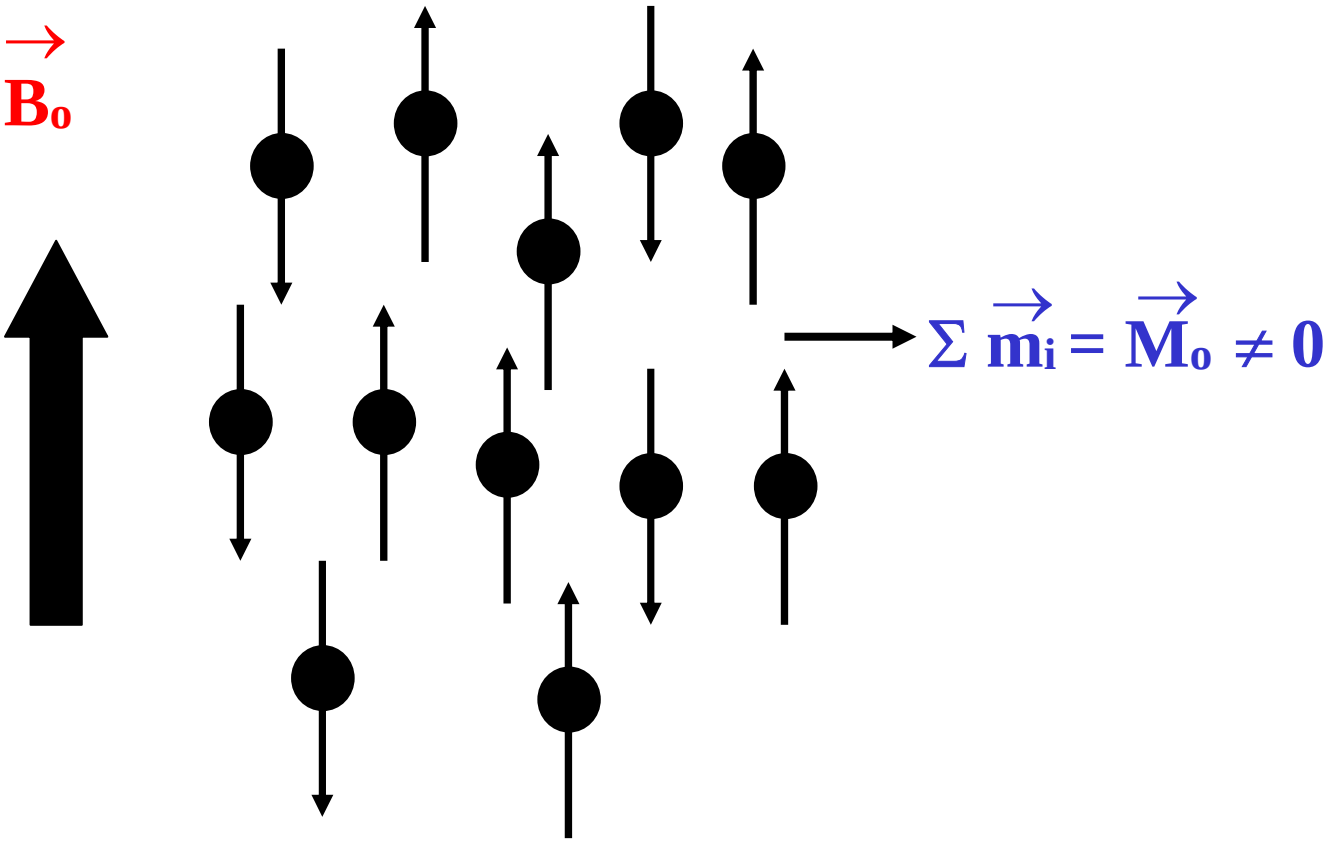

$$\vec{B}_o \gg \vec{M}_o$$

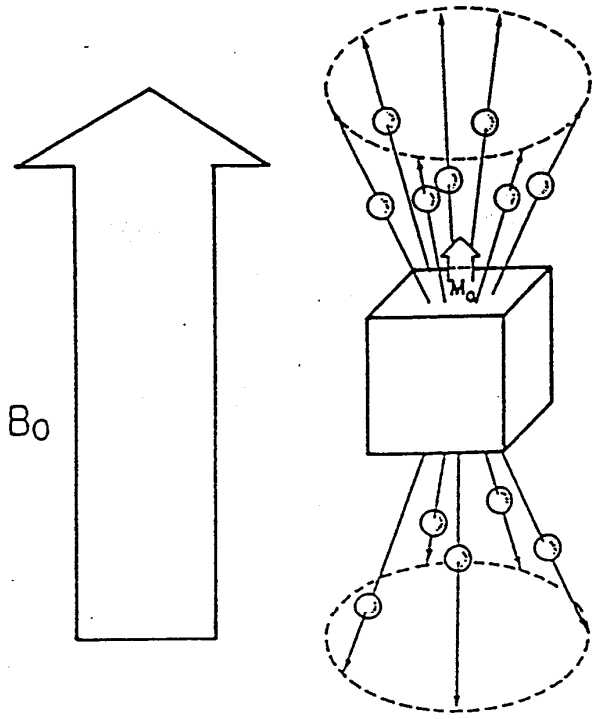

Figure 5. The net magnetization (M_0) resulting from the imbalance of hydrogen nuclear dipoles points along B_0 but is small compared with B_0.

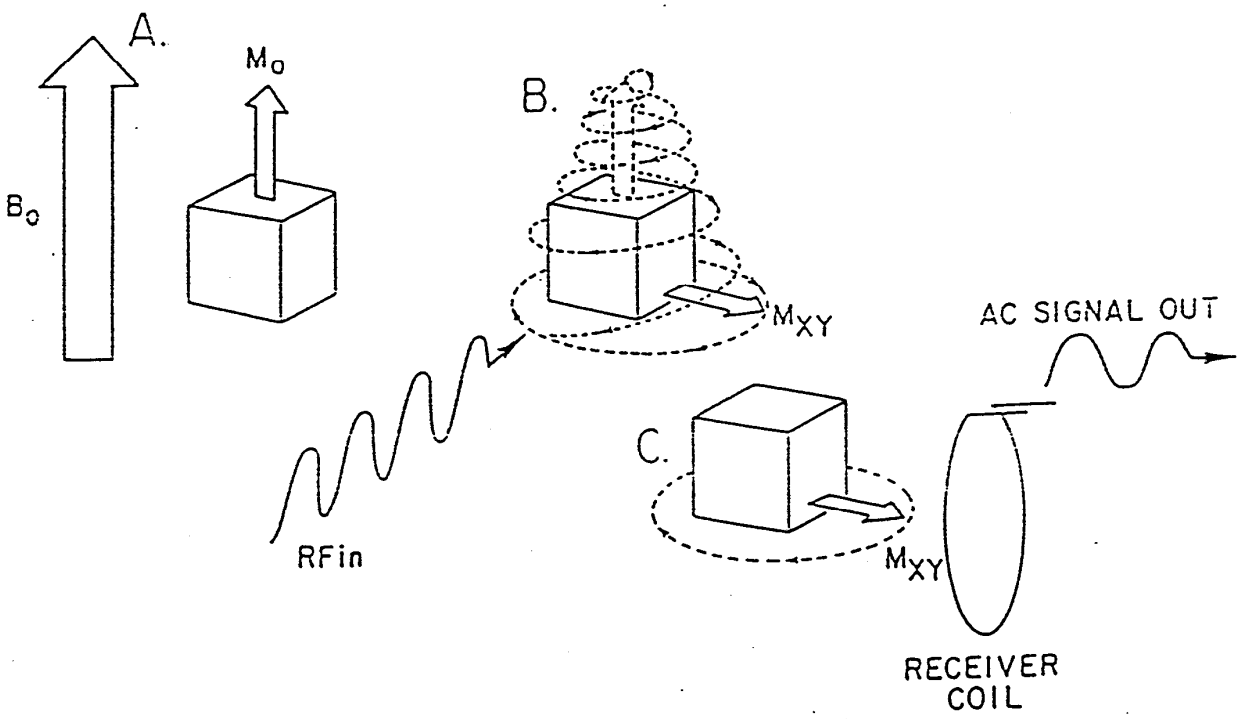

Figure 6. *A.* Net magnetization of the sample M_0 initially is aligned with the main magnetic field B_0, but it is so small in comparison to B_0 that it is undetectable. *B.* A radio-frequency (RF) field applied at the Larmor frequency tips tissue magnetization into the transverse plane, rendering it measurable as transverse magnetization, M_{xy}. *C.* Measurement of M_{xy} is possible because of its precession, which produces a changing magnetic flux linking a properly oriented loop receiver coil. The changing magnetic flux linking the coil induces an alternating current (AC) (alternating at the Larmor frequency) in the receiver coil. This alternating current, when amplified and digitized, becomes the signal from which the MR image is reconstructed.

3D-FID (Free Induction Decay)

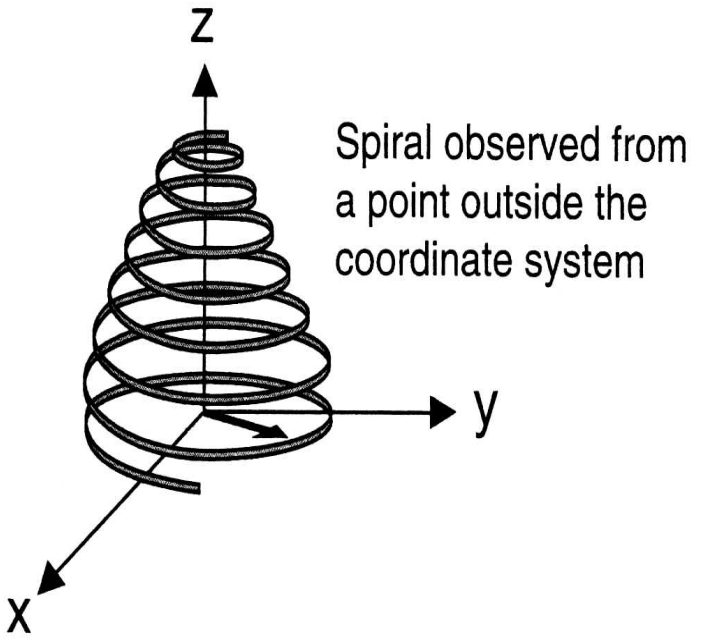

The outside observer sees a spiral motion of the magnetization vector towards the x-y plane.

共振後磁向量的軌跡

Fourier Transform

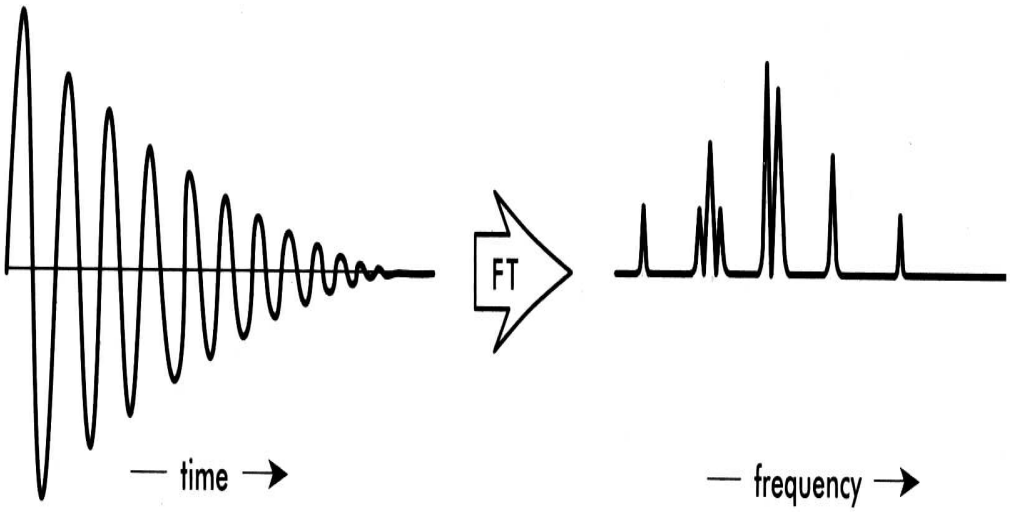

Nuclear spin (I) :

$$A = Z + N$$

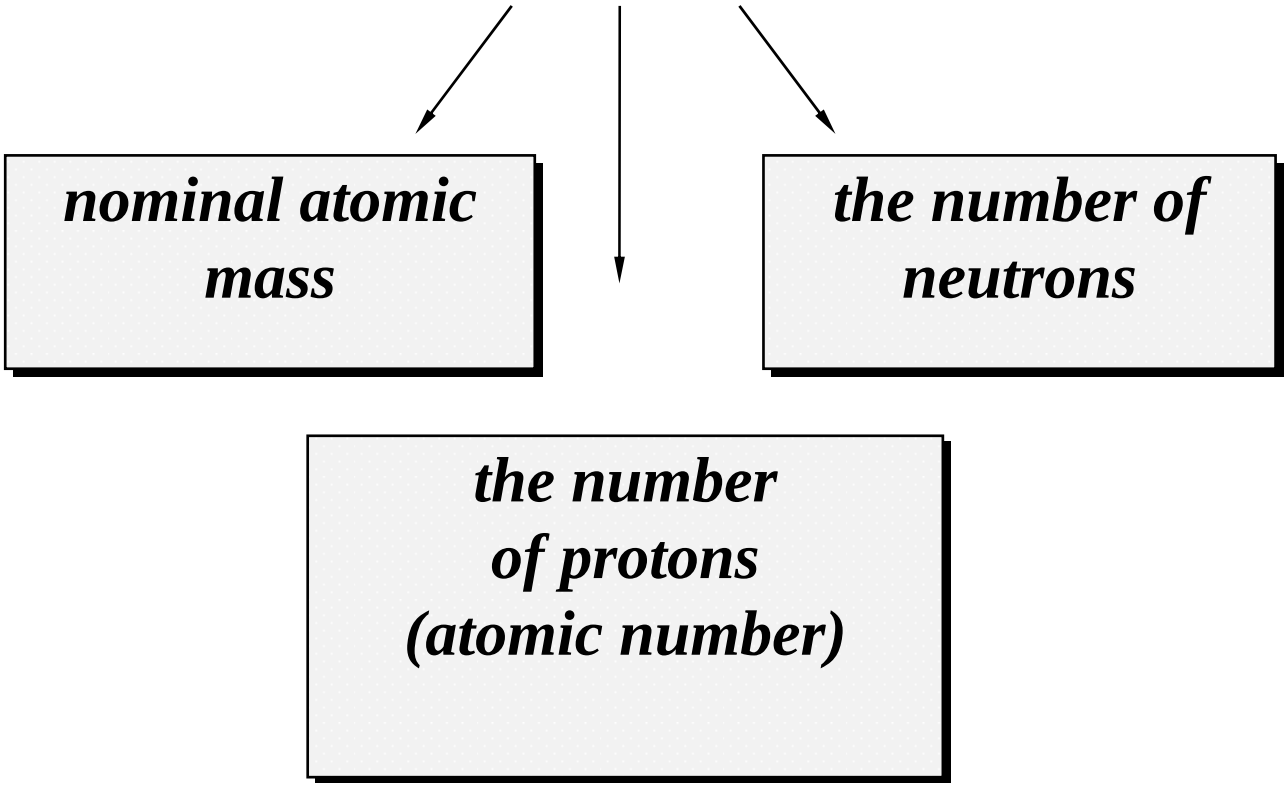

A nucleus with an even mass A and even charge Z, and therefore also an even N, will have a nuclear spin I of zero. (^{12}C, ^{16}O, and ^{18}O).

$$\mathbf{N + Z\ (P) = A}$$

$$^{12}C:\ 6 + 6\ (6) = 12$$
$$^{16}O:\ 8 + 8\ (8) = 16$$
$$\Big\} \quad I = 0$$

A nucleus with an even mass and odd charge (both Z and N odd) will exhibit an integer value of I. ($^{2}H(I=1)$, $^{14}N(I=1)$, and $^{10}B(I=3)$)

$$^{14}N:\ 7 + 7\ (7) = 14$$
$$^{2}H\ :\ 1 + 1\ (1) = 2$$
$$\Big\} \quad I = 1$$

A nucleus with odd mass (Z odd and N even, or Z even and N odd) will have nuclear spin with an I value that we can express as n/2, where n is an odd integer. ($^{1}H(I=1/2)$, $^{13}C(I=1/2)$, and $^{17}O(I=5/2)$)

$$^{1}H:\ 0 + 1\ (1) = 1$$
$$^{13}C:\ 7 + 6\ (6) = 13$$
$$\Big\} \quad I = 1/2$$

- ***Nuclei with I = 0 cannot be detected NMR.***
- ***Nuclei with $I \neq 0$ can be detected NMR.***
- ***Different isotopes of the same element have different nuclear spins, some of which are detectable by NMR, others of which are not.***

Properties of nuclei of interest in NMR studies of protein

Isotope	Spin	Frequency (MHz) at 11.74 T	Nature abundance(%)	Relative sensitivity
^{1}H	1/2	500.0	99.98	1.00
^{2}H	1	76.7	1.5×10^{-2}	9.65×10^{-3}
^{3}H	1/2	533.3	0	1.21
^{12}C	0	------	98.89	------
^{13}C	1/2	125.7	1.108	1.59×10^{-2}
^{14}N	1	36.1	99.63	1.01×10^{-3}
^{15}N	1/2	50.7	0.37	1.04×10^{-3}
^{16}O	0	------	$\sim$100	------
^{17}O	5/2	67.8	3.7×10^{-2}	2.91×10^{-2}
^{19}F	1/2	470.4	100	0.83
^{31}P	1/2	202.4	100	6.63×10^{-2}

The magnetic shielding and chemical shift

Consider an indirect coupling of the nuclei to external static magnetic field by interacting with the surrounding electrons. This interaction leads to magnetic shielding in resonance frequencies that are a reflection of the chemical environment of a nucleus in an atom or molecule and are therefore important in the analytical application of NMR, as well as in testing theoretical descriptions of molecules.

Energy States for I = 1/2, 1, 3/2

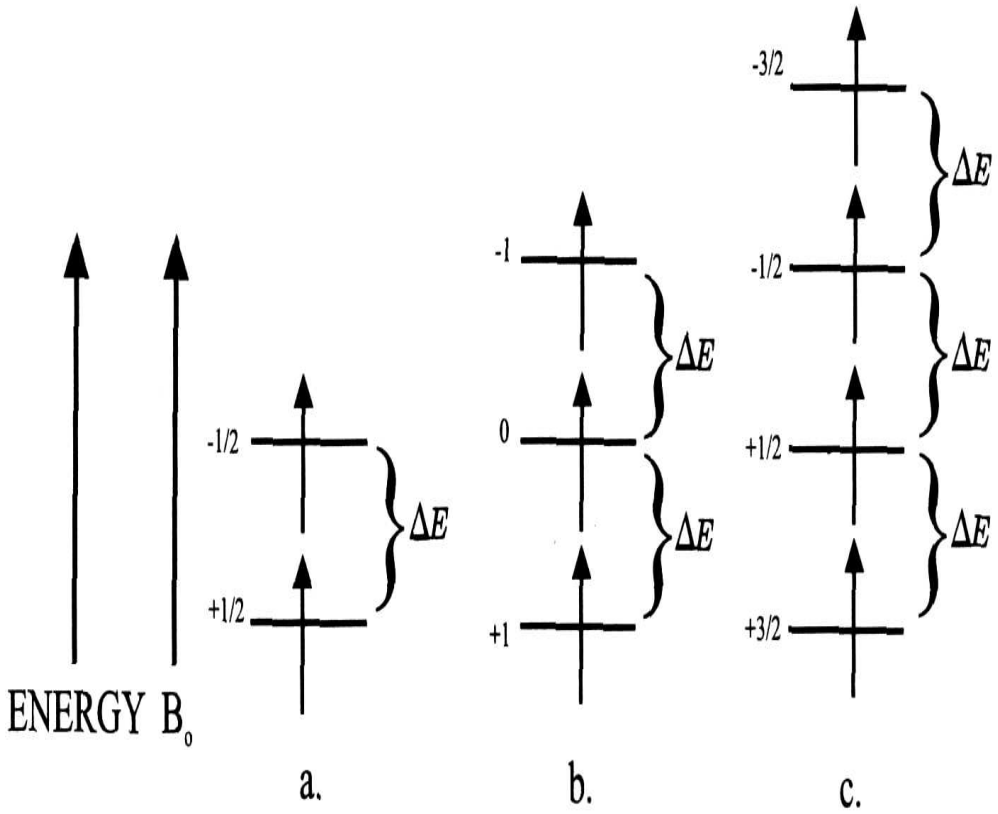

Figure 2.6. Zeeman interaction. In the presence of a magnetic field, the energy states for a spin become unequal. The difference in energy ΔE between any two states is the same and is proportional to B_0. For most spin ½ nuclei, the $z = +½$ level is lowest in energy (*a*); for most spin 1 nuclei, the $z = +1$ level is lowest in energy (*b*); for most spin ³⁄₂ nuclei, the $z = +³⁄₂$ level is lowest in energy (*c*).

Resonance

Larmor precession,

its angular velocity :

$\omega_0 = \gamma B_0$ ， 故 $\omega_0 = 2\pi\nu$

We can apply a radio frequeny radiation to match the Larmor frequency, namely to excite the nuclear resonance.

With External Magnetic Field

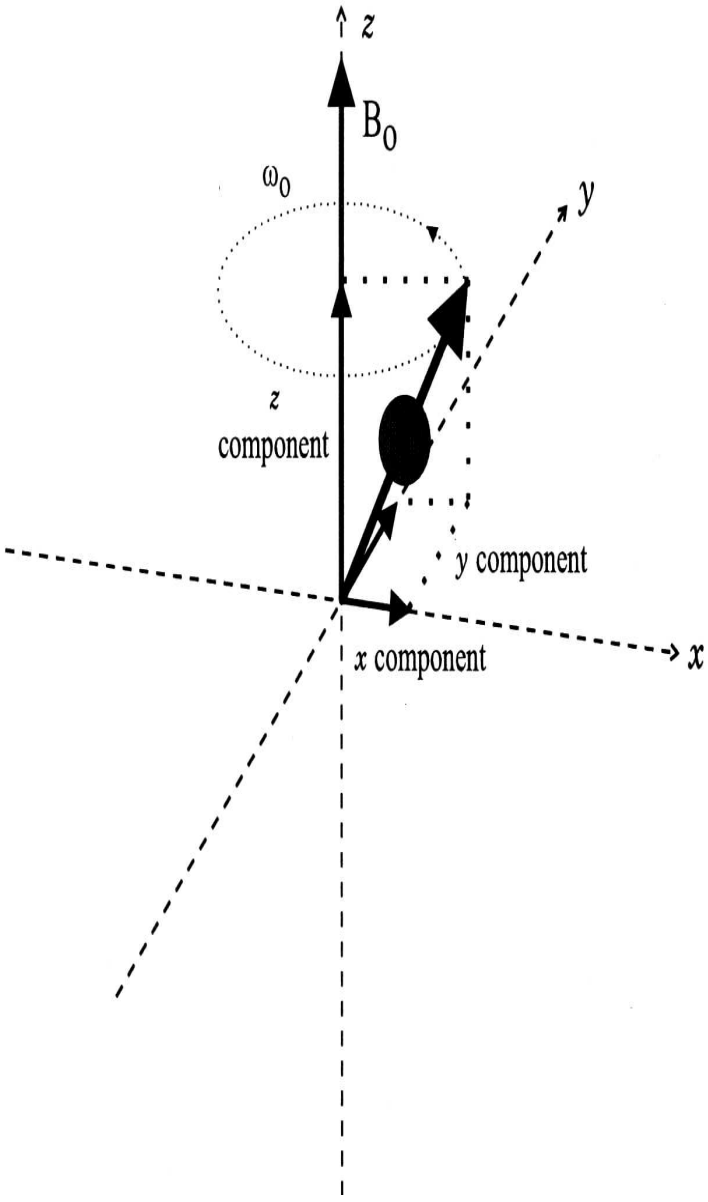

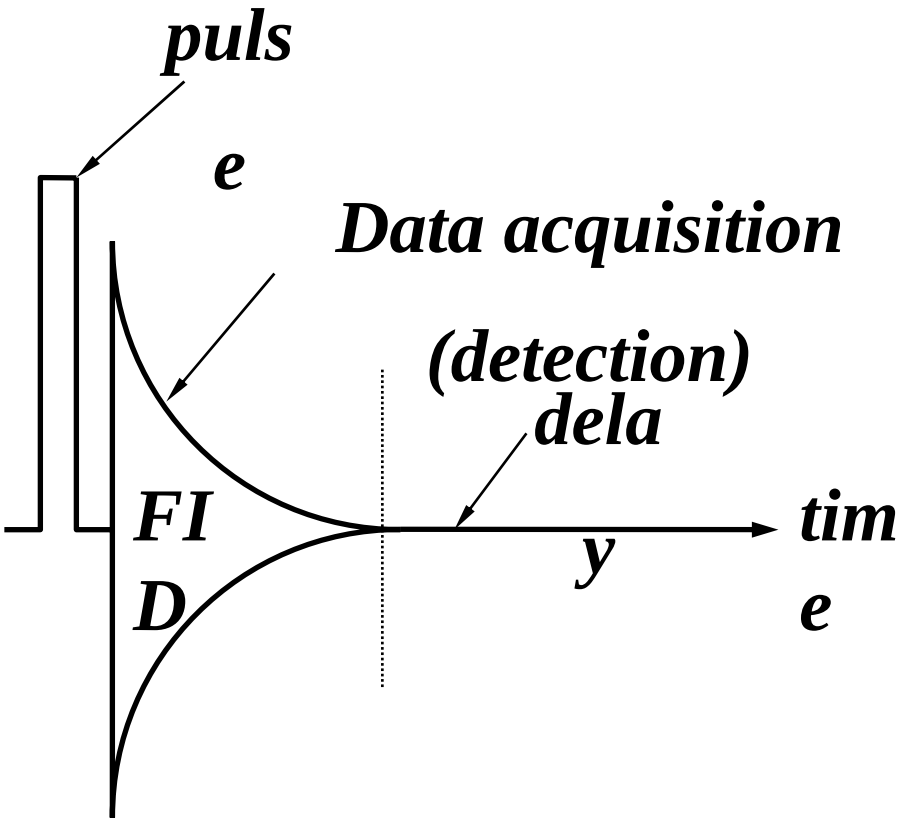
puls
e
Data acquisition
(detection)
dela
FI
D
y
tim
e

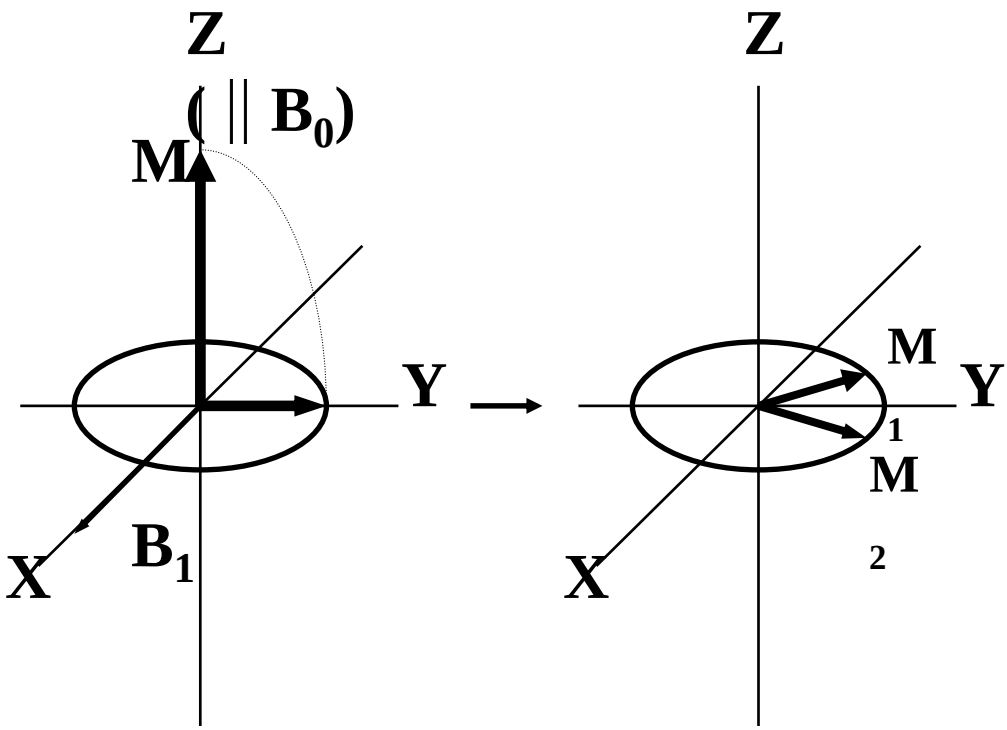
Z
(‖ B0)
M
Y
X
B1
Z
M
Y
1
M
2
X

FID its projection along y-axis

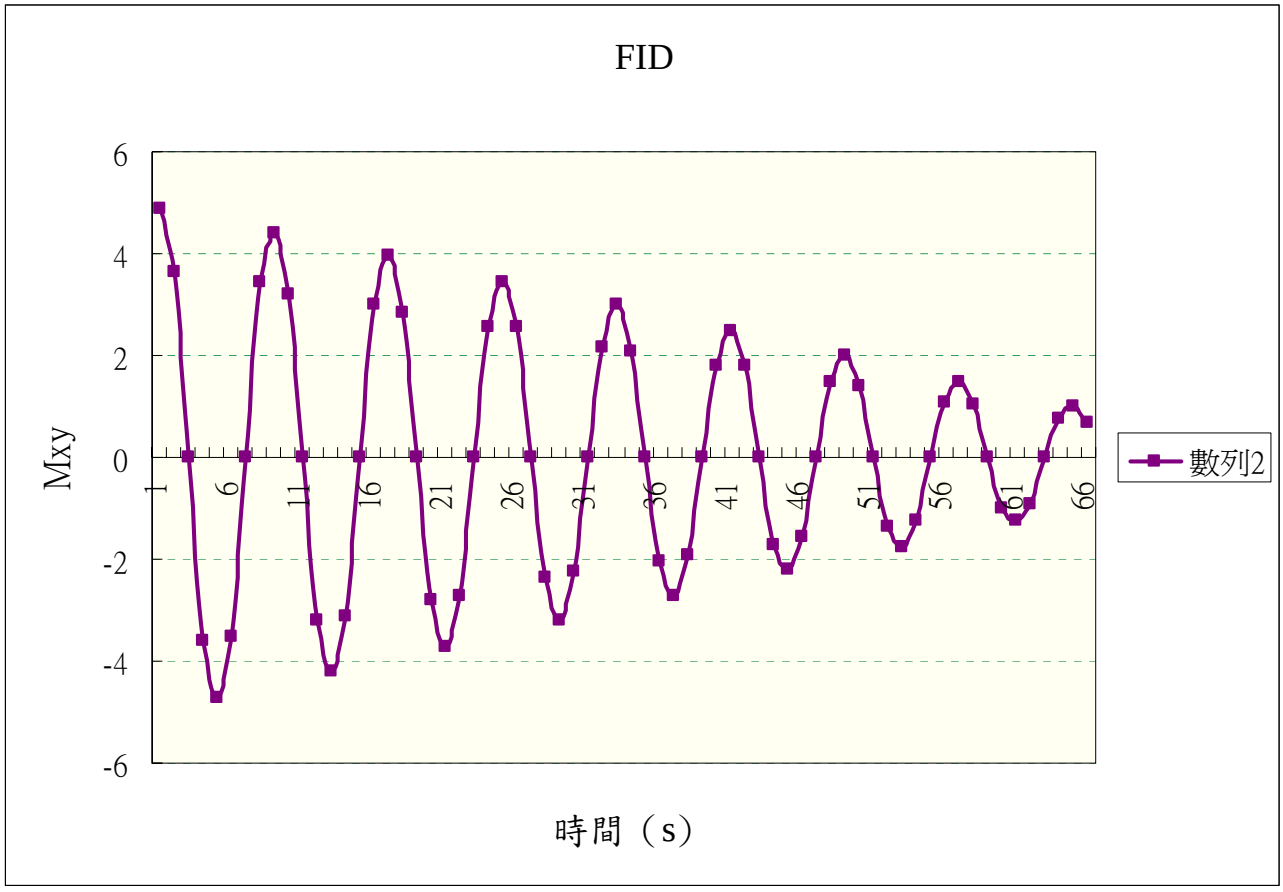

Longitudinal and transverse relaxation following a pulse

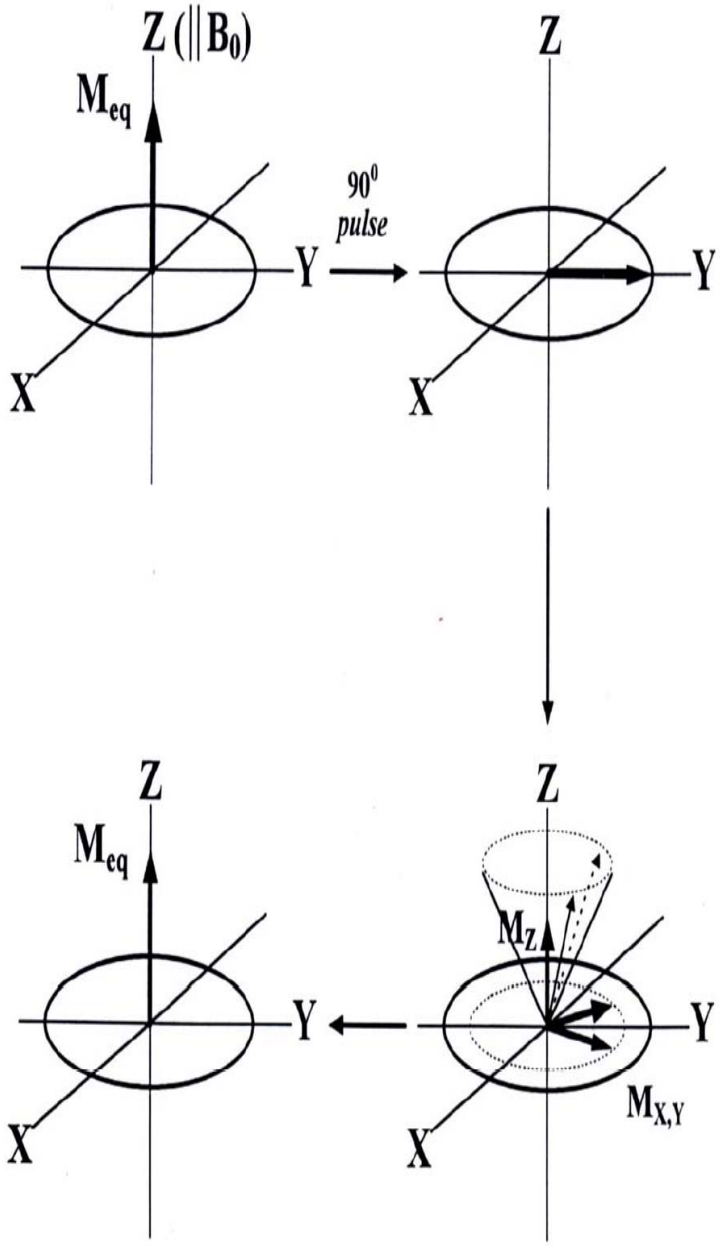

Longitudinal relaxation or spin-relaxation relaxation T_1

Longitudinal relaxation (T_1) is the mechanism by which an excited magnetization vector returns to equilibrium (conventionally shown along the *z* axis).

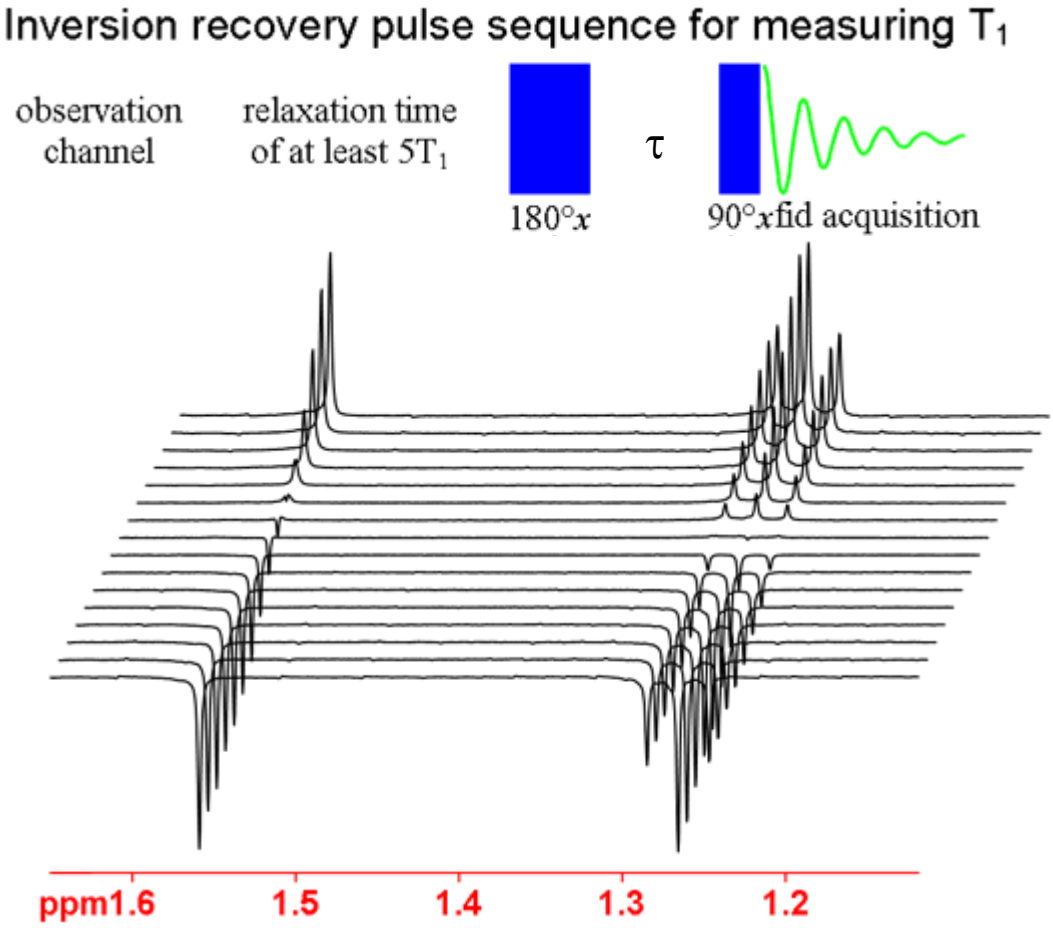

Inversion recovery curve for the methyl protons of ethylbenzene (0.1%) in $CDCl_3$ at 400 Mhz

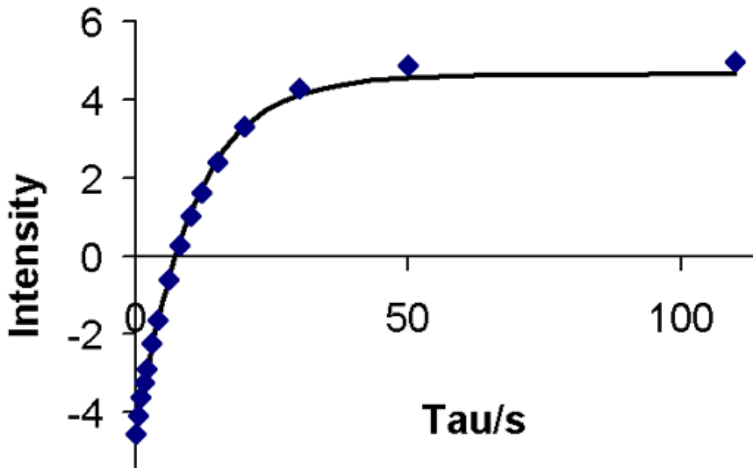

The inversion recovery (*T*1) pulse sequence yields a signal of intensity $I_0\left[1 - 2\exp\left(\frac{\tau}{T_1}\right)\right]$

Transverse relaxation T_2, spin-spin relaxation

Transverse relaxation (*T*2) is the mechanism by which the excited magnetization vector (conventionally shown in the x-y plane) decays. This is always at least slightly faster than longitudinal relaxation.

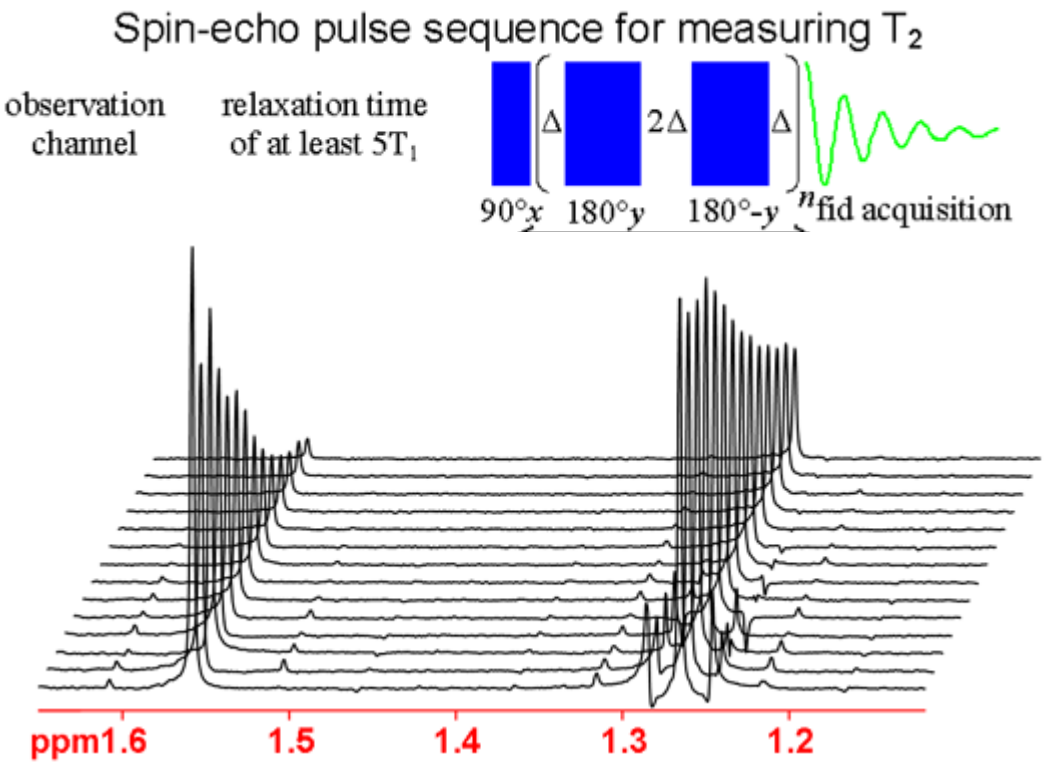

Spin-echo experiment for proton spectrum of ethylbenzene (0.1%) in $CDCl_3$ at 400 MHz, the residual water peak on the left relaxes faster than the methyl on the right.

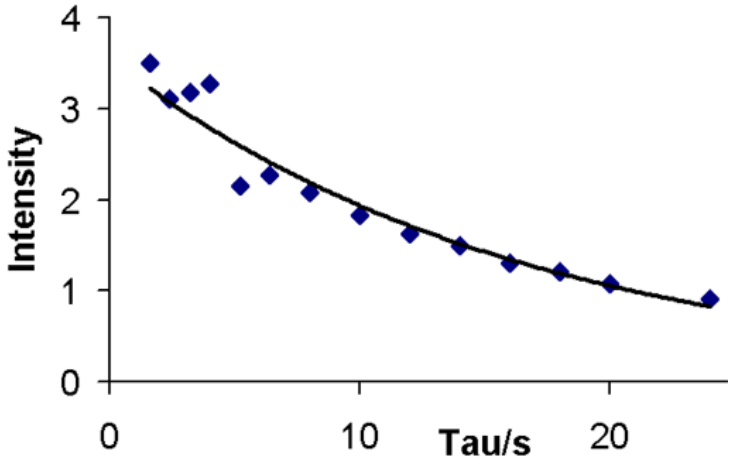

Exponential decay curve for the methyl protons of ethylbenzene (0.1%) in CDCl3 at 400 MHz

The spin-echo (*T2*) pulse sequence yields a signal of intensity $I_0[1-\exp(-\frac{\tau}{T_2})]$

Chemical shift

Chemical shift (δ) ***the frequency of specific spin for solutions or liquids depends on the chemical environment of the nucleus. Such differences in resonance conditions are referred to as chemical shifts.***

$B=B_o(1-\sigma)$, The dimensionless number σ is a small fraction, describing the electron shielding in the external magnetic field.

It is measured relative to a reference compound. In frequency units the chemical shift is proportional to the applied static magnetic field, and therefore chemical shifts are customarily quoted in parts per million (ppm) units.

Chemical shift references

Chemical shift (δ) defines the location of a NMR line along the rf axis. It is measured relative to a reference compound. In frequency units the chemical shift is proportional to the applied static magnetic field, and therefore chemical shifts are customarily quoted in parts per million (ppm) units.

$$\Delta\nu = \nu_{\text{signal}} - \nu_{\text{reference}}$$

$$\delta\ (\text{ppm}) = (\Delta\nu/\nu_0)\times 10^6$$

Examples :

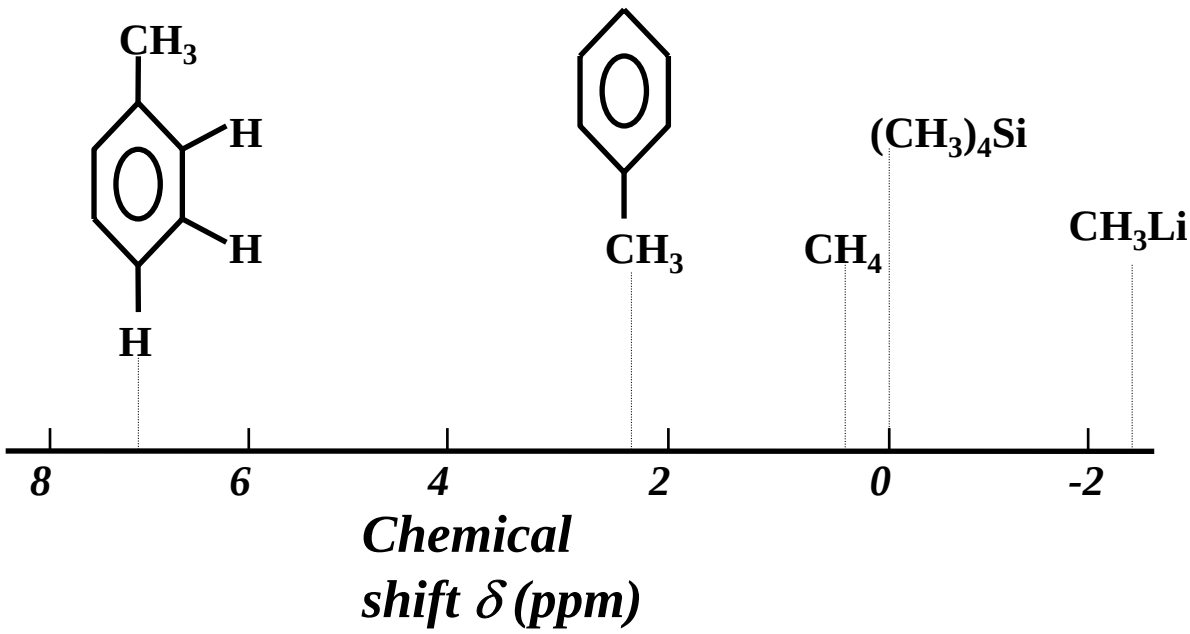

downfield
high frequency

Increased shielding

Increased deshielding

upfield
low frequency

One Dimensional NMR Spectroscopy

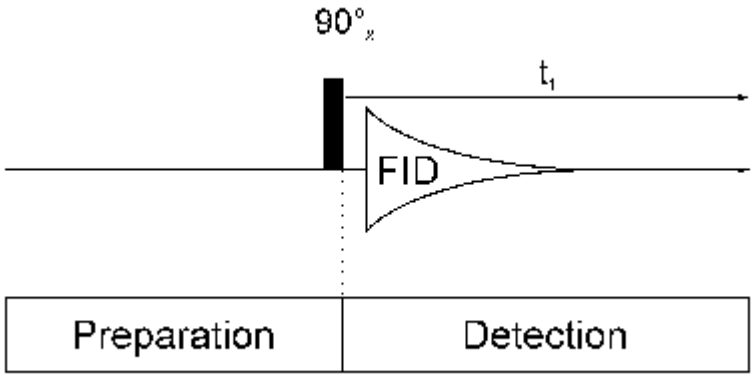

The 1D experiment

Each 1D NMR experiment consists of two sections: preparation and detection. During preparation the spin system is set to a defined state. During detection the resulting signal is recorded. In the simplest case the preparation is a 90 degree pulse (in our example applied along the x axis) which rotates the equilibrium magnetization M_z onto the y axis (M_y). After this pulse each spin precesses with its own Larmor frequency around the z axis and induces a signal in the receiver coil. The signal decays due to T2 relaxation and is therefore called free induction decay (FID).

Usually, the experiment is repeated several times and the data are summed up to increase the signal to noise ratio. After summation the data are fourier transformed to yield the final 1D spectrum.

One Dimensional 1H NMR Spectrum

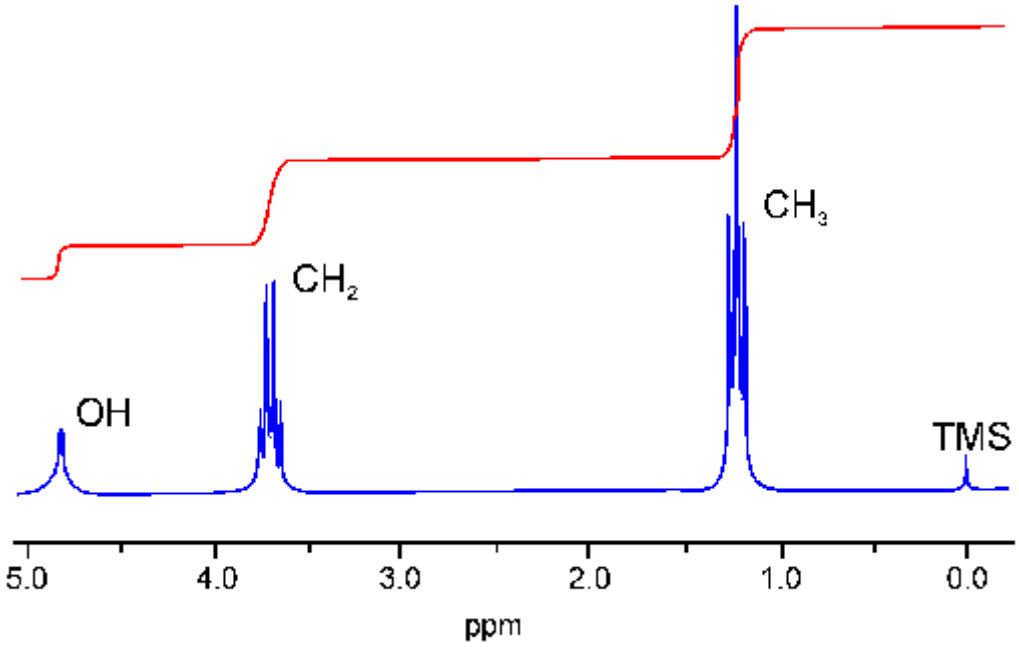

The ethanol 1H spectrum contains three signals two of which are in part split up into several lines (the split signals are called multiplets). The three signals can be assigned to the OH, CH_2 and CH_3 protons, respectively. The three methyl protons are equivalent to each other and give only one signal. The same is true for the two methylene protons. The number of protons which cause a specific signal can be calculated by integration over the signal:

The steps in the red integration curve over the signals show a ratio of 1:2:3 which is equivalent to the number of corresponding protons.

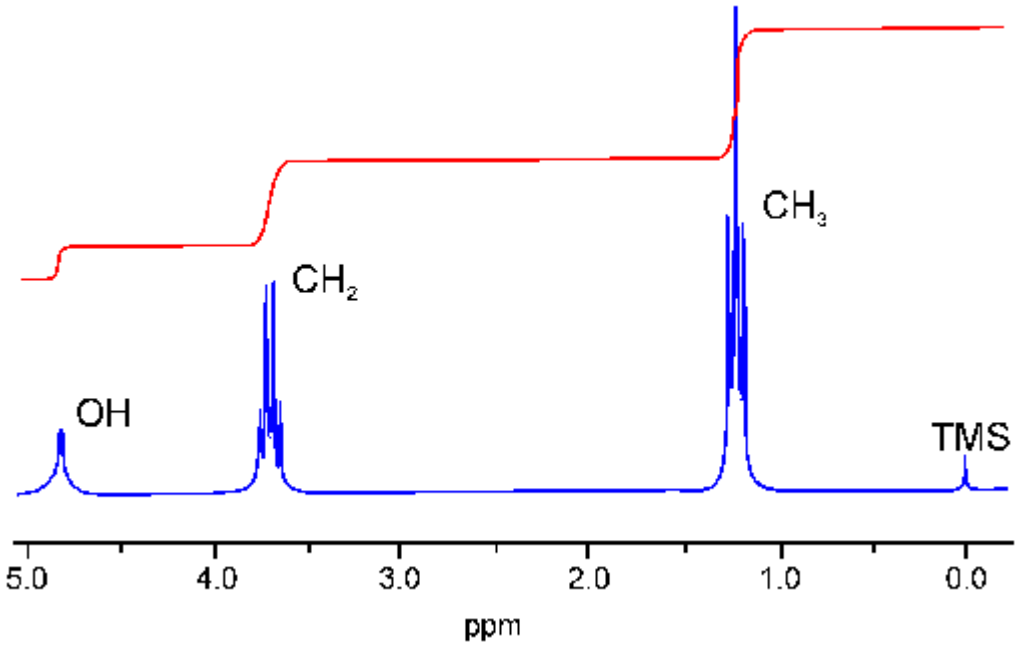

Chemical Shift:

The electrons in a molecule surround the nuclei and create a small magnetic field which shields the nuclei slightly from the external field. Therefore, the larmor frequencies of different nuclei vary due to their different chemical environment. This effect is called 'chemical shift'. It is one of the major parameters of NMR spectroscopy since it causes the different positions of the signals in a NMR spectrum (see spectrum above).

The value of a signals chemical shift (*delta*) in ppm (parts per million) is defined as:

$$delta = ((w_{signal} - w_{reference}) / w_{reference}) * 10^6$$

In the case if the 1H NMR spectrum of ethyl benzene, the methyl (CH3) group is the most electron withdrawing (electronegative) and therefore resonates at the lowest chemical shift.

The aromatic phenyl group is the most electron donating (electropositive) so that it has the highest chemical shift. The methylene (CH2) falls somewhere in the middle. However, if the chemical shift of the aromatics were due to electropositivity alone, then they would resonate between four and five ppm. The increased chemical shift is due to the delocalized ring current of the phenyl group.

Spin-spin coupling constant (J) ***characterizes scalar interactions (through-bond) between nuclei linked via a small number of covalent bonds in a chemical structure.***

If two nuclei couple with non-zero spin in the molecule having, say, spin I_1 and I_2, then it is found that the resonance of spin I_1 is split into $2I_2+1$ lines of equal intensity and that of spin I_2 is similarly split into $2I_1+1$ lines. The line separations are equal. The interaction is known as spin-spin coupling. And J is field independent and is customarily quoted in hertz (Hz).

1H-1H spin-spin J-coupling observed by NMR

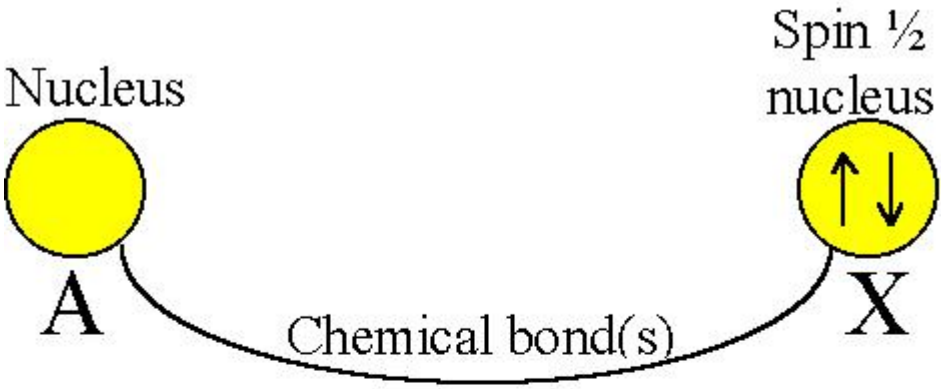

The resonant frequency of A is dependent on the alignment of X. A's signal is split into two equal parts because X is about equally divided between alignments.

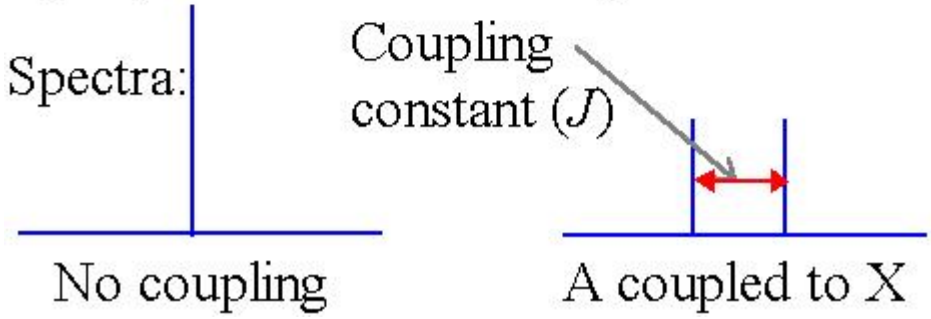

The effective magnetic field is also affected by the orientation of neighboring nuclei. This effect is known as spin-spin coupling which can cause splitting of the signal for each type of nucleus into two or more lines.

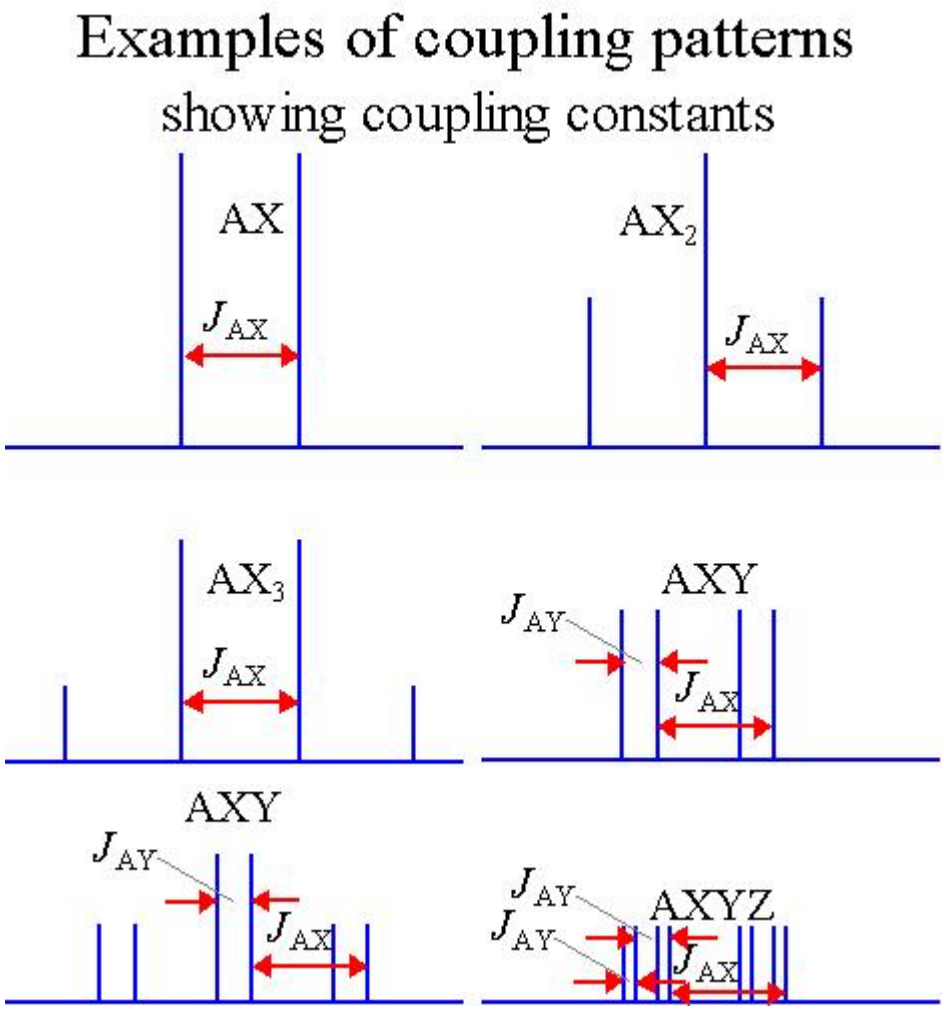

The size of the splitting (coupling constant or *J*) is independent of the magnetic field and is therefore measured as an absolute frequency (usually Hertz). The number of splittings indicates the number of chemically bonded nuclei in the vicinity of the observed nucleus.

The above patterns are a first order approximation and are correct provided that all the coupled spins have widely separated chemical shifts. The different nuclei are labeled with the letters A and X (in a system of this type the letters come from widely separated parts of the alphabet). If the chemical shifts are similar then distortions in peak height occur as in the diagram below (the letters are also close together in the alphabet). For more than two spins, extra signals may appear.

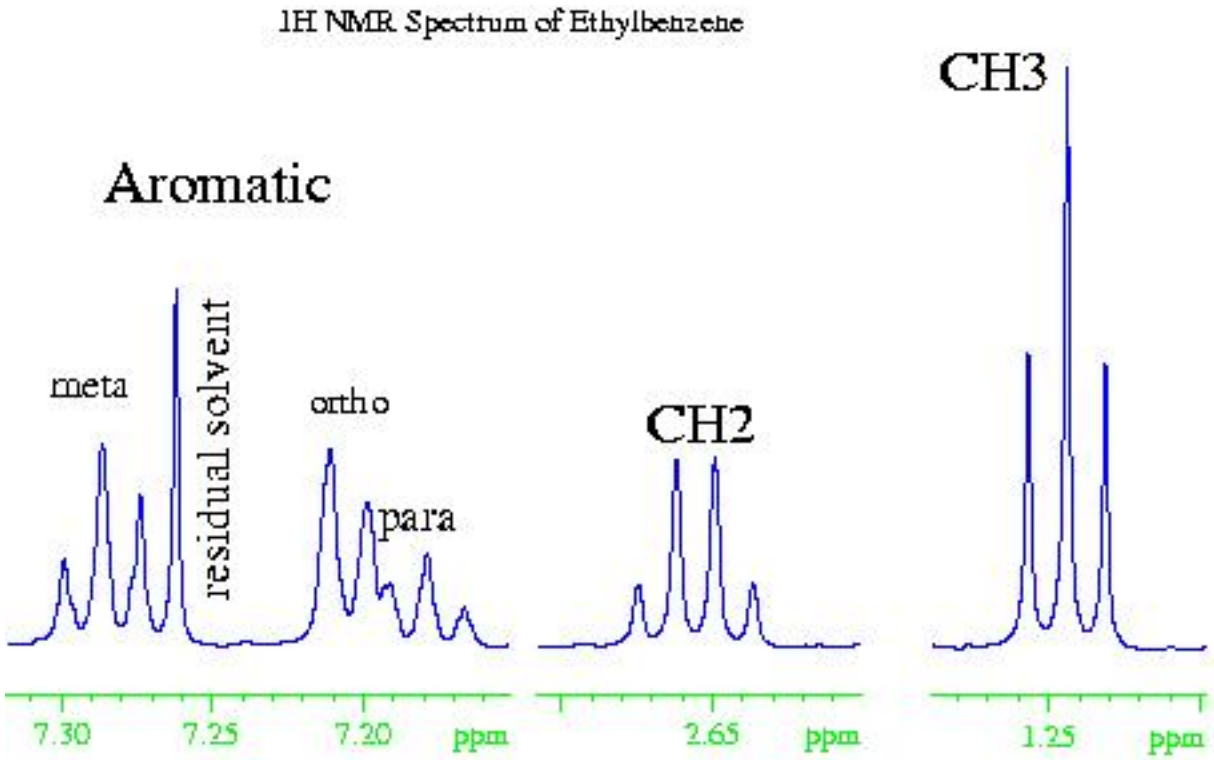

Returning to the example of ethylbenzene, the methyl (CH3) group has a coupling pattern in the form of A3X2 which to a first order approximation looks like an AX2 multiplet. Likewise, the methylene (CH2) group has the form A2X3 that is equivalent to AX3. The first order approximation works because the groups are widely separated in the spectrum. The aromatic signals are close together and display second order effects. The *ortho* signal is a doublet AX while the *meta* and *para* signals are triplets

Summary

Isolated spins (Zeeman effect, Larmor Frequency)

Electron cloud (chemical shift)

Scalar coupling (J-coupling through chemical bonds)

Dipolar interaction (NOE through space)

* Spin dynamics (T1, T2… relaxations)

One Dimensional 1H NMR Spectrum

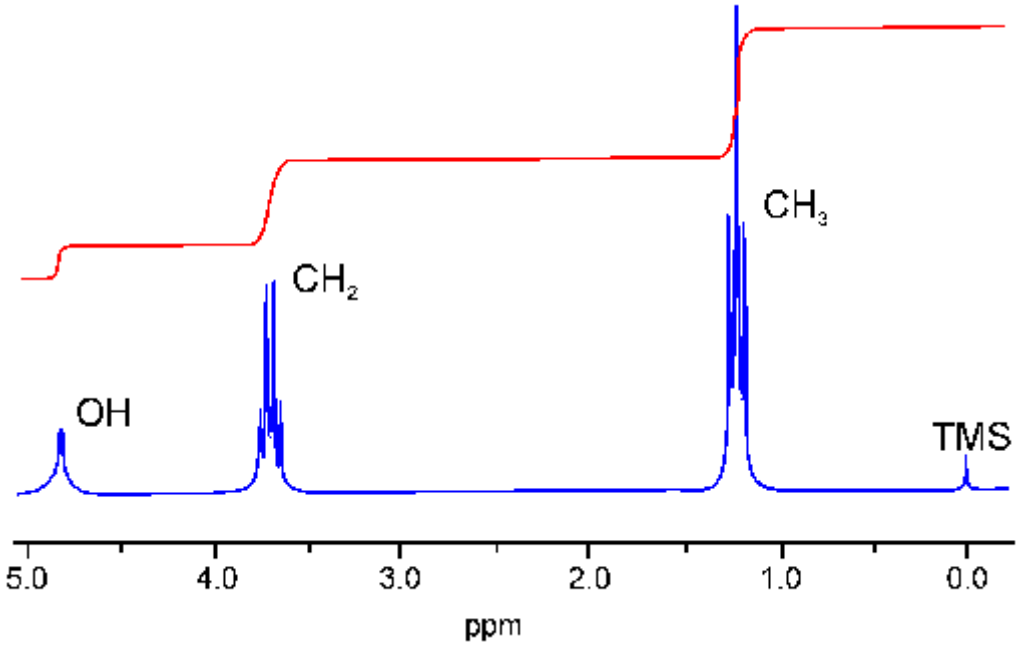

The ethanol 1H spectrum contains three signals two of which are in part split up into several lines (the split signals are called multiplets). The three signals can be assigned to the OH, CH_2 and CH_3 protons, respectively. The three methyl protons are equivalent to each other and give only one signal. The same is true for the two methylene protons. The number of protons which cause a specific signal can be calculated by integration over the signal:

The steps in the red integration curve over the signals show a ratio of 1:2:3 which is equivalent to the number of corresponding protons.

Coupling of 1H to 31P

Long-range couplings to 31P (phosphorus) appear in the 1H spectrum of phosphorus containing molecules. The couplings have effects over three to four bonds. The 31P spectrum also shows 1H couplings.

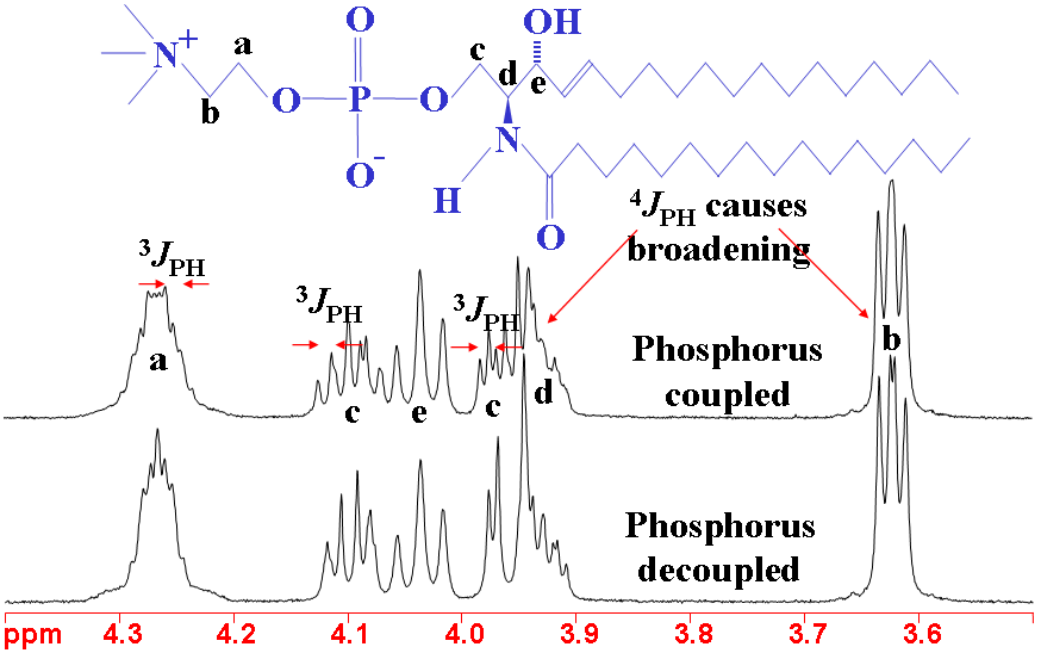

^{31}P spectrum of sphingomyelin shows the effects of ^{1}H coupling

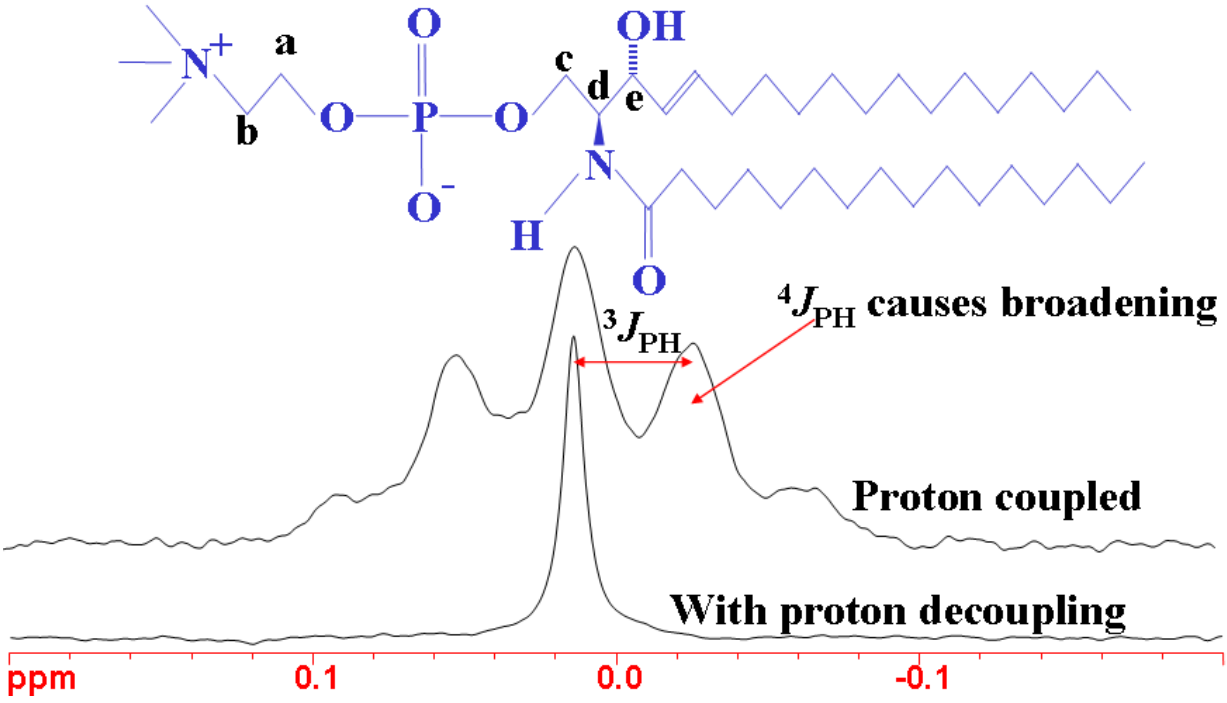

What’s happening during the pulse sequence ?

RF pulse :

$$I_\beta \xrightarrow{(\phi I_\alpha)} I_\beta \cos\phi + I_\gamma \sin\phi$$

α, β and γ represent permutations of the x, y and z axes and ϕ is the pulse flip angle

Example :

$$I_y \xrightarrow{(90 I_x)} I_z$$

$$I_x \xrightarrow{(90 I_y)} -I_z$$

Chemical shift :

$$I_x \xrightarrow{(w_I t I_z)} I_x \cos(w_I t) + I_y \sin(w_I t)$$

$$I_y \xrightarrow{(w_I t I_z)} I_y \cos(w_I t) - I_x \sin(w_I t)$$

$$2I_z S_x \xrightarrow{(\phi I_x)} 2I_z S_x \cos\phi - 2I_y S_x \sin\phi$$

$$2I_x S_z \xrightarrow{(w_I t I_z)} 2I_x S_z \cos(w_I t) + 2I_y S_z \sin(w_I t)$$

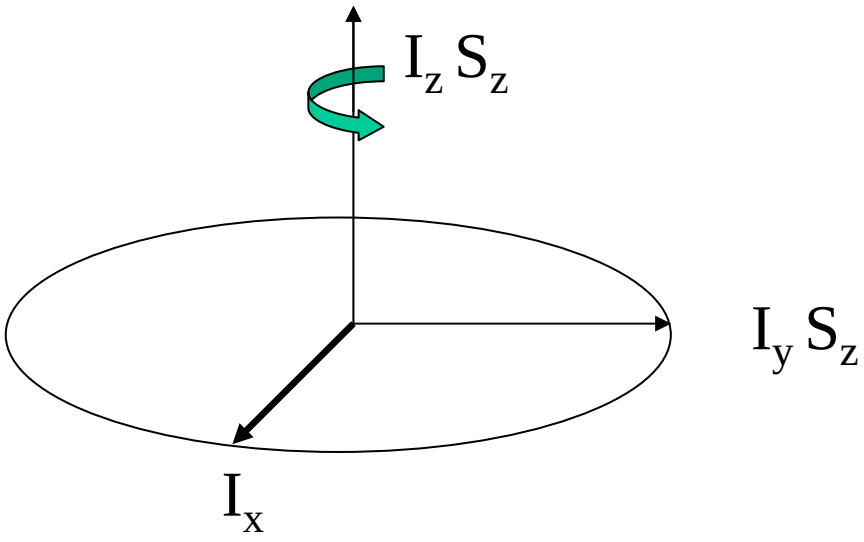

J-coupling :

$$I_x \xrightarrow{(\pi J_{IS} t 2 I_z S_z)} I_x \cos(\pi J_{IS} t) + 2 I_y S_z \sin(\pi J_{IS} t)$$

$$2 I_y S_z \xrightarrow{(\pi J_{IS} t 2 I_z S_z)} 2 I_y S_z \cos(\pi J_{IS} t) - I_x \sin(\pi J_{IS} t)$$

Example :

$$I_x \xrightarrow{(\pi J_{IS} t 2 I_z S_z)} 2 I_y S_z \quad (t = 1/2 J_{IS})$$

$$2 I_y S_z \xrightarrow{(\pi J_{IS} t 2 I_z S_z)} - I_x \quad (t = 1/2 J_{IS})$$

COSY :

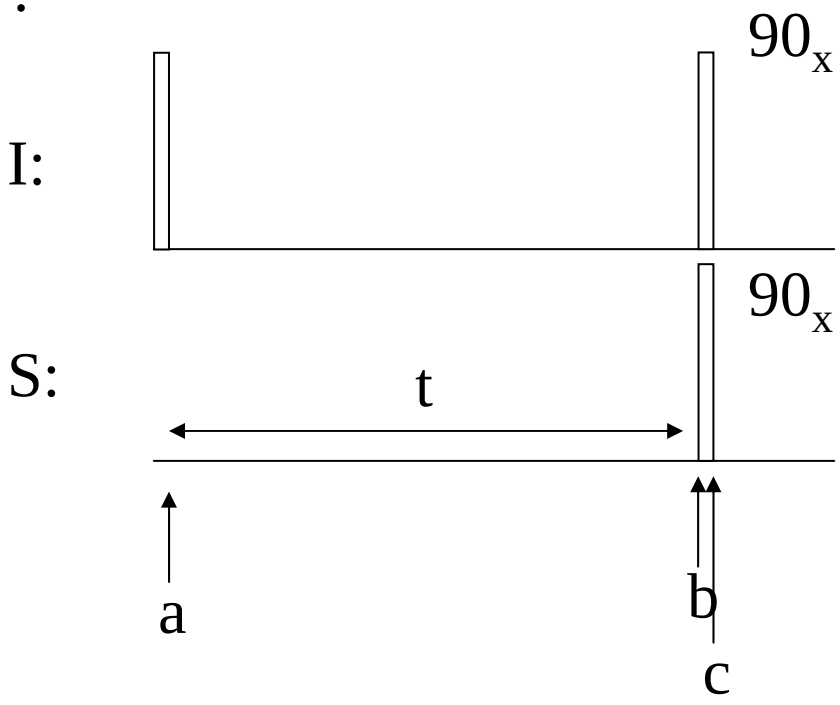

$$a \rightarrow b: I_x \xrightarrow{(wtI_z)} I_x \cos(w_I t) + I_y \sin(w_I t)$$

$$\xrightarrow{(\pi J_{IS} t 2 I_z S_z)} [I_x \cos(w_I t) + I_y \sin(w_I t)] \cos(\pi J_{IS} t)$$

$$+ [2 I_y S_z \cos(w_I t) - 2 I_x S_z \sin(w_I t)] \sin(\pi J_{IS} t)$$

$$b \rightarrow c: \xrightarrow{(90I_x)} \xrightarrow{(90S_x)} [I_x \cos(w_I t) + I_z \sin(w_I t)] \cos(\pi J_{IS} t)$$

$$+ [-2 I_z S_y \cos(w_I t) + 2 I_x S_y \sin(w_I t)] \sin(\pi J_{IS} t)$$

$$I_x \xrightarrow{(COSY)} -2 I_z S_y \cos(w_I t) \sin(\pi J_{IS} t)$$

NOESY:

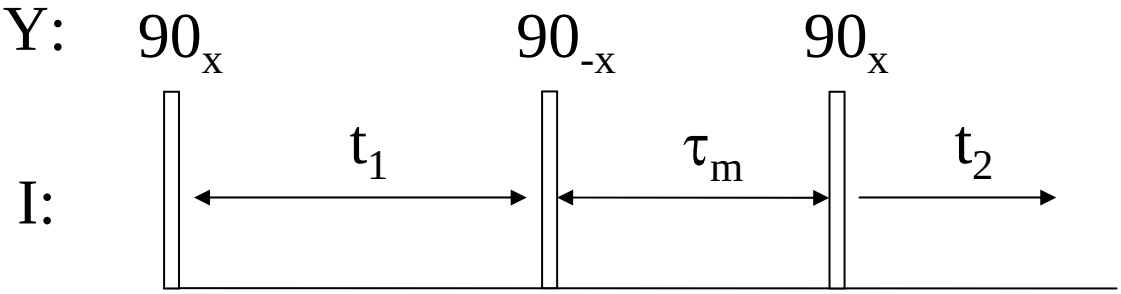

S:

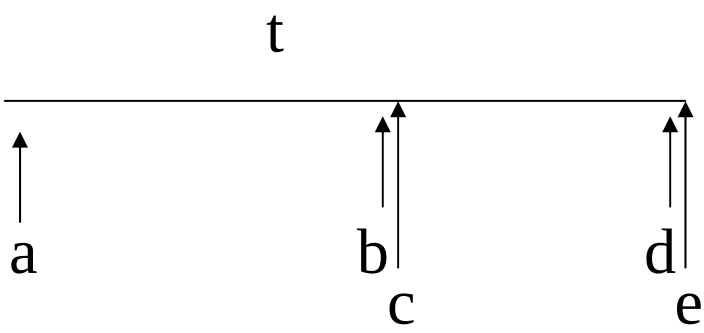

$$a \rightarrow b: I_x \xrightarrow{(wtI_z)} I_x \cos(w_I t) + I_y \sin(w_I t)$$

$$\xrightarrow{(\pi J_{IS} t 2 I_z S_z)} [I_x \cos(w_I t) + I_y \sin(w_I t)] \cos(\pi J_{IS} t)$$

$$+ [2 I_y S_z \cos(w_I t) - 2 I_x S_z \sin(w_I t)] \sin(\pi J_{IS} t)$$

$$b \rightarrow c: \xrightarrow{(90 I_x)} [I_x \cos(w_I t) + I_z \sin(w_I t)] \cos(\pi J_{IS} t)$$

$$+ [2 I_z S_z \cos(w_I t) + 2 I_x S_z \sin(w_I t)] \sin(\pi J_{IS} t)$$

$c \rightarrow d: \rightarrow$ **?**

HMQC :

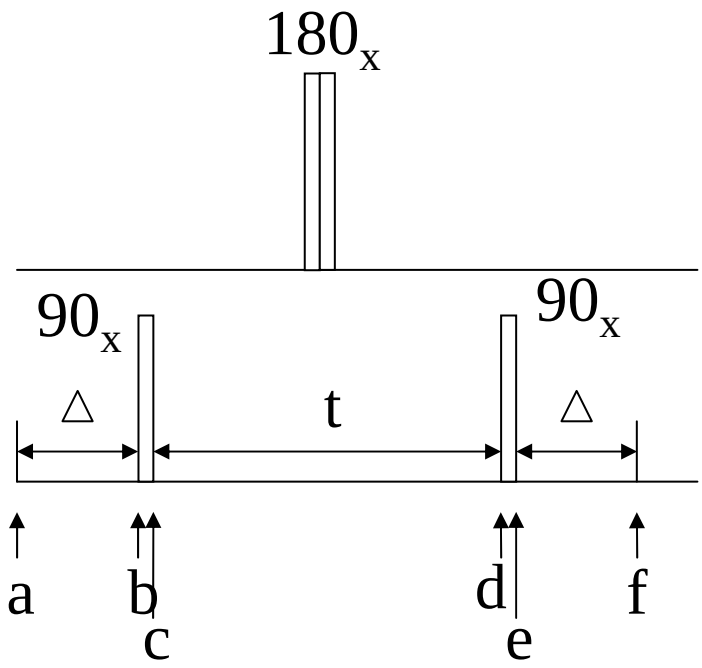

$a \rightarrow b$: $I_x \xrightarrow{(\pi J_{IS} t 2I_z S_z)} 2I_y S_z$ ($\triangle = 1/2J_{IS}$)

$b \rightarrow c$: $\xrightarrow{(90S_x)} -2I_y S_y$

$c \rightarrow d$: $\xrightarrow{(\text{Dec CS})} -2I_y S_y \cos(w_S t) + 2I_y S_x \sin(w_S t)$

$d \rightarrow e$: $\xrightarrow{(90S_x)} -2I_y S_z \cos(w_S t) + 2I_y S_x \sin(w_S t)$

$e \rightarrow f$: $\xrightarrow{(\pi J_{IS} t 2I_z S_z)} I_x \cos(w_S t) + 2I_y S_x \sin(w_S t)$

HMQC: $I_x \rightarrow I_x \cos(w_S t)$ ($\triangle = 1/2J_{IS}$)

Anatomy of a 3D experiment

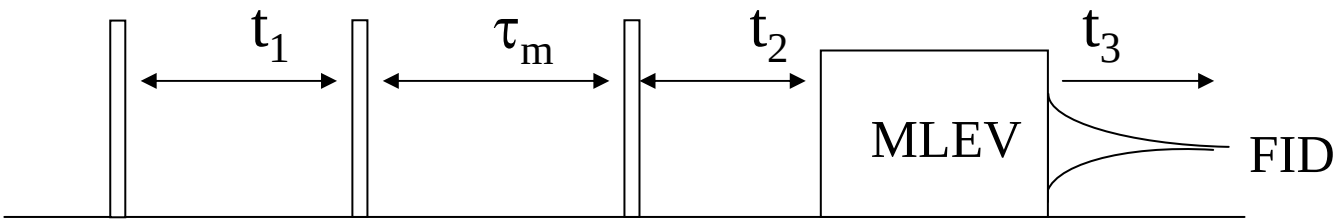

Preparation	Evolution	Mixing Time	Evolution	Mixing Time	Detection

A three dimensional NMR experiment (see picture above) can easily be constructed from a two-dimensional one by inserting an additional indirect evolution time and a second mixing period between the first mixing period and the direct data acqusition. Each of the different indirect time periods (t1, t2) is incremented separately.

Triple resonance experiments are the method of choice for the sequential assignment of larger proteins (> 150 AA). These experiments are called 'triple resonance' because three different nuclei (1H, 13C, 15N) are correlated. The experiments are performed on doubly labelled (13C, 15N) proteins.

2D NMR Spectroscopy

A two-dimensional NMR experiment involves a series of one-dimensional experiments. Each experiment consists of a sequence of radio frequency pulses with delay periods in between them. It is the timing, frequencies, and intensities of these pulses that distinguish different NMR experiments from one another.

During some of the delays, the nuclear spins are allowed to freely precess (rotate) for a determined length of time known as the **evolution time**. The frequencies of the nuclei are detected after the final pulse.

By incrementing the evolution time in successive experiments, a two-dimensional data set is generated from a series of one-dimensional experiments

Correlation spectroscopy is one of several types of two-dimensional NMR spectroscopy.

Other types of two-dimensional NMR include **J-spectroscopy**, **exchange spectroscopy** (EXSY), and Nuclear Overhauser effect spectroscopy (NOESY).

Two-dimensional NMR spectra provide more information about a molecule than one-dimensional NMR spectra and are especially useful in determining the structure of a molecule, particularly for molecules that are too complicated to work with using one-dimensional NMR. The first two-dimensional experiment, **COSY**, was proposed by Jean Jeener, a professor at Université Libre de Bruxelles, in 1971. This experiment was later implemented by Walter P. Aue, Enrico Bartholdi and Richard R. Ernst, who published their work in 1976

NOESY

NOESY (Nuclear Overhauser Effect Spectroscopy) spectra provide information about protons that are 5 Angstroms or less apart in space. The information is through space and not through bond, like a COSY or TOCSY. The presence of a NOE peak is direct evidence that two protons are within 5 Angstroms through space. The absence of a NOE peak between protons does not necessarily mean that they are not within 5 Angstroms since other factors can reduce a NOE peak even if the protons are close in space. A mid-size molecule (~1000-1500MW range) may have NOEs that are close to zero and a ROESY may be required to see them. Large molecules generally give better NOEs at higher field, but small molecules may actually give better NOEs at lower field. A 2-D NOESY of a small molecule will have cross peaks of opposite phase to the diagonal. A 2-D NOESY of a large molecule will have cross peaks of the same phase as the diagonal. Theoretically, these experiments should be symmetrical, but it is typical to see more intense peaks on one side of the diagonal than the other.

Nuclear **O**verhauser **E**ffect **S**pectroscop**Y** is a 2D spectroscopy method whose aim is to identify spins undergoing cross-relaxation and to measure the cross-relaxation rates. Most commonly, NOESY is used as a homonuclear ^{1}H technique. In NOESY, direct dipolar couplings provide the primary means of cross-relaxation, and so spins undergoing cross-relaxation are those which are close to one another in space. Thus, the cross peaks of a NOESY spectrum indicate which ^{1}H's are close to which other ^{1}H's in space. This can be distinguished from COSY, for example, which relies on J-coupling to provide spin-spin correlation, and whose cross peaks indicate which ^{1}H's are close to which other ^{1}H's through the bonds of the molecule.

2D NOESY spectrum of 50 mM Gramicidin in DMSO-d6

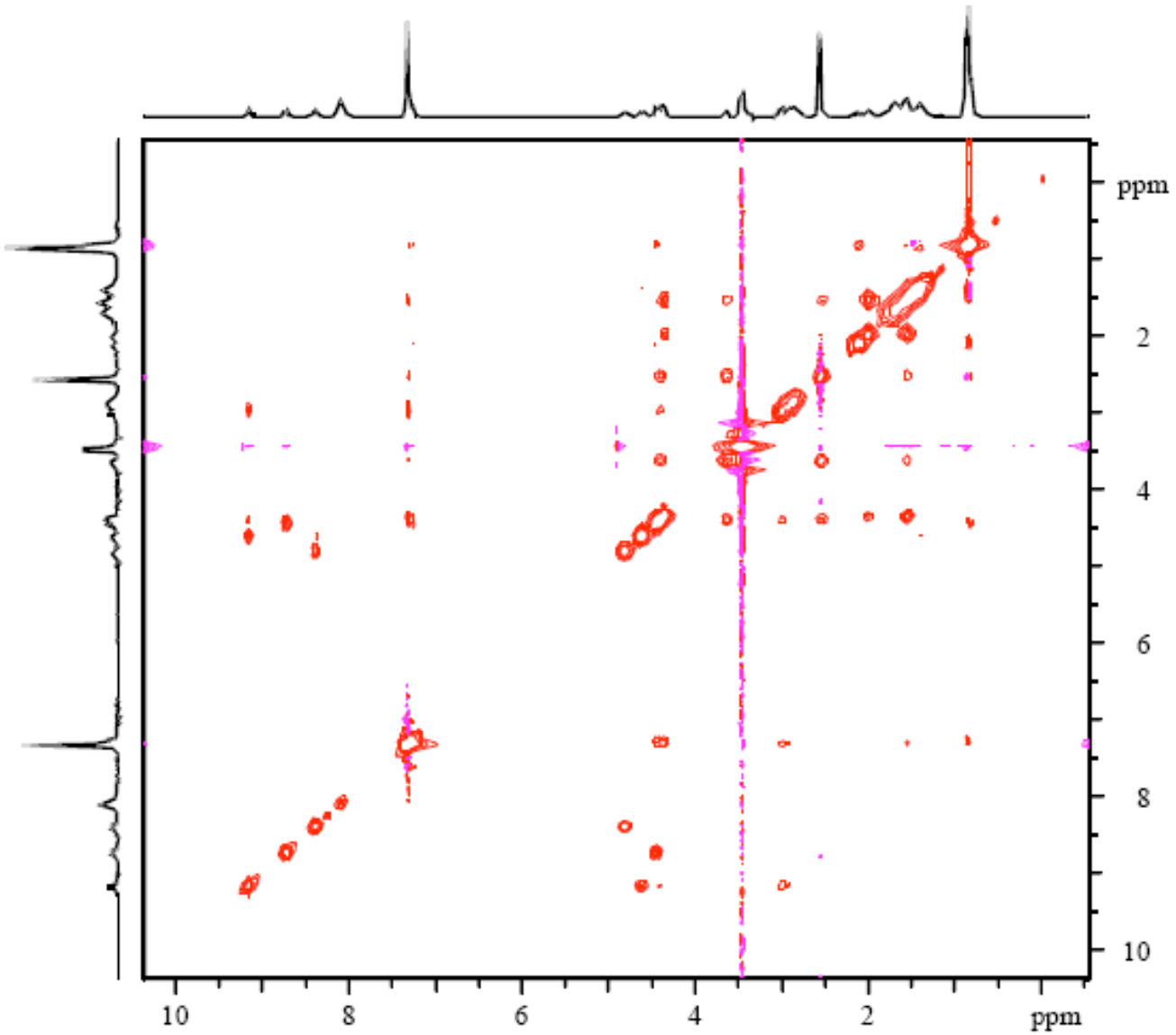

2D NOESY spectrum of ethylbenzene

The basic NOESY sequence consists of three π/2 pulses. The first pulse creates transverse spin magnetization. This precesses during the evolution time t_1, which is incremented during the course of the 2D experiment. The second pulse produces longitudinal magnetization equal to the transverse magnetization component orthogonal to the pulse direction. Thus, the basic idea is to produce an initial situation for the mixing period τ_m (the time during which cross relaxation occurs) where the longitudinal polarization of each spin is labelled by its resonance frequency. The longitudinal magnetization is allowed to relax during the mixing time τ_m. Note that, for the basic NOESY experiment, τ_m is kept constant throughout the 2D experiment. The third pulse creates transverse magnetization from the remaining longitudinal magnetization. Acquisition begins immediately following the third pulse, and the transverse magnetization is observed as a function of the time t_2. The NOESY spectrum is generated by a 2D Fourier transform with respect to t_1 and t_2.

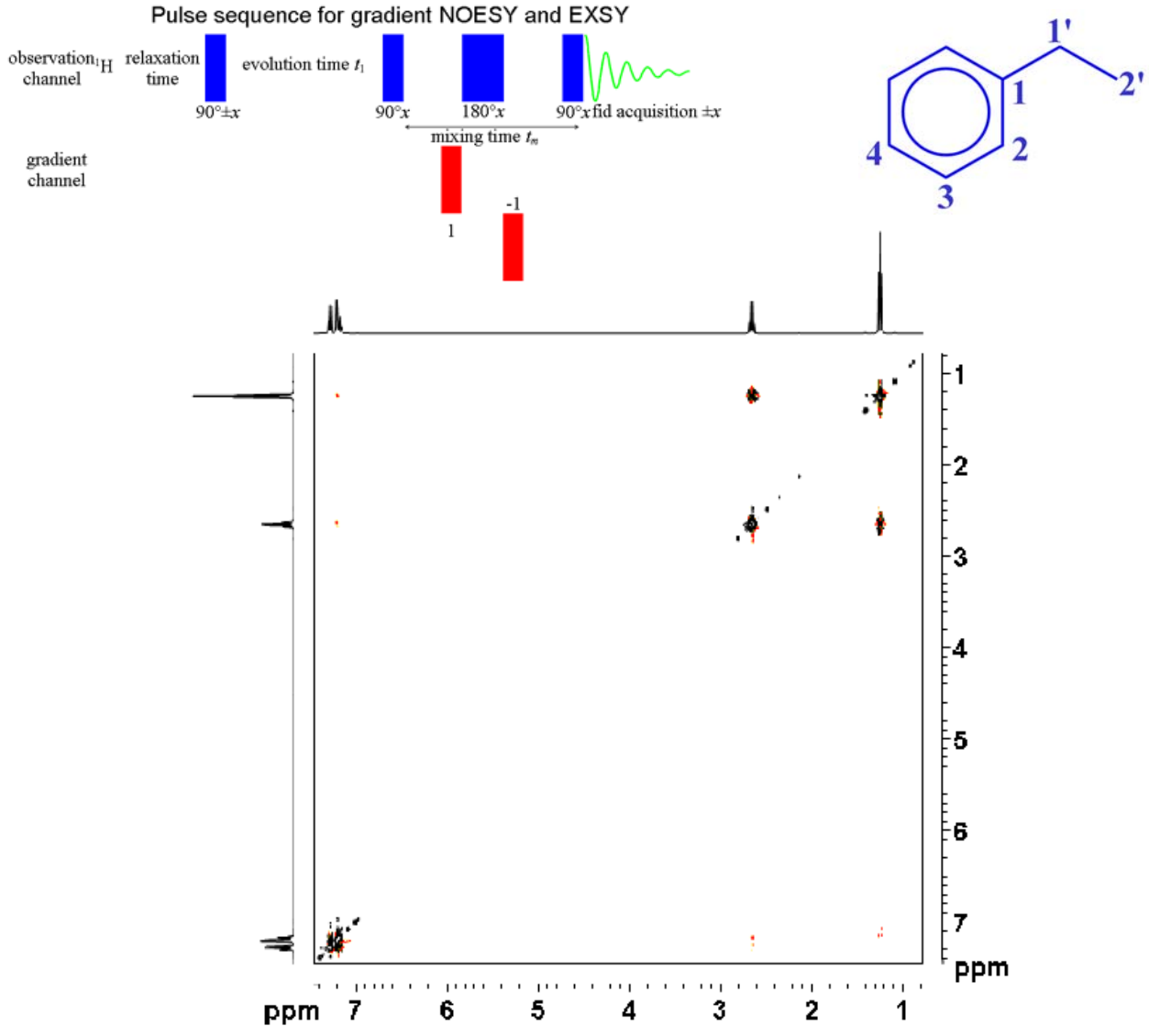

2D NOESY spectrum of aromatic region of 12,14-ditbutylbenzo[g]chrysene

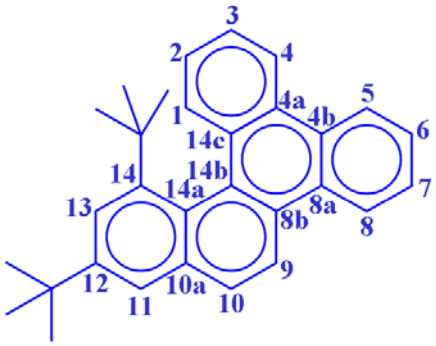

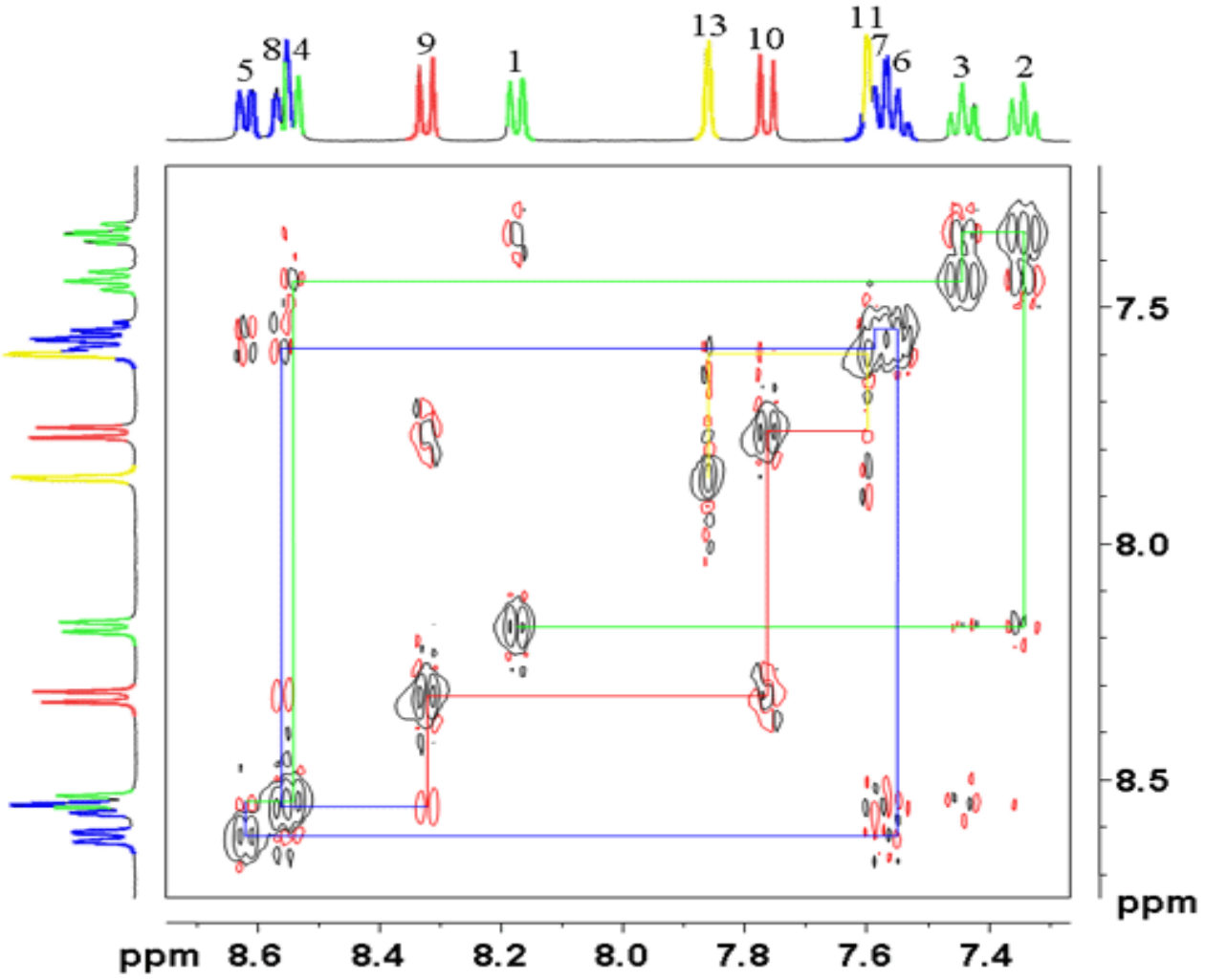

Continuing the connectivity, we can assign H10 as 7.76 ppm H11 as 7.60 ppm and H13 as 7.86 ppm. In the opposite direction, H7 is at 7.59 ppm , H6 at 7.55 ppm, H5 at 8.62 ppm, H4 at 8.54 ppm, H3 at 7.44 ppm, H2 at 7.34 ppm and H1 at 8.17 ppm. Aromaric region shows connectivity and separation into four color-coded proton groups

^{1}H-^{1}H TOCSY

^{1}H-^{1}H TOCSY (TOtal Correlated SpectroscopY also known as HOHAHA – HOmonuclear HArtmann HAhn) is useful for dividing the proton signals into groups or coupling networks, especially when the multiplets overlap or there is extensive second order coupling.

A TOCSY spectrum yields through bond correlations *via* ***spin-spin coupling***. Correlations are seen throughout the coupling network and intensity is not related in a simple fashion to the number of bonds connecting the protons. Therefore a five-bond correlation may or may not be stronger than a three-bond correlation. TOCSY is usually used in large molecules with many separated coupling networks such as peptides, proteins, oligosaccharides and polysaccharides. If an indication of the number of bonds connecting the protons is required, for example in order to determine the order in which they are connected, a COSY spectrum is preferable.

The pulse sequence used in our laboratory is the gradient enhanced TOCSY. The spin-lock is a composite pulse and should be applied for between 20 and 200 ms with a pulse power sufficient to cover the spectral width. A short spin-lock makes the TOCSY more COSY-like in that more distant correlations will usually be weaker than short-range ones. A long spin-lock allows correlations over large coupling networks. Too long a spin-lock will heat the sample causing signal distortion and can damage the electronics of the spectrometer.

The attenuation should be set so that the 90° pulse with will be less than 1/(4SWH) (SWH is the spectral width in Hz) and typically 1/(6SWH). An attenuation of 12 dB with a 50 W amplifier yielding a 90° pulse width of 35 μs is typical.

2D TOCSY spectrum of ethylbenzene

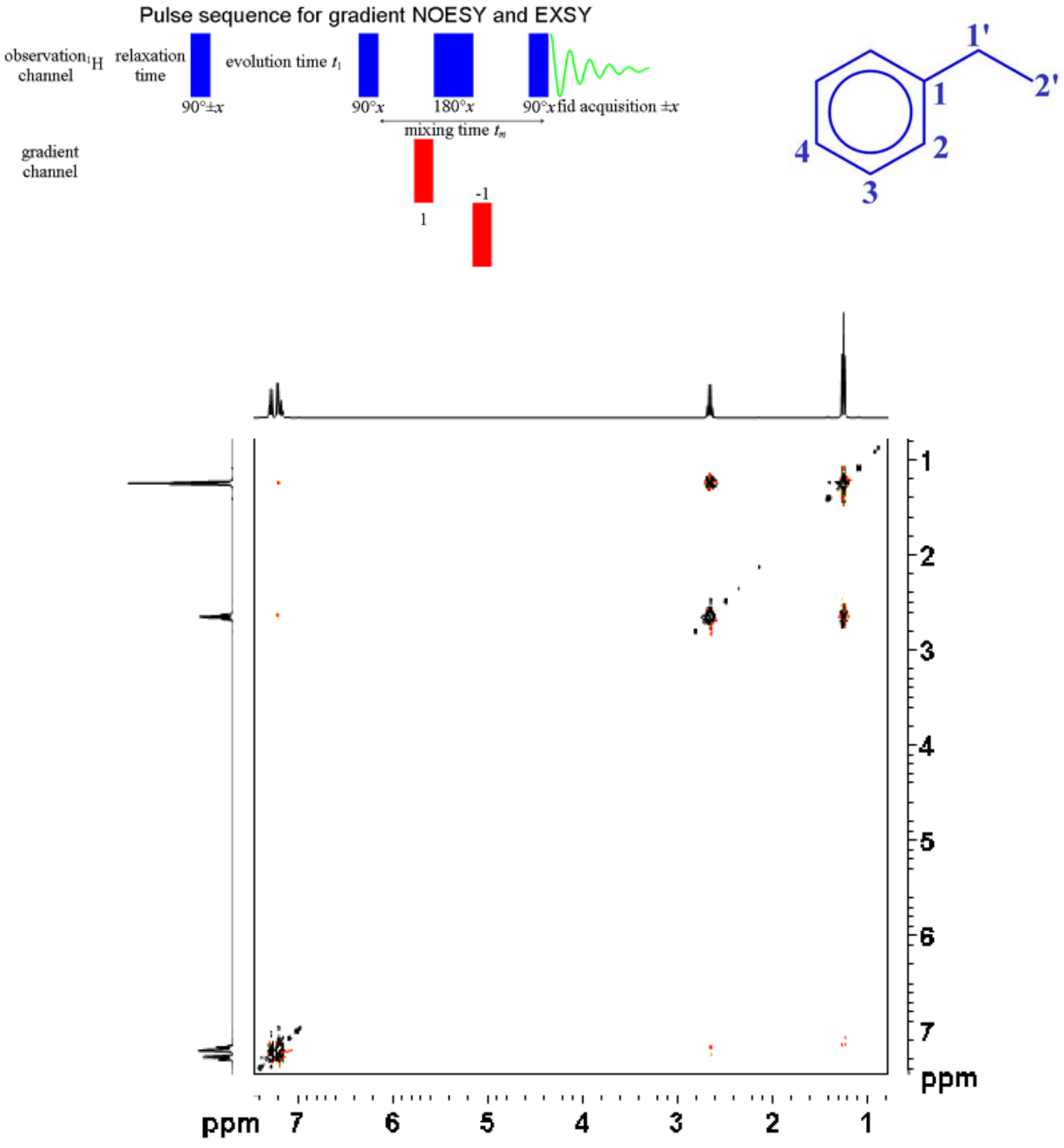

^{1}H-^{1}H COSY Spectroscopy

1H-1H COSY (COrrelated SpectroscopY) is useful for determining which signals arise from neighboring protons, especially when the multiplets overlap or there is extensive second order coupling.

A COSY spectrum yields through bond correlations *via* spin-spin coupling. If a homonuclear coupling is resolved in the 1D spectrum, a correlation will appear in the COSY but if no splitting is observed then no correlation is likely. Two and three bond and sometimes four bond correlations yield COSY signals.

2D COSY spectrum of ethylbenzene

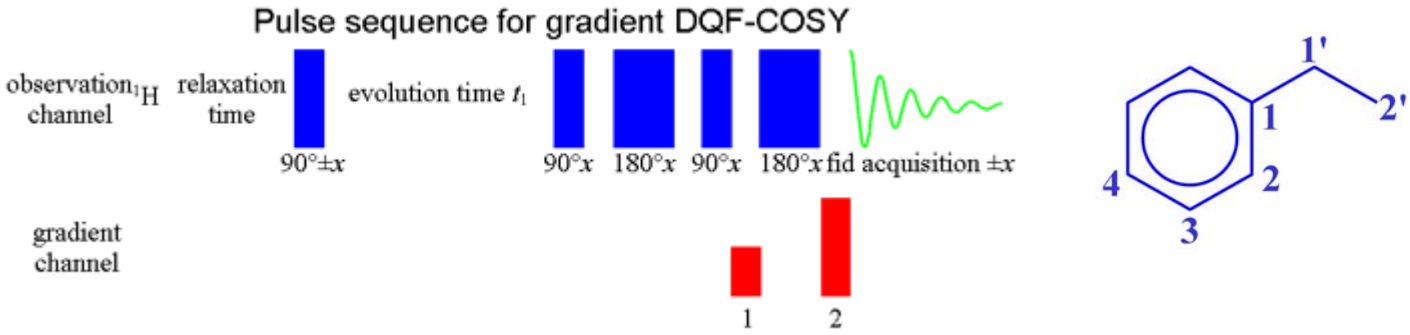

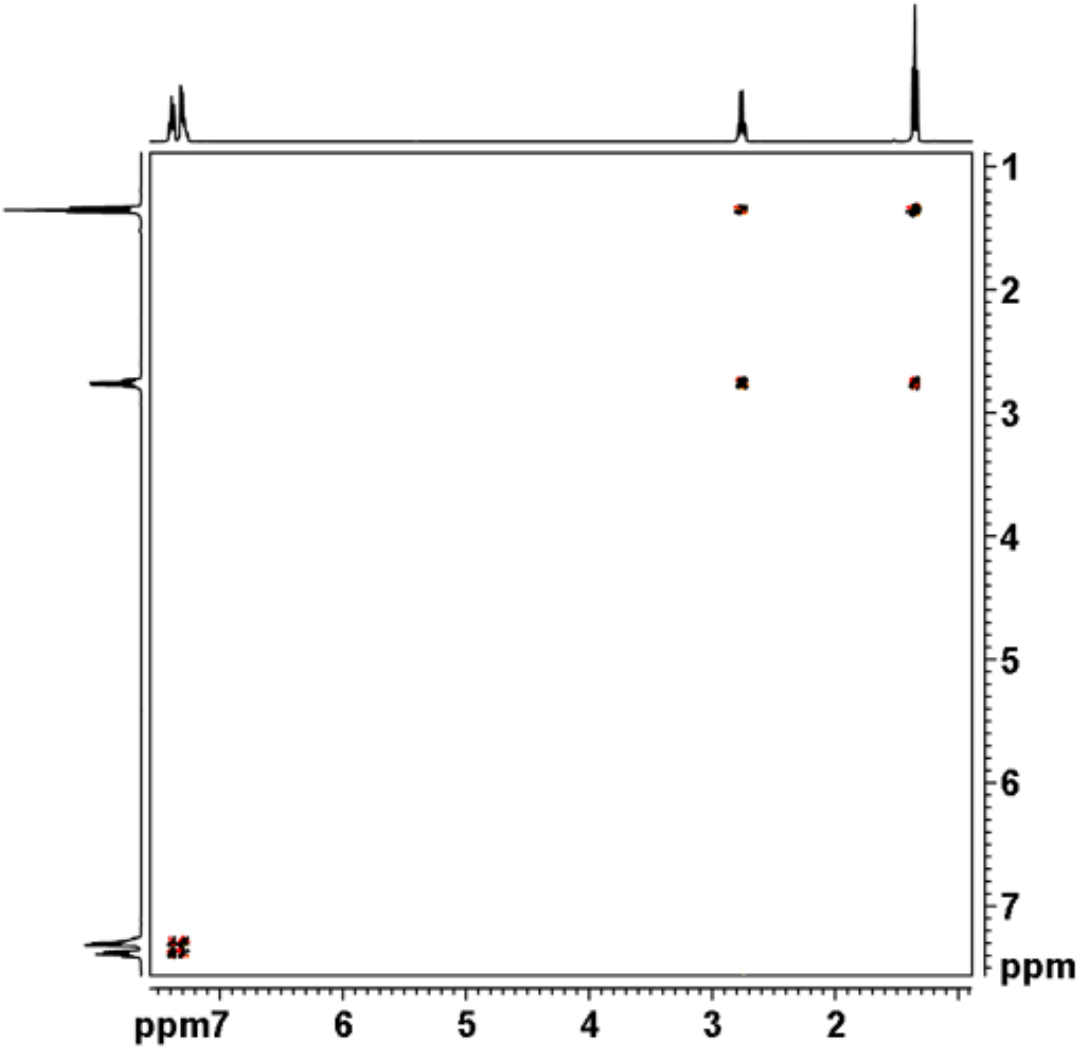

2D COSY spectrum of aromatic region of 12,14-ditbutylbenzo[g]chrysene

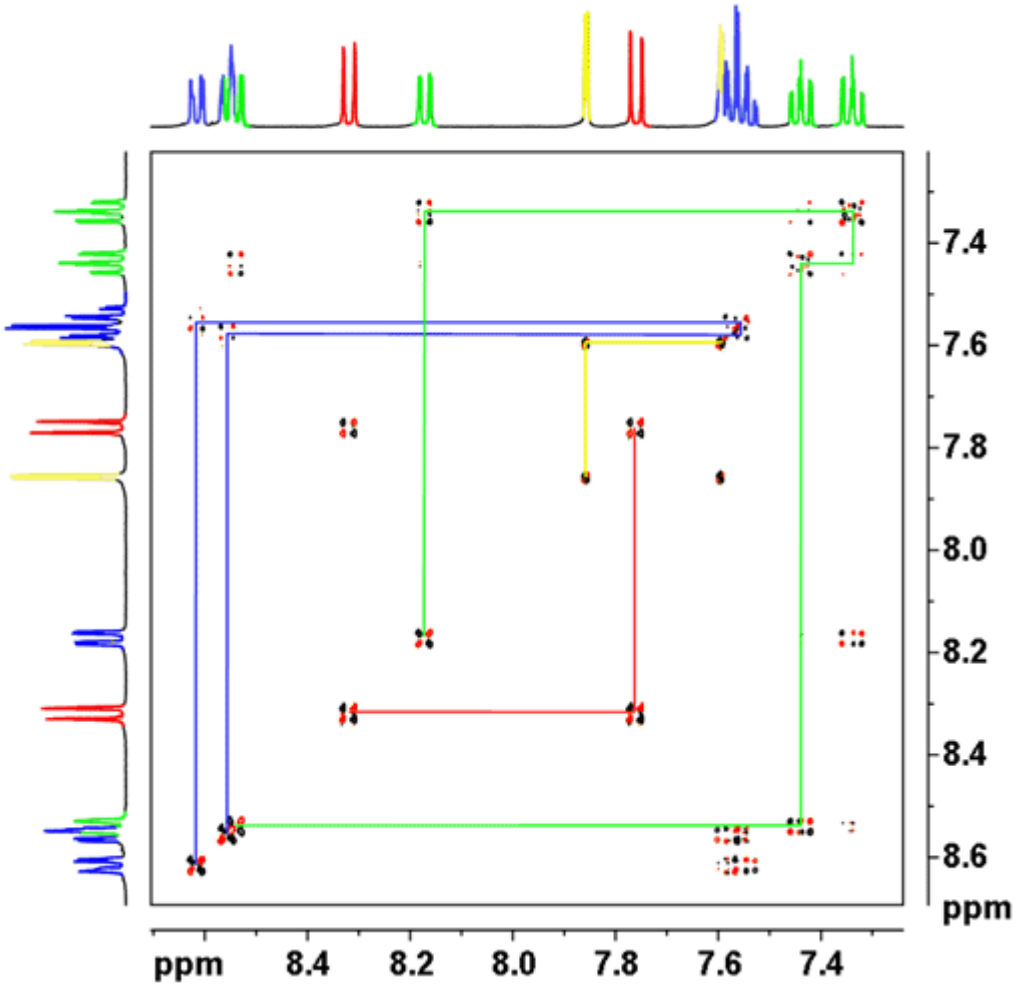

There are separated into four color-coded proton groups showing connectivity. Using horizontal and vertical lines, it is possible to separate each group and follow its connectivity. The **blue** group of four protons is connected in the order 8.62 ppm to 7.55 to 7.59 to 8.56, the **green** group of four protons in the order 8.54 to 7.34 to 7.44 to 8.17 and the **red** group or two protons, that correspond to H9 and 10 because they are the only group of two protons expected to have a three-bond coupling constant (8.9 Hz), are at 7.76 and 8.32 ppm. The **yellow** group of two protons correspond to H11 and 13 because the coupling constant is small (1.9 Hz) and consistent with a four bond correlation.

HMQC NMR Spectrum of of codeine

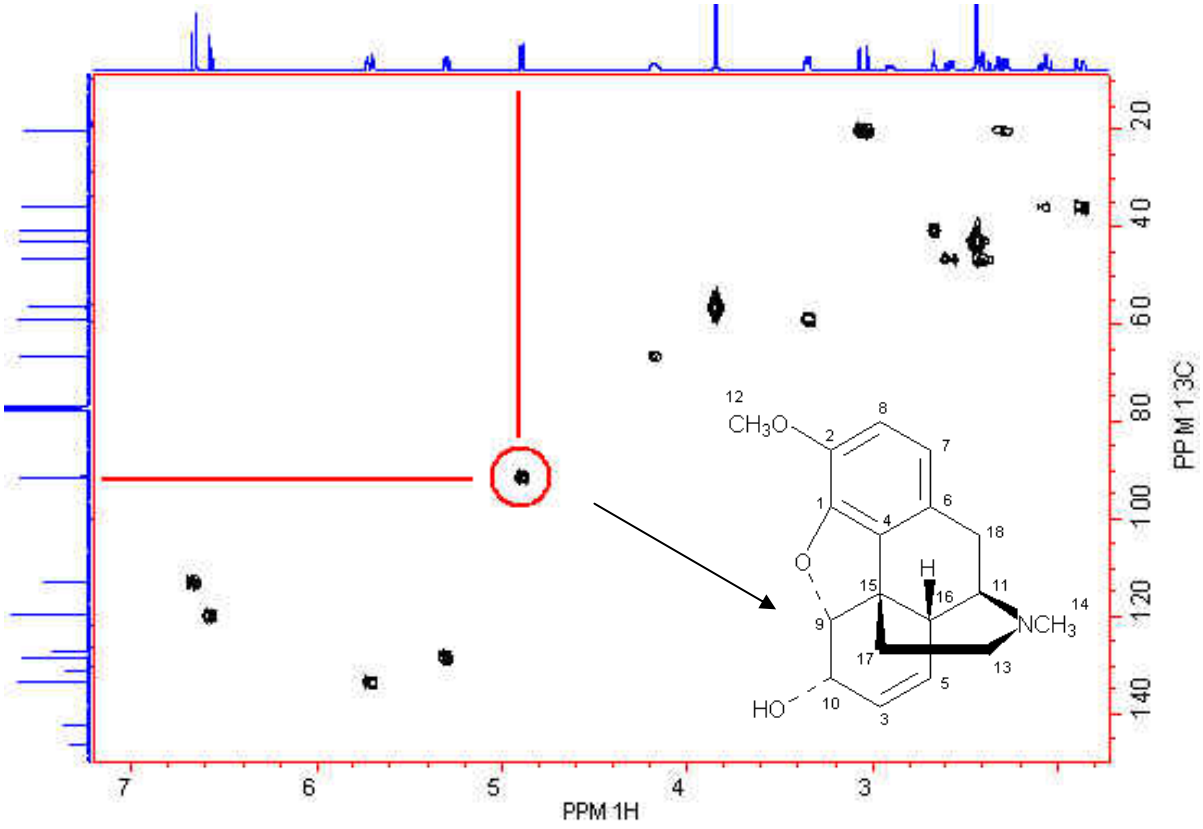

This is a 2D experiment used to correlate, or connect, 1H and 13C peaks for directly bonded C-H pairs. The coordinates of each peak seen in the contour plot are the 1H and 13C chemical shifts. This is helpful in making assignments by comparing 1H and 13C spectra.

This experiment yields the same information as the older "HETCOR" experiment, but is more sensitive, so can be done in less time and/or with less material. This is possible because in the HMQC experiment, the signal is detected by observing protons, rather than carbons, which is inherently more sensitive, and the relaxation time is shorter. This so-called "inverse detection" experiment is technically more difficult and is possible only on newer model spectrometers.

Contour plot of the HMQC spectrum. Because it is a heteronuclear experiment, the 2 axes are different, and the plot is not symmetrical. Unlike a COSY spectrum, there are no diagonal peaks.

HMQC NMR Spectrum of of codeine

Expanded aliphatic region:

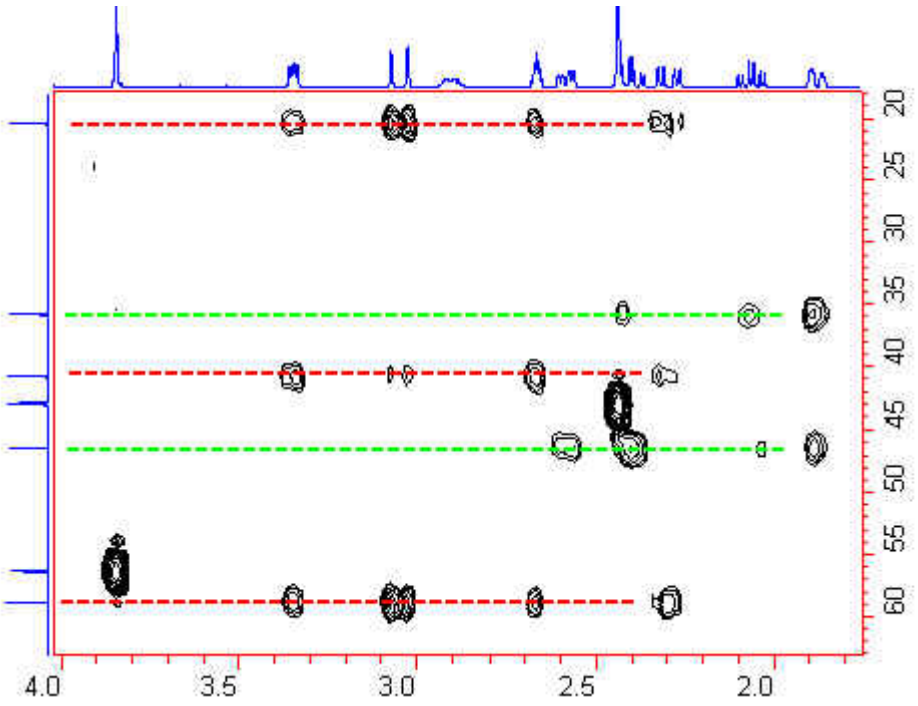

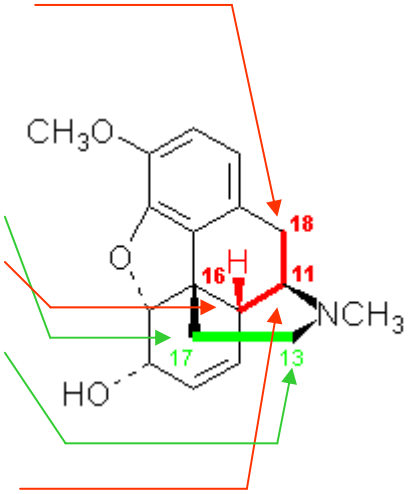

	^{13}C	^{1}H			
3	133	3 and 5	12	56	none
5	128	3 and 5	13	46	13, 13', 17, 17'
7	120	7 and 8	14	43	none
8	113	7 and 8	16	40	11, 16, 18, 18'
9	91	10			
10	66	9	17	36	13', 17, 17'
11	59	11, 16, 18, 18'	18	20	11, 16, 18, 18'

Table 6.4 *^1H Chemical Shifts of the Amino Acid Residues in the Random Coil Conformation*[a]

Residue	Chemical Shift (ppm)			
	NH	$C^{\alpha}H$	$C^{\beta}H$	Others
Gly	8.39	3.97		
Ala	8.25	4.35	1.39	
Val	8.44	4.18	2.13	$C^{\gamma}H_3$ 0.97, 0.94
Ile	8.19	4.23	1.90	$C^{\gamma}H_2$ 1.48, 1.19
				$C^{\gamma}H_3$ 0.95
				$C^{\delta}H_3$ 0.89
Leu	8.42	4.38	1.65, 1.65	$C^{\gamma}H$ 1.64
				$C^{\delta}H_3$ 0.94, 0.90
Pro (*trans*)		4.44	2.28, 2.02	$C^{\gamma}H_2$ 2.03, 2.03
				$C^{\delta}H_2$ 3.68, 3.65
Ser	8.38	4.50	3.88, 3.88	
Thr	8.24	4.35	4.22	$C^{\gamma}H_3$ 1.23
Cys	8.31	4.69	3.28, 2.96	
Asp	8.41	4.76	2.84, 2.75	
Glu	8.37	4.29	2.09, 1.97	$C^{\gamma}H_2$ 2.31, 2.28
Asn	8.75	4.75	2.83, 2.75	$N^{\gamma}H_2$ 7.59, 6.91
Gln	8.41	4.37	2.13, 2.01	$C^{\gamma}H_2$ 2.38, 2.38
				$N^{\delta}H_2$ 6.87, 7.59
Met	8.42	4.52	2.15, 2.01	$C^{\gamma}H_2$ 2.64, 2.64
				$C^{\epsilon}H_3$ 2.13
Lys	8.41	4.36	1.85, 1.76	$C^{\gamma}H_2$ 1.45, 1.45
				$C^{\delta}H_2$ 1.70, 1.70
				$C^{\epsilon}H_2$ 3.02, 3.02
				$N^{\epsilon}H_3^+$ 7.52
Arg	8.27	4.38	1.89, 1.79	$C^{\gamma}H_2$ 1.70, 1.70
				$C^{\delta}H_2$ 3.32, 3.32
				NH, NH_2^+ 7.17, 6.62
His	8.41	4.63	3.26, 3.20	$C^{\delta 2}H$ 7.14
				$C^{\epsilon 1}H$ 8.12
Phe	8.23	4.66	3.22, 2.99	$C^{\delta}H$ 7.30
				$C^{\epsilon}H$ 7.39
				$C^{\zeta}H$ 7.34
Tyr	8.18	4.60	3.13, 2.92	$C^{\delta}H$ 7.15
				$C^{\epsilon}H$ 6.86
Trp	8.09	4.70	3.32, 3.19	$C^{\delta 1}H$ 7.24
				$C^{\epsilon 3}H$ 7.65
				$C^{\zeta 3}H$ 7.17
				$C^{\eta}H$ 7.24
				$C^{\zeta 2}H$ 7.50
				$N^{\epsilon 1}H$ 10.22

[a] Measured at pH 7.0 and 35°C as peptide Xaa in tetrapeptide Gly-Gly-Xaa-Ala.

From K. Wüthrich, *NMR of Proteins and Nucleic Acids*, Wiley Interscience, New York, 1986.

Structural information

1. ***Interproton distances :***

   $NOE \propto R^{-6}$

2. ***Dihedral angles :***

   J-coupling and Karplus equations

3. ***Chemical Shift Index (CSI) :***

   Chemical shift of H^{α}, C^{α}, C^{β}, *CO*

4. ***Hydrogen bonding :***

   Amide proton exchange rates

NMR data with structural content :

Chemical shifts (H_α)

β-sheet *Random coil* *α-helix*

down field ←

$<\Delta\delta>$ ($\delta_{\beta\text{–sheet}} - \delta_{\beta\text{–sheet}} \approx 0.76$ ppm)

Coupling constants (^3J)

For L-amino acid :

$$^3J = 6.4\cos^2(\phi - 60^o) - 1.4\cos(\phi - 60^o) + 1.9$$

For D-amino acid :

$$^3J = 6.4\cos^2(\phi + 60^o) - 1.4\cos(\phi + 60^o) + 1.9$$

$^3J > 9$ Hz, $\phi = -120^o \pm 30^o$

$^3J < 4$ Hz, $\phi = -30^o \pm 40^o$

Structural information

1. Interproton distances :

$NOE \propto R^{-6}$

2. Dihedral angles :

J-coupling and Karplus equations

3. Chemical Shift Index (CSI) :

Chemical shift of H^{α}, C^{α}, C^{β}, CO

4. Hydrogen bonding :

Amide proton exchange rates

(a) COSY spectroscopy and its structural connectivities

(A) 1D ^{1}H spectrum

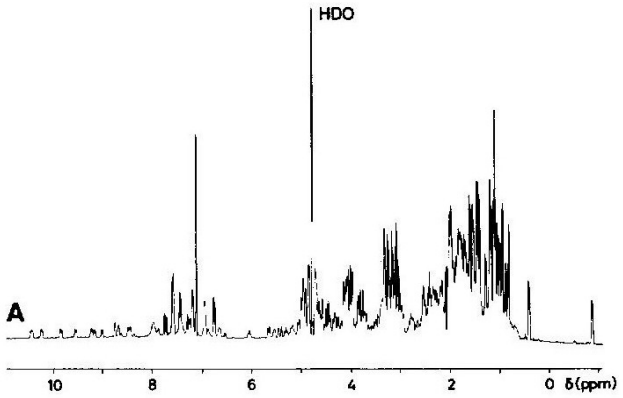

(B) 2D COSY spectrum

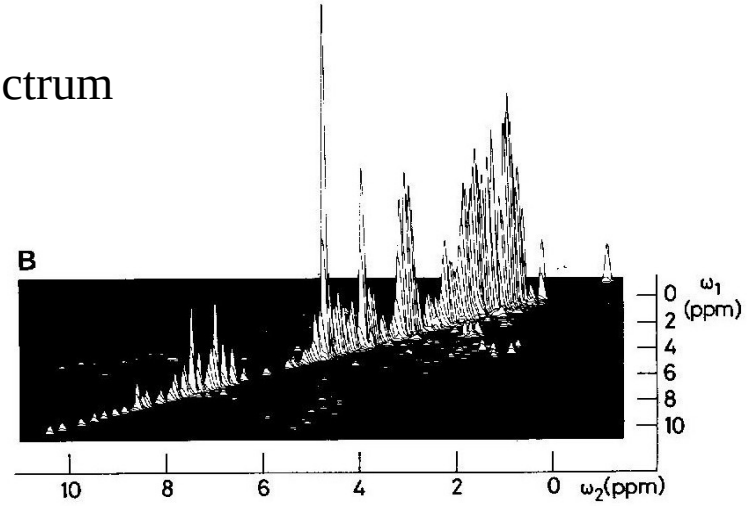

(C) Same as (b), contour plot

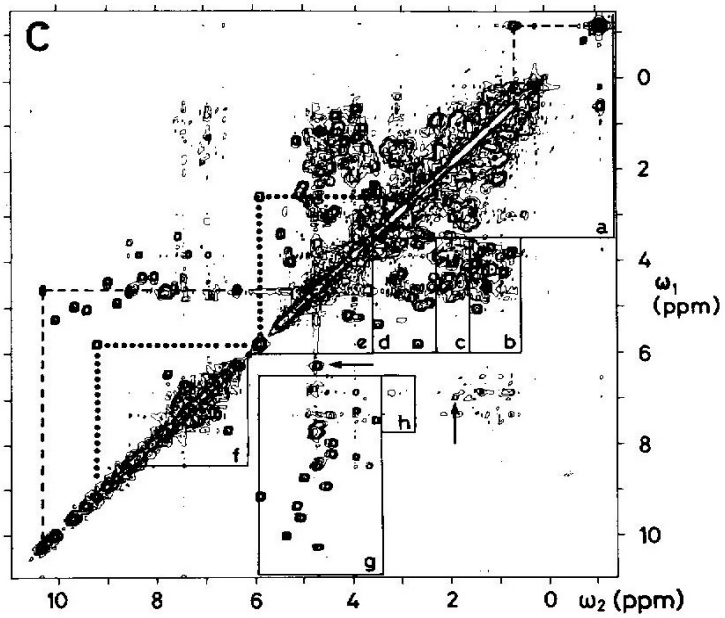

Figure 5.8. (*Continued*)

Figure 5.8. ^{1}H COSY of a freshly prepared D_2O solution of inhibitor *K* (0.01 *M*, pD 3.4, 25°C; 360 MHz; absolute value). *(A)* 1D ^{1}H NMR. *(B)* Stacked plot of COSY spectrum. *(C)* Contour plot of COSY spectrum. Above the diagonal, broken and dotted lines indicate how connectivities between distinct diagonal peaks are established via the cross peaks. Below the diagonal, solid lines define the regions a–h, which contain cross peaks between distinct proton types (see text). The arrows are explained in the text.

TABLE 2.4. Groups of Hydrogen Atoms in the Common Amino Acid Residues with Similar Random Coil ^1H Chemical Shifts[a]

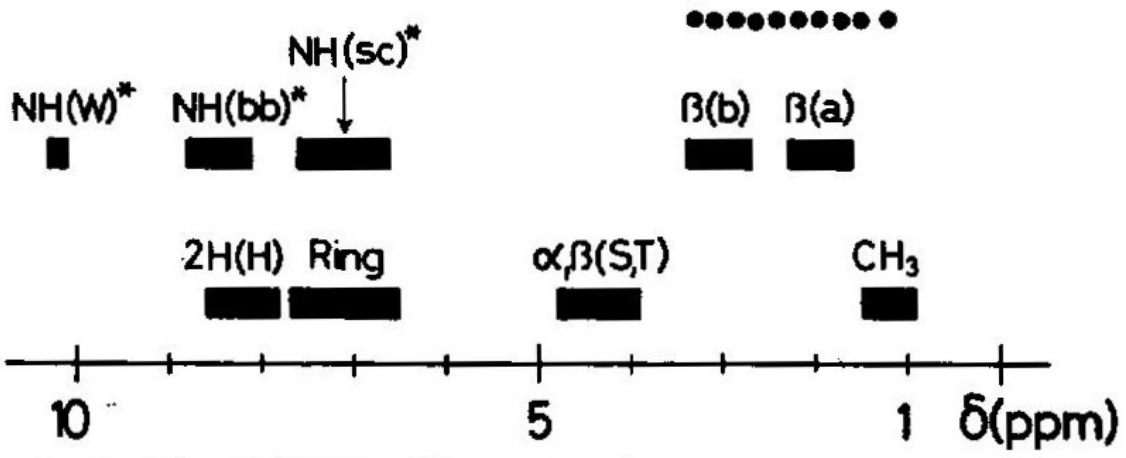

Code	δ (ppm)	Comments
CH_3	0.9-1.4	
β(a)	1.6-2.3	βH of V,I,L,E,Q,M,P,R,K
β(b)	2.7-3.3	βH of C,D,N,F,Y,H,W
••••	1.2-3.3	Other Aliphatic CH
α,β(S,T)	3.9-4.8	All αH, βH of S and T
Ring	6.5-7.7	Aromatic CH of F,Y,W; 4H of H
2H(H)	7.7-8.6	2H of H in the pH range 1-11
NH(sc)*	6.6-7.6	Side Chain NH of N,Q,K,R
NH(bb)*	8.1-8.8	Backbone NH
NH(W)*	10.2	Indole NH of W

[a] In model peptides the labile protons (identified by *) are only observed in H_2O solution. The singlet resonance of εCH_3 in Met is at 2.13 ppm (Table 2.3).

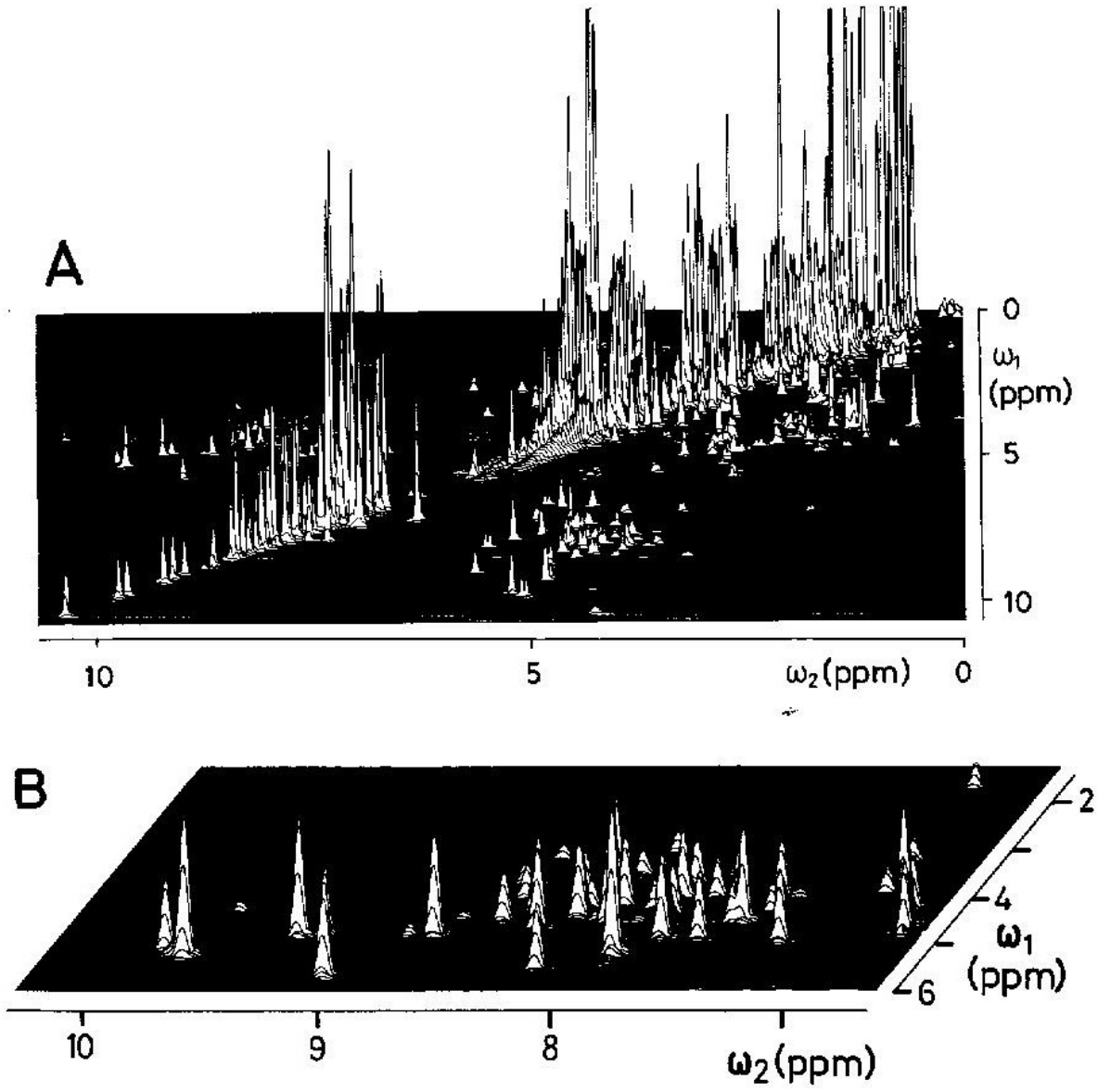

Figure 5.9. ^{1}H COSY spectrum of BPTI (0.02 *M*, H_2O, pH 4.6, 80°C; 500 MHz; absolute value). *(A)* Stacked plot of the entire spectrum. *(B)* Expanded presentation of the COSY fingerprint in the region (ω_1 = 1.8–6.0 ppm, ω_2 = 6.7–10.3 ppm) (from Wagner and Wüthrich, 1982a).

Eight areas containing different connectivities :

- a. All nonlabile, nonaromatic amino acid side chain protons except βH-γCH_3 of Thr, δH-δH of Pro, and βH-βH of Ser.
- b. αH-βCH_3 of Ala and βH-γCH_3 of Thr.
- c. αH-βH of Val, Ile, Leu, Glu, Gln, Met, Pro, Arg, and Lys.
- d. αH-βH of Cys, Asp, Asn, Phe, Tyr, His, and Trp.
- e. αH-αH of Gly, αH-βH of Thr, δH-δH of Pro, αH-βH and βH-βH of Ser.
- f. Aromatic ring protons, including the four-bond connectivity 2H-4H of His and side chain amide protons of Asn and Gln
- g. Backone NH-αH.
- h. δCH_3–εNH of Arg.

(A) 1D ^{1}H spectrum

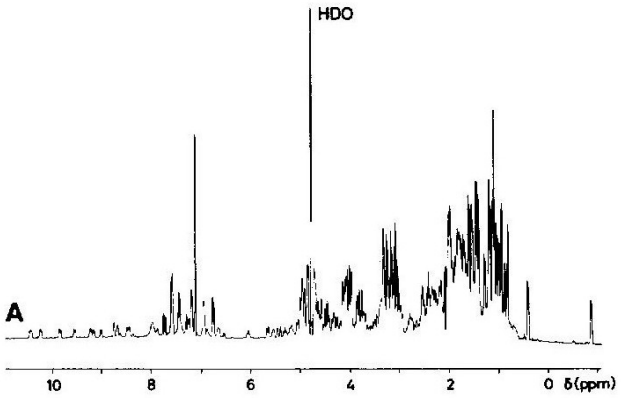

(B) 2D COSY spectrum

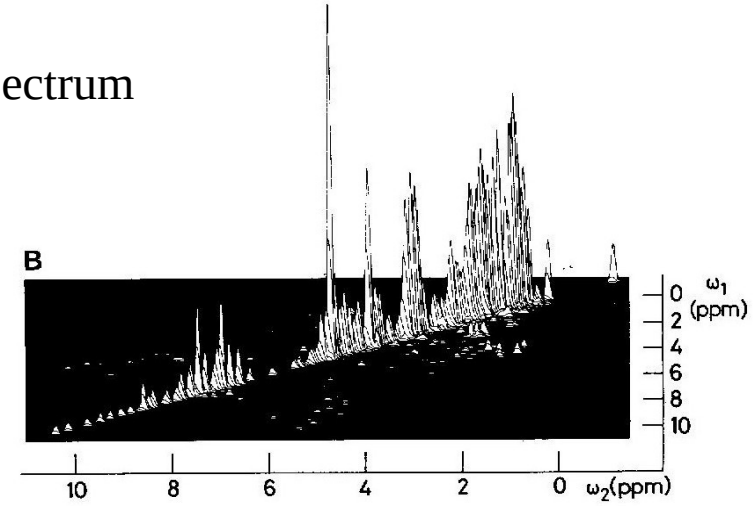

(C) Same as (b), contour plot

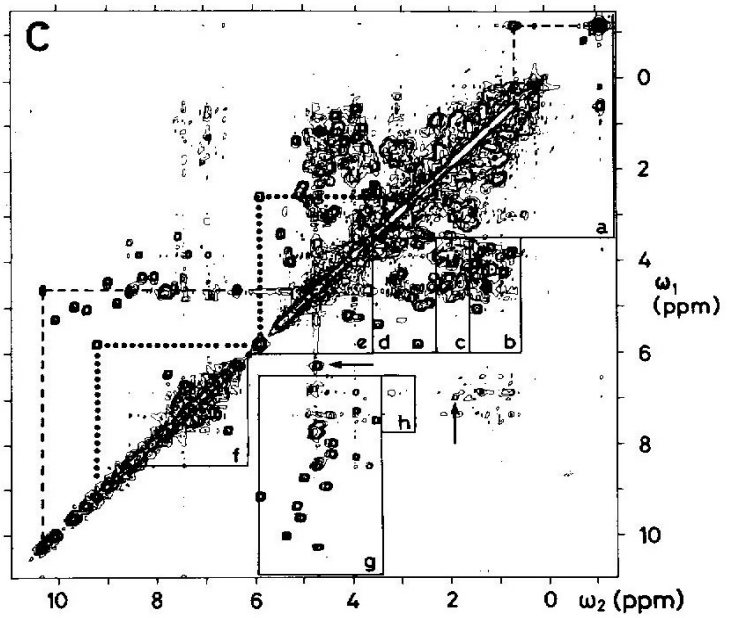

Figure 5.8. (*Continued*)

Figure 5.8. ^{1}H COSY of a freshly prepared D_2O solution of inhibitor *K* (0.01 *M*, pD 3.4, 25°C; 360 MHz; absolute value). *(A)* 1D ^{1}H NMR. *(B)* Stacked plot of COSY spectrum. *(C)* Contour plot of COSY spectrum. Above the diagonal, broken and dotted lines indicate how connectivities between distinct diagonal peaks are established via the cross peaks. Below the diagonal, solid lines define the regions a–h, which contain cross peaks between distinct proton types (see text). The arrows are explained in the text.

(b) NOE spectroscopy and its Applications to Macromolecules

Nuclear Overhauser Effects (NOE)

- The NOE phenomenon is intimately related to spin relaxation. Analogous to the spin relaxation T_1 and T_2, the NOE varies as a function of the product of the Larmor frequency ω_o, and the rotational correlation time τ_c.

- Considering a pair of closely spaced spins *i* and *j*, connected by the vector $\boldsymbol{r}_{ij}$, and located either in a small or large spherical molecule. As a result of the collisions with the surrounding solvent and solute molecules, the thermal motions of these spheres consist of a random walk, which includes both translational and rotational movements. The relevant quantity for dipole-dipole relaxation and NOE is the rotational tumbling of the vector $\boldsymbol{r}_{ij}$, and the concomitant time variation of the angle θ_{ij} between $\boldsymbol{r}_{ij}$ and $\mathbf{B}_o$.

- If the mobility of this vector is restricted to the overall rotations of the molecule, $\boldsymbol{r}_{ij}$ will change orientation much more frequently in the small molecule than in the large molecule. For spherical particles of radius ***a*** in a solvent of viscosity η, a correlation time characterizing the frequency range for these stochastic motions can be estimated as

$$\tau_c = 4\pi\eta\boldsymbol{a}^3/3kT$$

The NOE is a consequence of modulation of the dipole-dipole coupling between different nuclear spins by the Brownian motion of the molecules in solution, and the NOE intensity can be related to the distance r between pre-irradiated and observed spin by an equation of the general form

$$NOE \propto 1/r^6 * f(\tau_c)$$

$f(\tau_c)$ is a function of the *correlation time* τ_c, which accounts for the influence of the motional averaging process on the observed NOE. It seems to indicate that distance measurements with the use of NOE's should be straightforward, provided that $f(\tau_c)$ can be independently assessed. In reality, a number of fundamental and technical obstacles tend to render quantitative distance measurements difficult. Thus, in all NOE experiments, and in particular in NOESY, processes other than NOE's may also be manifested and can lead to falsification of apparent NOE intensities. Quite generally, because of the low sensitivity for observation of NOE's, the accuracy of integration of line intensities is also limited by low S/N. Fundamental difficulties can then also arise when trying to correlate experimental NOE intensities with distances, for example, because of spin diffusion or the prevalence of intramolecular mobility in macromolecules.

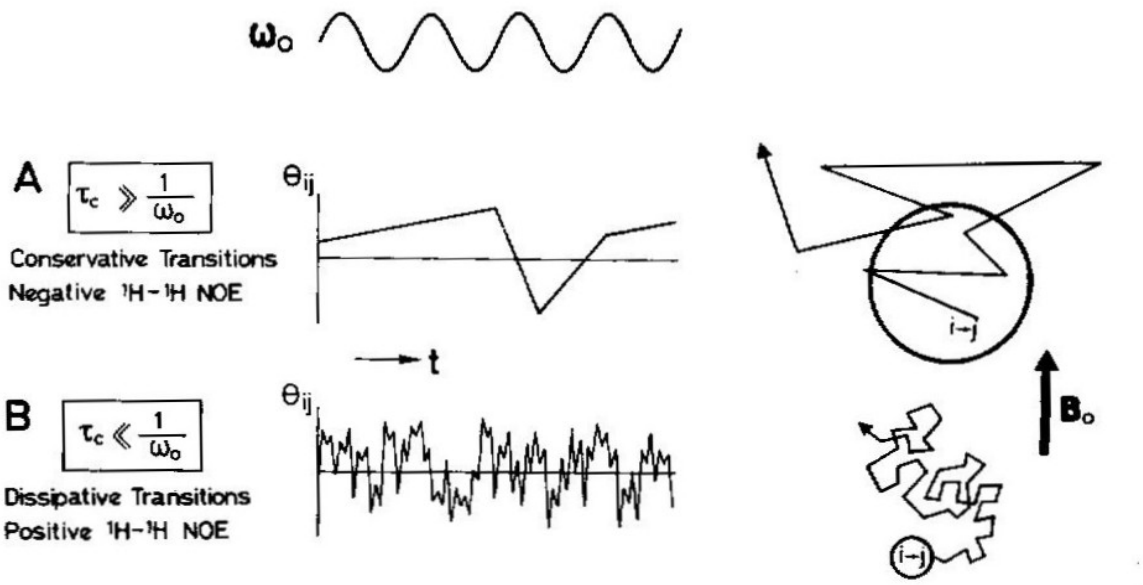

Figure 6.3. Brownian motion and NOE. The scheme considers two spins *i* and *j*, separated by the vector $\mathbf{r}_{ij}$ and located either in a large *(A)* or small *(B)* spherical molecule. θ_{ij} is the angle between $\mathbf{r}_{ij}$ and the magnetic field $\mathbf{B}_0$. The drawings on the right are a pictorial presentation of the rotational motions of $\mathbf{r}_{ij}$, where the length of the segments in the random walk indicates the time after which a distinct rotation state is again interrupted by collisions with other molecules. In the center, the variations of θ_{ij} are plotted versus time, and compared with the Larmor frequency of the spins ω_0.

In a small molecules, for example, a tripeptide or dinucleotide in aqueous solution, τ_c is short relative to ω_o^{-1} (at 500 MHz, $\omega^{-1} = 3 \times 10^{-10}$s). In this extreme motional situation, the frequency range covered by the rotational motion of r_{ij} includes ω_o^{-1} and $2\omega_o$, which enables dissipative transitions between different spin states. In contrast, for macromolecules τ_c is long relative to ω_o^{-1}, and the frequencies of the rotational motions are too low to allow efficient coupling with the nuclear spin transitions. Therefore, energy-conserving transitions of the type $\alpha_i\beta_i$-$\beta_i\alpha_j$ (cross relaxation) are favored.

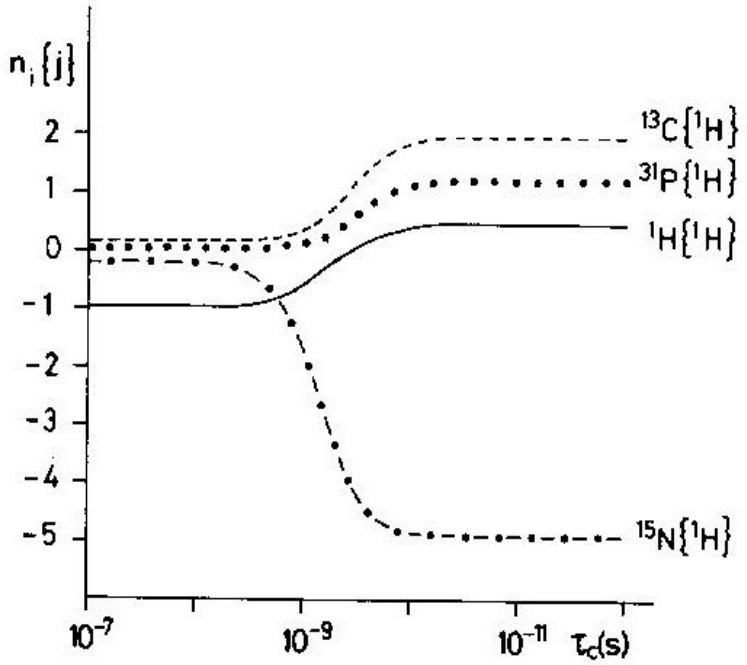

Figure 6.4. Plots of the maximum NOE (Eq. 6.3) versus log τ_c for ^1H, ^{13}C, ^{15}N, and ^{31}P interacting with ^1H. $\mathbf{B}_0 = 11.74$ T, preirradiation on ^1H, it is assumed that the relaxation is entirely by dipole–dipole coupling with the preirradiated proton.

- In the 1D experiments with relative line intensities I in the absence of NOE's, the line intensities with NOE then become

$$I = 1 + \gamma_i / 2\gamma_j \text{ (NOE factor)}$$

- The $^{1}H\{^{1}H\}$ NOE, which is of prime interest for conformational studies, is +0.5 for the extreme motional narrowing situation. For τ_c, longer than approximately 1 x 10^{-9} s it adopts a value of -1.0. For ^{13}C and ^{31}P {1H} the NOE factor is positive over the entire τ_c range and becomes very small for long τ_c. For ^{15}N {1H}, the NOE factor is negative throughout because of the negative value of γ. The NOE's 1H{31P}, 1H{13C}, and 1H{15N}, are very small and relatively of little practical importance in macromolecules.

- In general, mechanisms other than dipole-dipole coupling with the preirradiated spin contribute to the T_1 relaxation. If $T_{1d}(j)$ accounts for the dipolar relaxation between *i* and *j* and T_{10} for all other contribution to T_1 of spin i, NOE factor becomes

$$(\gamma_i/2\gamma_j)\,(T_{1d}(j)^{-1}/(T_{1d}(j)^{-1} + T_{10}^{-1})$$

- Accordingly, the NOE can be partially or completely ***quenched*** in the presence of alternative, efficient relaxation pathways, for example, through proximity of spin *i* to a paramagnetic center.

NOE and structural determination

- In principle, all hydrogen atoms of a protein form a single network of spins, coupled by the dipole-dipole interaction. Magnetization can be transferred from one spin to another not only directly but also indirectly via other spins in the vicinity-an effect called spin diffusion.

- The approximation of isolated spin pairs is only valid for short mixing time in the NOESY experiment. However, the mixing time cannot be made arbitrarily short because the intensity of a NOE is proportional to the mixing time.

- In practice, a compromise has to be made between the suppression of spin diffusion and sufficient cross-peak intensities, usually with mixing time in the range of 40-80 ms. Spin diffusion effects can also be included in the structure calculation by complete relaxation matrix refinement, care has to be taken not to bias the structure determination by over-interpretation of the data.

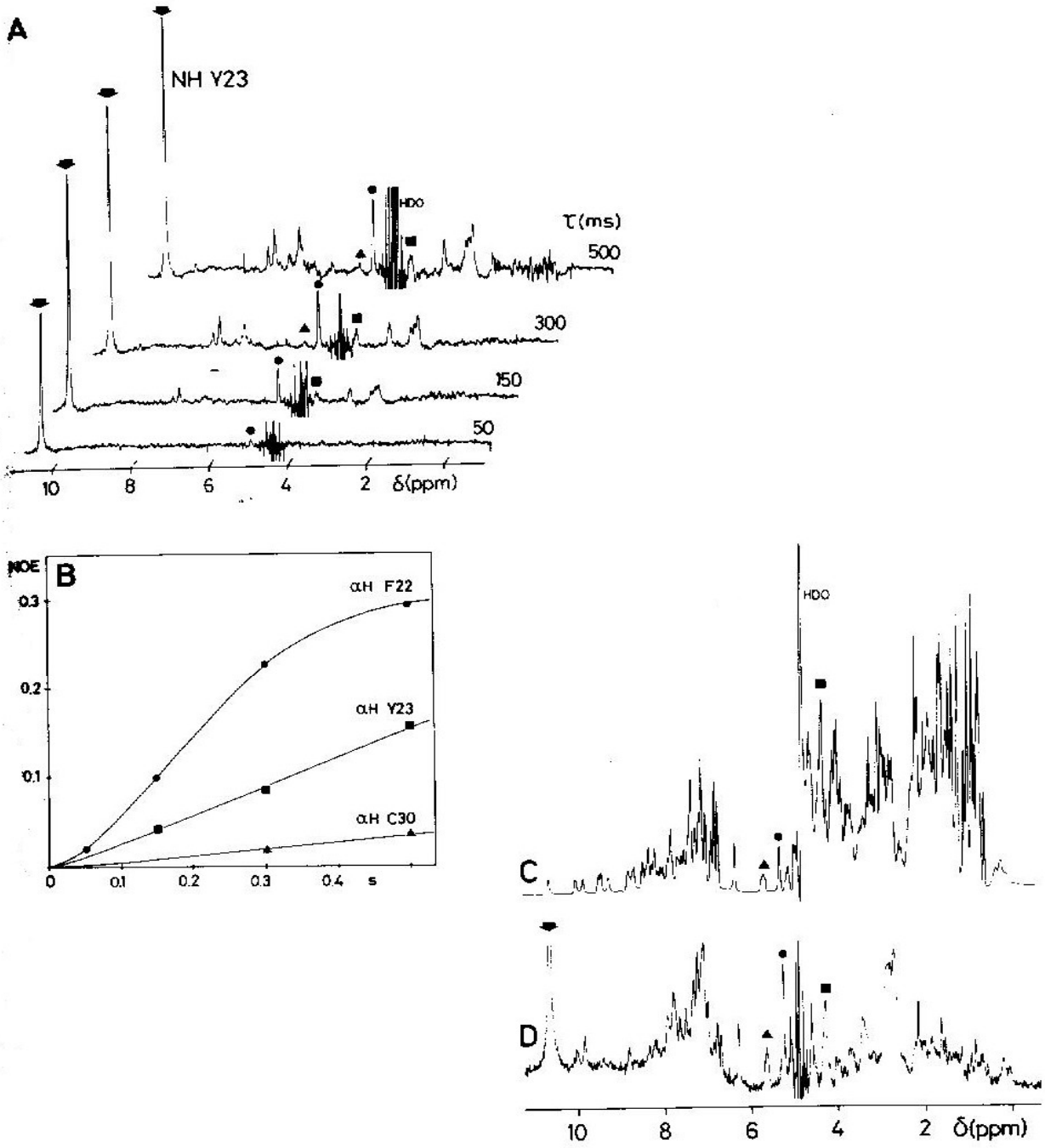

Figure 6.6. NOE buildup observed in 1D TOE difference spectra of a freshly prepared D_2O solution of BPTI (0.02 *M*, pD 4.5, 15°C; 360 MHz). *(A)* TOE difference spectra recorded with preirradiation on the lowest-field amide-proton line (arrow) during different intervals, τ. *(B)* Plots of NOE intensity versus τ for the three lines identified in *(A)*. *(C)* Normal 1D ^1H NMR spectrum. *(D)* Steady-state NOE difference spectrum obtained with selective preirradiation (arrow) during 4 s (from Dubs et al., 1979).

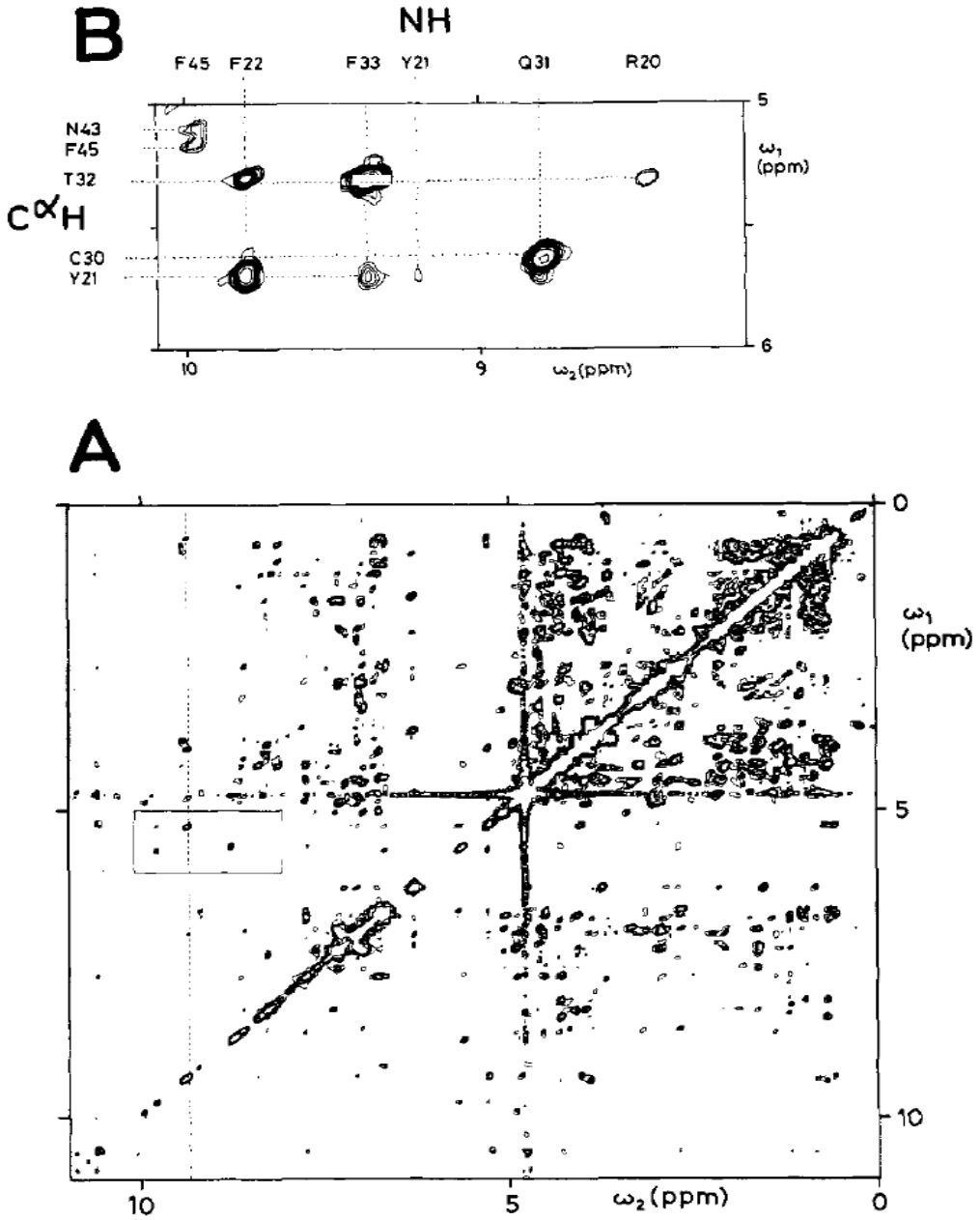

Figure 2. (A) Contour plot of a proton NOESY spectrum at 360 MHz of a 0.02 M solution of the basic pancreatic trypsin inhibitor (BPTI) in ^2H_2O, T = 24 °C, p^{2}H 4.6. The mixing time, τ_m, was 300 ms. The spectral width was 4000 Hz. The data set consisted of 512 points in both dimensions, 48 free induction decays were accumulated for each value of t_1, and the total accumulation time was 18 h. Before Fourier transformation the free induction decays were multiplied with a phase-shifted sine bell, sin $[\pi(t + t_0)/t_s]$, where t_s was the experimental acquisition time and t_0/t_s was 1/64.[30] After Fourier transformation the spectrum was further improved by triangular multiplication.[21] An absolute value plot is shown. The vertical and horizontal spikes at 4.8 ppm are due to the resonance of the residual solvent protons. The dotted, vertical line at 9.39 ppm inidicates where the cross sections of Figure 4 were taken. (B) Plot on an expanded scale of the spectral region from 5.0 to 6.0 ppm in ω_1 and 8.1 to 10.1 ppm in ω_2, which is indicated by a solid rectangle in spectrum A. Lower contour levels were plotted than in A, so that additional peaks appear in spectrum B. The cross peaks are identified by the IUPAC-IUB one-letter symbols for amino acids and the position in the amino acid sequence of the C$^\alpha$ and amide protons.

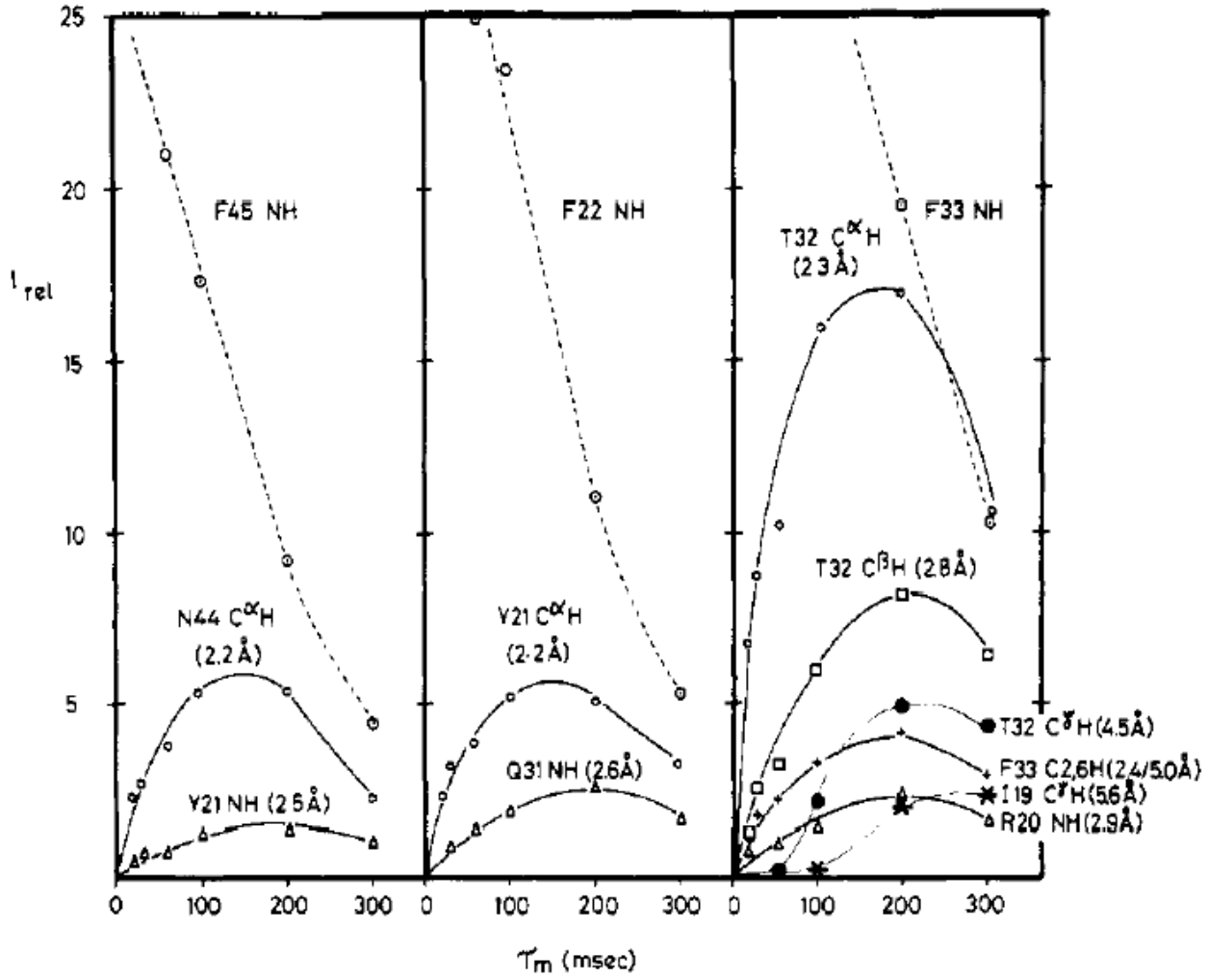

Figure 5. Dependence of the relative peak heights on the mixing time τ_m of cross-peaks in the NOESY spectrum of BPTI (Figures 2–4). The data were measured in cross sections through the diagonal peaks of the amide protons of Phe-45 at 9.98 ppm, Phe-22 at 9.82 ppm, and Phe-33 at 9.39 ppm (Figure 4). The broken lines show the decay of the intensity of the diagonal peaks and are identified by the assignment of these peaks. The time course of the NOE's for protons located near the proton corresponding to the diagonal peak is indicated by the solid curves which connect the experimental points. Resonance assignments and, in parentheses, the proton–proton distances in the X-ray structure[27] are added for each curve, whereby an average proton position was assumed for methyl groups. Two cases of second-order NOE's are clearly evidenced in the diagram on the right, i.e., for Thr-32 $C^{\gamma}H_3$ and Ile-19 $C^{\gamma}H_3$ (see also Figure 4).

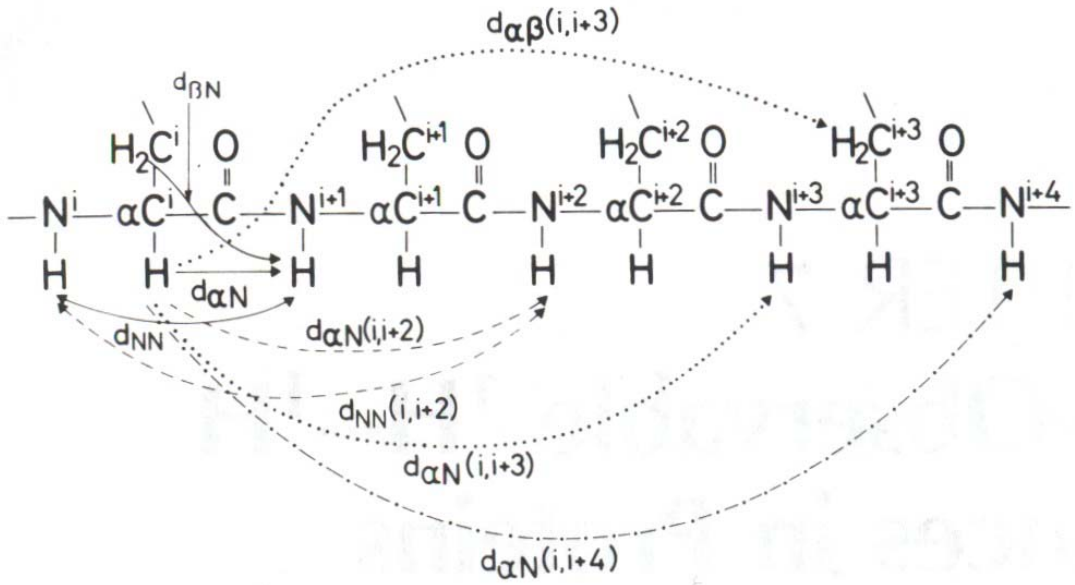

Figure 7.1. Selected sequential and medium-range $^1H-^1H$ distances in polypeptide chains (from Wüthrich et al., 1984a).

^1H-^1H distance in Proteins

- Notation for ^1H-^1H distances

$$d_{\alpha N}(i,j) \equiv d(\alpha H_i, NH_j)$$

$$d_{NN}(i,j) \equiv d(NH_i, NH_j)$$

$$d_{\beta N}(i,j) \equiv \min\{d(\beta H_i, NH_j)\}$$

$$d_{\alpha\alpha}(i,j) \equiv d(\alpha H_i, \alpha H_j)$$

$$d_{\alpha\beta}(i,j) \equiv \min\{d(\alpha H_i, \beta H_j)\}$$

- ***Sequential distances*** are those between backbone protons or between a backbone proton and a β proton in residues that are nearest neighbors in the sequence. For simplicity, the indices i and j are omitted for the sequential distance; for example,

$$d_{\alpha N}(i,i+1) \equiv d_{\alpha N}$$

$$\text{and } d_{NN}(i,i+1) \equiv d_{NN}$$

- ***Medium-range*** distances are all non-sequential inter-residue distances between backbone protons or between a backbone proton and a β proton within a segment of five consecutive residues.

- ***Long-range backbone*** distances are between backbone protons in residues that at least six positions apart in the sequence, that is $|i-j| \geq 5$. All other inter-residue distances are referred to as long-range distances.

Short sequential and medium-range ^{1}H-^{1}H distances, vicinal coupling constants, and amide hydrogen exchange rates

Parameter	*α-helix*	*3_{10}-helix*	*β*	*β_P*
$d_{\alpha N(i,i)}$	2.6	2.6	2.8	2.8
$d_{\alpha N(i,i+1)}$	3.5	3.4	2.2	2.2
$d_{\alpha N(i,i+2)}$	4.4	3.8		
$d_{\alpha N(i,i+3)}$	3.4	3.3		
$d_{\alpha N(i,i+4)}$	4.2	(>4.5)		
$d_{NN(i,i+1)}$	2.8	2.6	4.3	4.2
$d_{NN(i,i+2)}$	4.2	4.1		
$d_{\beta N(i,i+1)}$	2.5-4.1	2.9-4.4	3.2-4.5	3.7-4.7
$d_{\alpha\beta(i,i+3)}$	2.5-4.1	3.1-5.1		
$d_{\alpha\alpha(i,j)}$			2.3	4.8
$d_{\alpha N(i,j)}$			3.2	3.0
$d_{NN(i,j)}$			3.3	4.0
$^{3}J_{HN}$ (Hz)	(≦4)	(≦4)	(≧9)	(≧9)
NH exchange rate	slow	slow	slow	slow

***$d_{\alpha\alpha(i,j)}$, $d_{\alpha N(i,j)}$, and $d_{NN(i,j)}$ refer to interstrand distances.

***The first four residues in the α-helix and the first three residues in the 3_{10}-helix will have fast amide proton exchange rates.

***Every second residue in the flanking strand will have slow amide proton exchange rates.

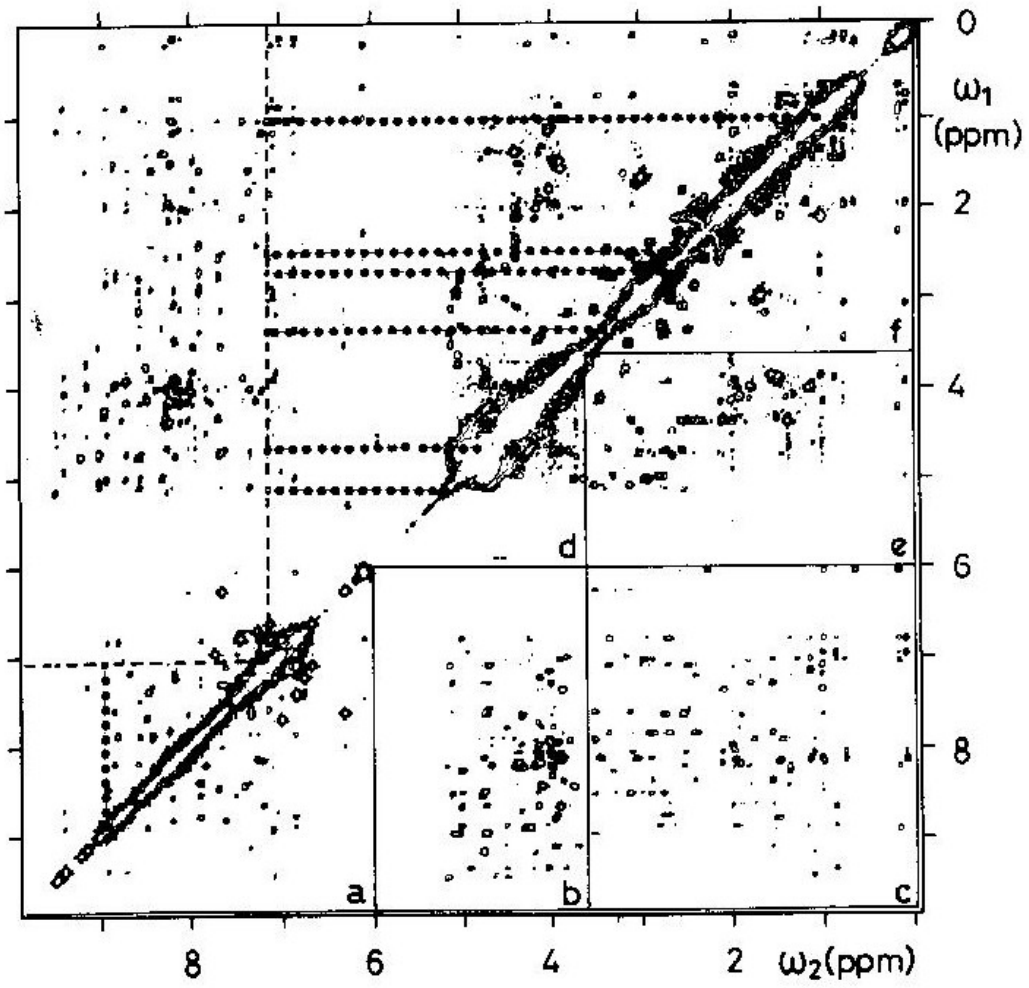

Figure 6.8. Protein ^{1}H NOESY spectrum (same as Fig. 5.37, symmetrized). Above the diagonal, broken and dotted lines indicate how connectivities between diagonal peaks are established via the cross peaks. Below the diagonal, the spectrum is divided into six regions a–f, which contain cross peaks between distinct proton types (see text).

Six areas containing different connectivities :

- a. NH; aromatics-NH; aromatics
- b. NH; aromatics-αH; δH of Pro; βH of Ser and Thr
- c. NH; aromatics-aliphatic side chains
- d. αH; δH of Pro; βH of Ser and Thr-αH; δH of Pro; βH of Ser and Thr
- e. αH; δH of Pro; βH of Ser and Thr-aliphatic side chains
- f. Aliphatic side chains-aliphatic side chains

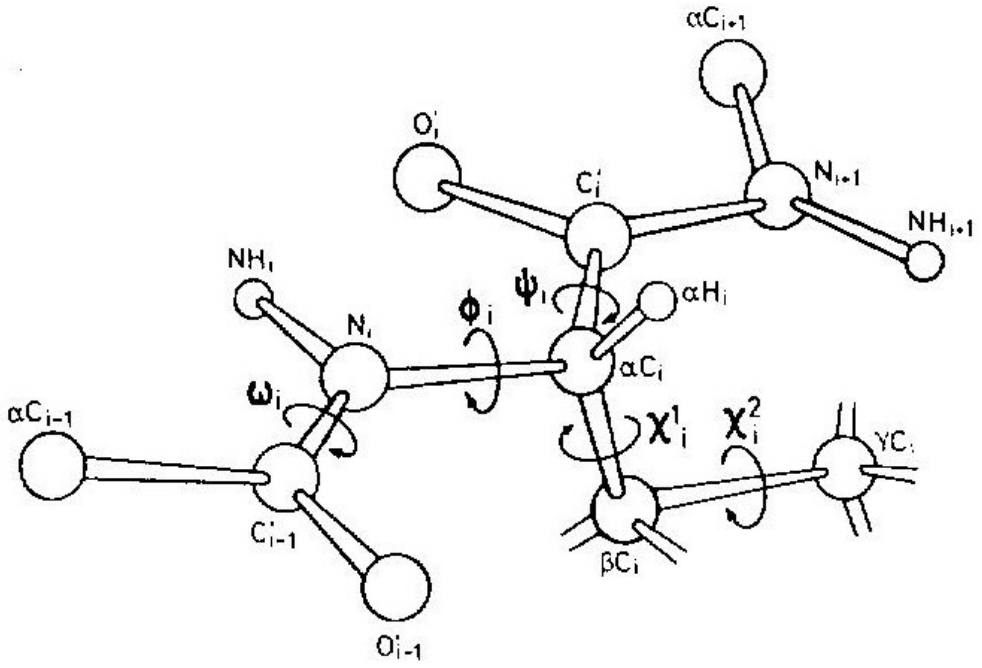

Figure 7.2. Standard nomenclature for the atoms and the torsion angles along a polypeptide chain (IUPAC–IUB Commission on Biochemical Nomenclature, 1970).

- The distances between vicinal protons vary between approximately 2.15 and 2.90 A, and the exact values are determined by the intervening torsion angle. For instance, the distances $d_{\alpha N}(i,i)$ and $d_{\alpha\beta}(i,i)$ are related with ϕ_i and χ_i, respectively.

Torsion angles for regular polypeptide conformations

Structure	Torsion angle (degree)	
	ϕ	ψ
Hypothetical fully extended	+180 ($\equiv$ -180)	+180
Anti-parallel β sheet	-139	+135
Parallel β sheet	-119	+113
Right-handed α-helix	-57	-47
Left-handed α-helix	~+60	~+60
3_{10} helix	-49	-26
Helix	-57	-70

(c) Distance d_{NN} and torsion angles relationship – Ramachandran plot

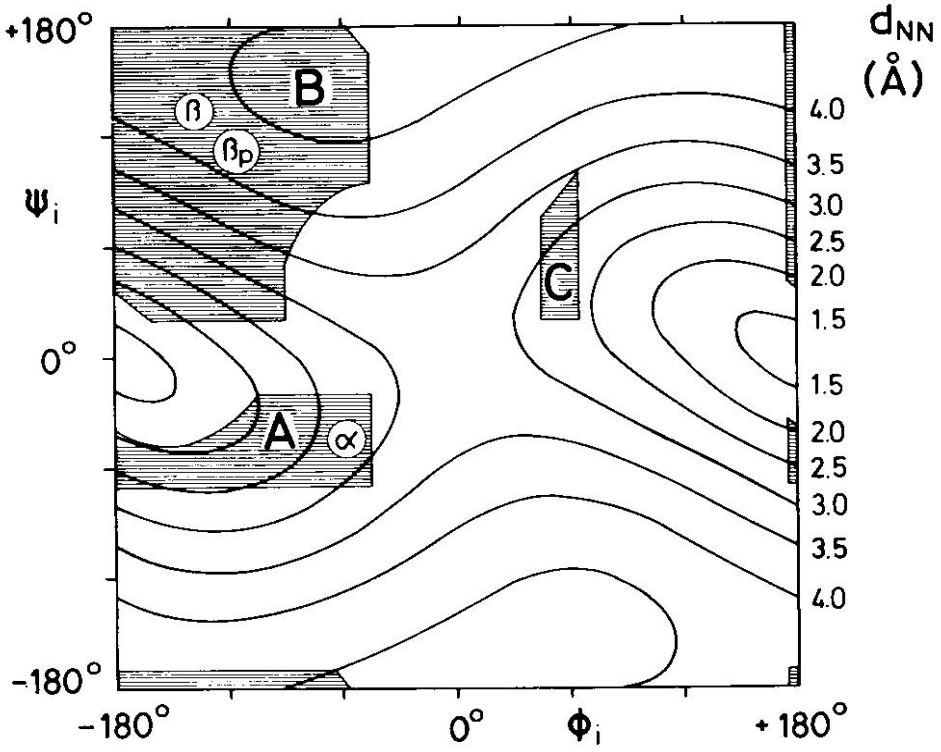

Figure 7.7. Sequential distance d_{NN} in the ϕ_i–ψ_i plane; solid contour lines represent fixed values of d_{NN} as indicated on the right. The shaded areas A, B, and C are sterically allowed for an alanyl dipeptide (Ramachandran and Sasisekharan, 1968). α, β, and β_p indicate the ϕ_i–ψ_i combinations for the regular α helix, antiparallel β sheet, and parallel β sheet (from Billeter et al., 1982).

Short (< 4.5 A) Sequential and Medium-Range ^1H-^1H Distances in Polypeptide Secondary Structures

Distance	α-helix	3_{10}-helix	β	β_P	turn I[a]	turn II[a]
					3.4	2.2
$d_{\alpha N}(i,i+1)$	3.5	3.4	2.2	2.2	3.2	3.2
$d_{\alpha N}(i,i+2)$	4.4	3.8			3.6	3.3
$d_{\alpha N}(i,i+3)$	3.4	3.3			3.1-4.2	3.8-4.7
$d_{\alpha N}(i,i+4)$	4.2					
					2.6	4.5
d_{NN}	2.8	2.6	4.3	4.3	2.4	2.4
$d_{NN}(i,i+2)$	4.2	4.1			3.8	4.3
					2.9-4.4	3.6-4.6
$d_{\beta N}$[b]	2.5-4.1	2.9-4.4	3.2-4.5	3.7-4.7	3.6-4.6	3.6-4.6
$d_{\alpha\beta}(i,i+3)$[b]	2.5-4.4	3.1-5.1				

[a] For the turns, the first of two numbers applies to the distance between residues 2 and 3, the second to that between residues 3 and 4. The range between indicated for $d_{\alpha N}(i,i+3)$ corresponds to the distances adopted if ψ_1 is varied between -180° and 180°.

[b] The ranges given correspond to the distances adopted by a β-methine proton if χ^1 is varied between -180° and 180°.

Other NMR data for structure determination

- NOEs and scalar coupling constants are the NMR data that most directly provide structural information. Additional NMR parameters that are sometimes used in structure determination include hydrogen exchange data and chemical shifts, in particular $^{13}C_{\alpha}$. Slow hydrogen exchange indicates that an amide proton is involved in a hydrogen bond.

- It was recognized that the deviations of $^{13}C_{\alpha}$ (and, to some extent $^{13}C_{\beta}$) chemical shifts from their random coil values are correlated with the local backbone conformation: $^{13}C_{\alpha}$ chemical shifts larger than the random coil values tend to occur for amino acid residues in α-helical conformation, whereas deviations toward smaller values are observed for residues in b-sheet conformation. Such information can be included in a structure calculation by restricting the local conformation for a residue to the α-helical or β-sheet region of the Ramachandran plot, although care should be applied because the correlation between chemical shift deviation and structure is not perfect.

(d) Chemical shifts and secondary structure

α-^{13}C Chemical Shift Values Categorized According to Secondary Structural Assignment[a-d]

Residue[e] type	Helix (DDS)	β Strand (DDS)	Coil (DDS)	Spera (1991) (TSP)	Richarz (1978) (dioxane)
Ala (112)	54.7	50.3	52.4	52.3	50.8
Cys (27)	60.0	56.1	56.0	56.9	53.9
Asp (97)	56.7	52.3	54.2	54.0	52.7
Glu (132)	59.2	54.6	56.4	56.4	55.4
Phe (74)	60.7	56.1	57.8	58.0	56.2
Gly (121)	46.5	44.6	45.4	45.1	43.9
His (24)	58.5	55.1	55.5	-	53.6
Ile (86)	64.7	59.8	61.3	61.3	59.6
Lys (138)	59.3	54.8	56.6	56.5	54.6
Leu (113)	57.8	53.9	55.7	55.1	53.8
Met (36)	57.8	54.1	55.7	55.3	54.0
Asn (71)	55.8	51.9	55.7	52.8	51.5
Pro (53)	65.9	62.5	53.2	63.1	61.9
Gln (61)	58.7	54.0	55.8	56.1	54.1
Arg (65)	59.4	54.8	56.7	56.1	54.6
Ser (88)	61.2	56.8	58.2	58.2	56.6
Thr (105)	65.8	60.6	62.0	62.1	60.1
Val (114)	65.7	60.0	62.3	62.3	60.7
Trp (12)	59.0	55.2	56.4	57.7	55.7
Tyr (43)	60.7	56.6	57.5	58.1	56.3

[a] Experimentally measured random coil values from Richarz and Wuthrich and from Spear and Bax are included for comparison. Data are given in ppm.

[b] The compounds (DDS, TMS, or dioxane) used in referencing the data are shown at the top of each column.

[c] To adjust DSS values to “old” dioxane standard, substract 1.5 ppm.

[d] To adjust DSS values to TSP, add 0.1 ppm.

[e] Total number of residues observed is given in parentheses. The data cover a grand total of 1572 amino acids.

Random Coil Chemical Shifts for Backbone Atoms in Peptides and Proteins[a]

Residue	α-^{1}H[b]	N-^{1}H	2-^{13}C	1-^{13}C	^{15}N
Ala	4.33	8.15	52.2	177.6	122.5
Cys	4.54	8.23	56.8	174.6	118.0
Asp	4.71	8.37	53.9	176.8	120.6
Glu	4.33	8.36	56.3	176.6	121.3
Phe	4.63	8.30	57.9	175.9	120.9
Gly	3.96	8.29	45.0	173.6	108.9
His	4.60	8.28	55.5	174.9	119.1
Ile	4.17	8.21	61.2	176.5	123.2
Lys	4.33	8.25	56.4	176.5	121.5
Leu	4.32	8.23	55.0	176.9	121.8
Met	4.48	8.29	55.2	176.3	120.5
Asn	4.74	8.38	52.7	175.6	119.5
Pro	4.42	-	63.0	176.0	128.1
Gln	4.33	8.27	56.0	175.6	120.3
Arg	4.35	8.27	56.0	176.6	120.8
Ser	4.47	8.31	58.1	174.4	116.7
Thr	4.35	8.24	62.0	174.8	114.2
Val	4.12	8.19	62.2	176.0	121.1
Trp	4.66	8.18	57.6	173.6	120.5
Tyr	4.55	8.28	58.0	175.9	122.0

[a] Proton and carbon shifts are relative to DDS, nitrogen shifts are relative to NH_3. Data are given in ppm.

[b] α-^{1}H shifts were measured using the hexapeptide GGXAGG in 1M urea at 25C.

Wishart and Skyes, Methods Enzymol. (1994), **239** ,363-392.

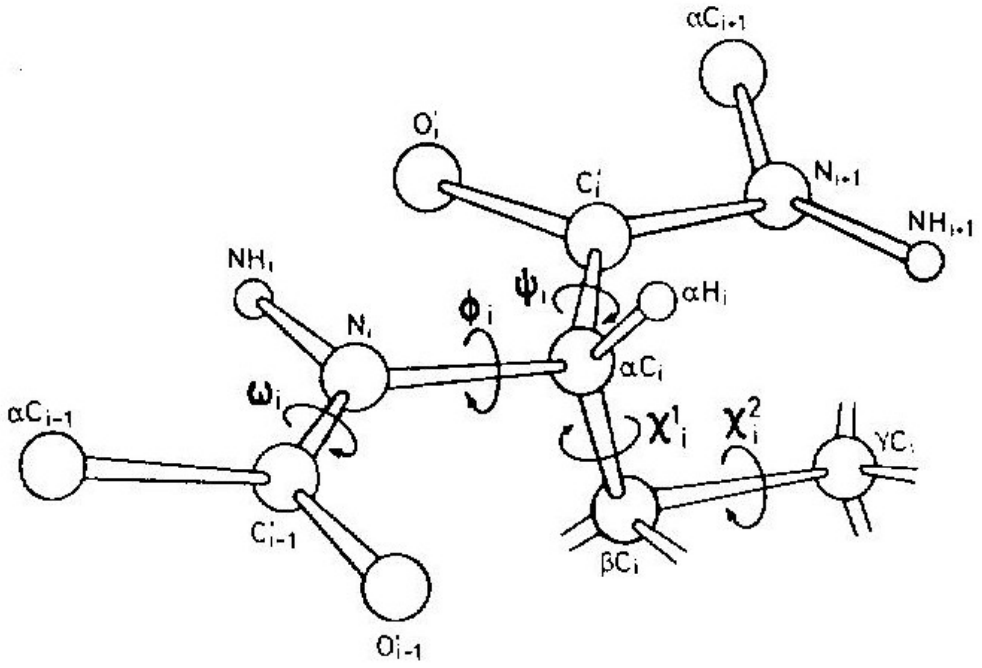

Figure 7.2. Standard nomenclature for the atoms and the torsion angles along a polypeptide chain (IUPAC–IUB Commission on Biochemical Nomenclature, 1970).

- The distances between vicinal protons vary between approximately 2.15 and 2.90 A, and the exact values are determined by the intervening torsion angle. For instance, the distances $d_{\alpha N}(i,i)$ and $d_{\alpha\beta}(i,i)$ are related with ϕ_i and χ_i, respectively.

Karplus relations

- For structure determination of proteins the most important Karplus relations are

  - $^3J_{NH\alpha} = 6.4\cos^2\theta - 1.4\cos\theta + 1.9$
  - $^3J_{\alpha\beta} = 9.5\cos^2\theta - 1.6\cos\theta + 1.8$
  - $^3J_{N\beta} = -4.4\cos^2\theta + 1.2\cos\theta + 0.1$
  - $^3J_{C'\beta} = 8.0\cos^2\theta - 2.0\cos\theta$

Structural information

1. ***Interproton distances :***

   $NOE \propto R^{-6}$

2. ***Dihedral angles :***

   J-coupling and Karplus equations

3. ***Chemical Shift Index (CSI) :***

   Chemical shift of H^{α}, C^{α}, C^{β}, *CO*

4. ***Hydrogen bonding :***

   Amide proton exchange rates

Resonance assignment strategies for small proteins

1. ***Spin system identification :***
   DQF-COSY and TOCSY experiments
2. ***Sequence-specific assignment :***
   NOESY experiment

For protein < 10 kDa, 2D homonuclear experiments may be sufficient for resolving overlapping NMR resonances.

DQF-COSY : Double-Quantum Filter-Correlation Spectroscopy

TOCSY : Total Correlation Spectroscopy

NOESY : Nuclear Overhauser Effect Spectroscopy

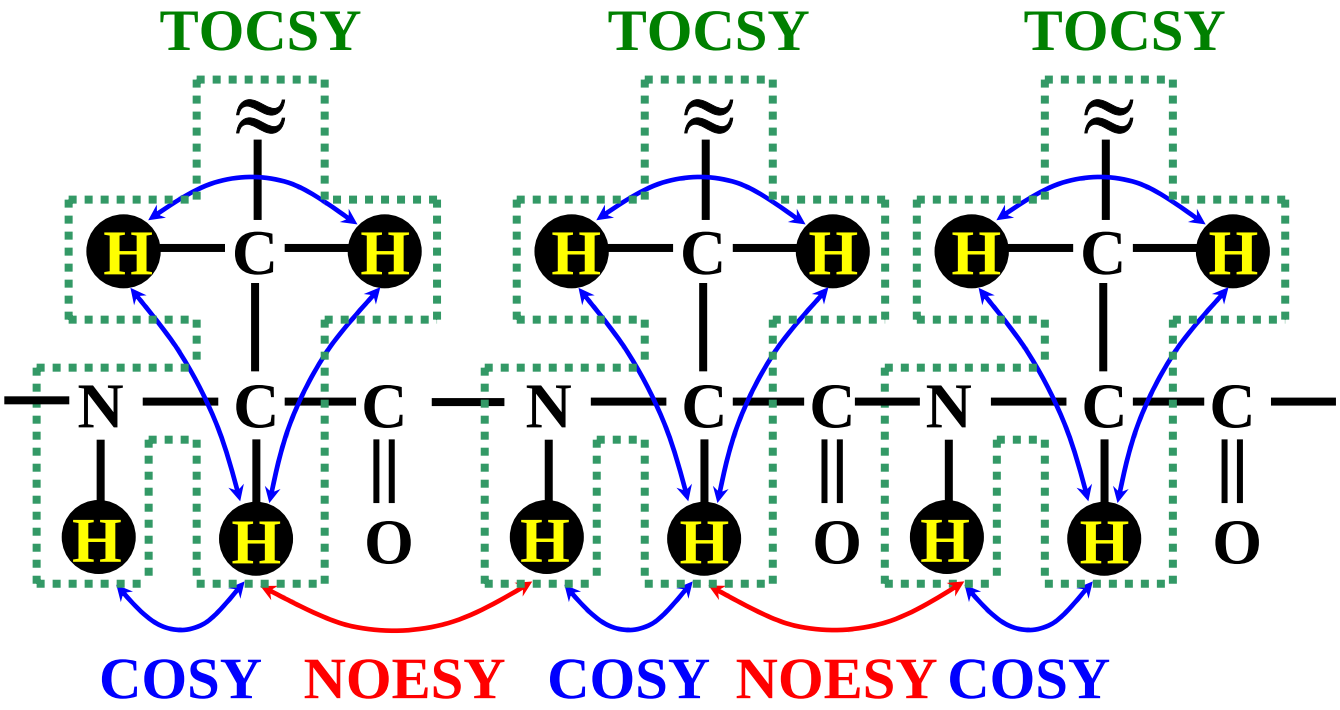
TOCSY
TOCSY
TOCSY
≈
H
C
H
N
C
C
H
H
O
COSY
NOESY
COSY
NOESY
COSY

Groups of Hydrogen Atoms in the Common Amino Acid Residues with similar Random Coil ^1H Chemical Shifts[a].

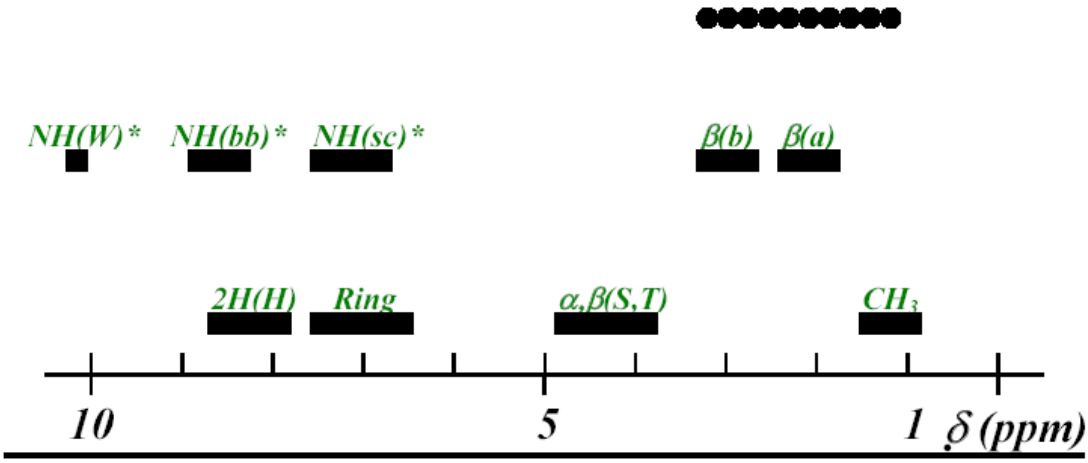

Code	(ppm)	Comments
CH_3	0.9-1.4	
β(a)	1.6-2.3	βH of V, I, L, E, Q, M, P, R, K
β(b)	2.7-3.3	βH of C, D, N, F, Y, H, W
●●●●●●●	1.2-3.3	Other aliphatic CH
α,β (S,T)	3.9-4.8	All αH, βH of S and T
Ring	6.5-7.7	Aromatic CH of F, Y, W; 4H of H
2H(H)	7.7-8.6	2H of H in the pH range 1-11
NH(sc)*	6.6-7.6	Side chain NH of N, Q, K, R
NH(bb)*	8.1-8.8	Backbone NH
NH(W)*	10.2	Indole NH of W

[a]In model peptides the labile protons (identified by *) are only observed in H_2O solution.
The singlet resonance of εCH_3 in Met is at 2.13 ppm.

CIEAKLTDTTTES (13-mer peptide)

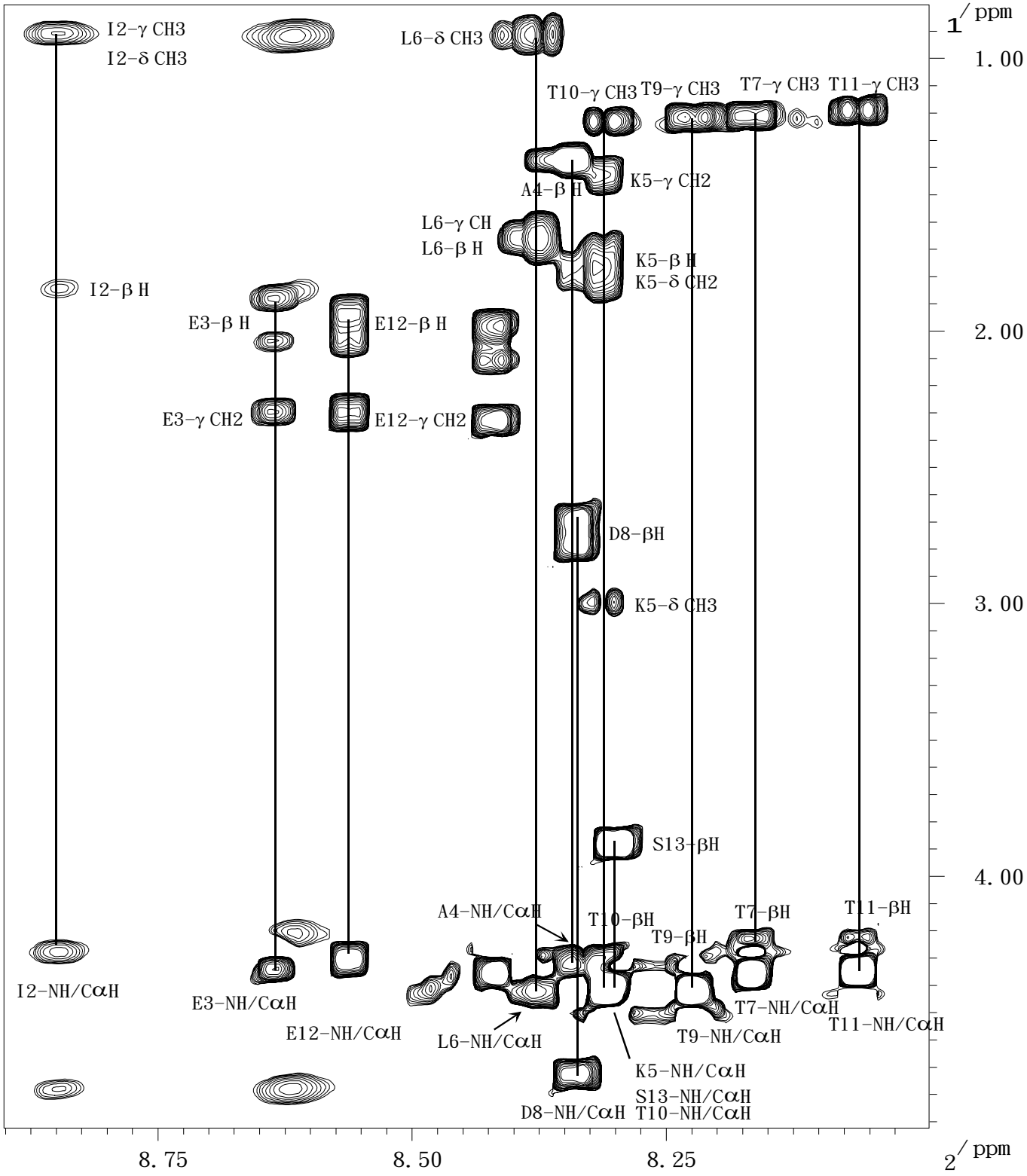

Fig 5-19 胜肽Den7 TOCSY光譜圖, pH 5.0的50mM phosphate buffer 300 μL及30 μL D2O,298K的條件下測得

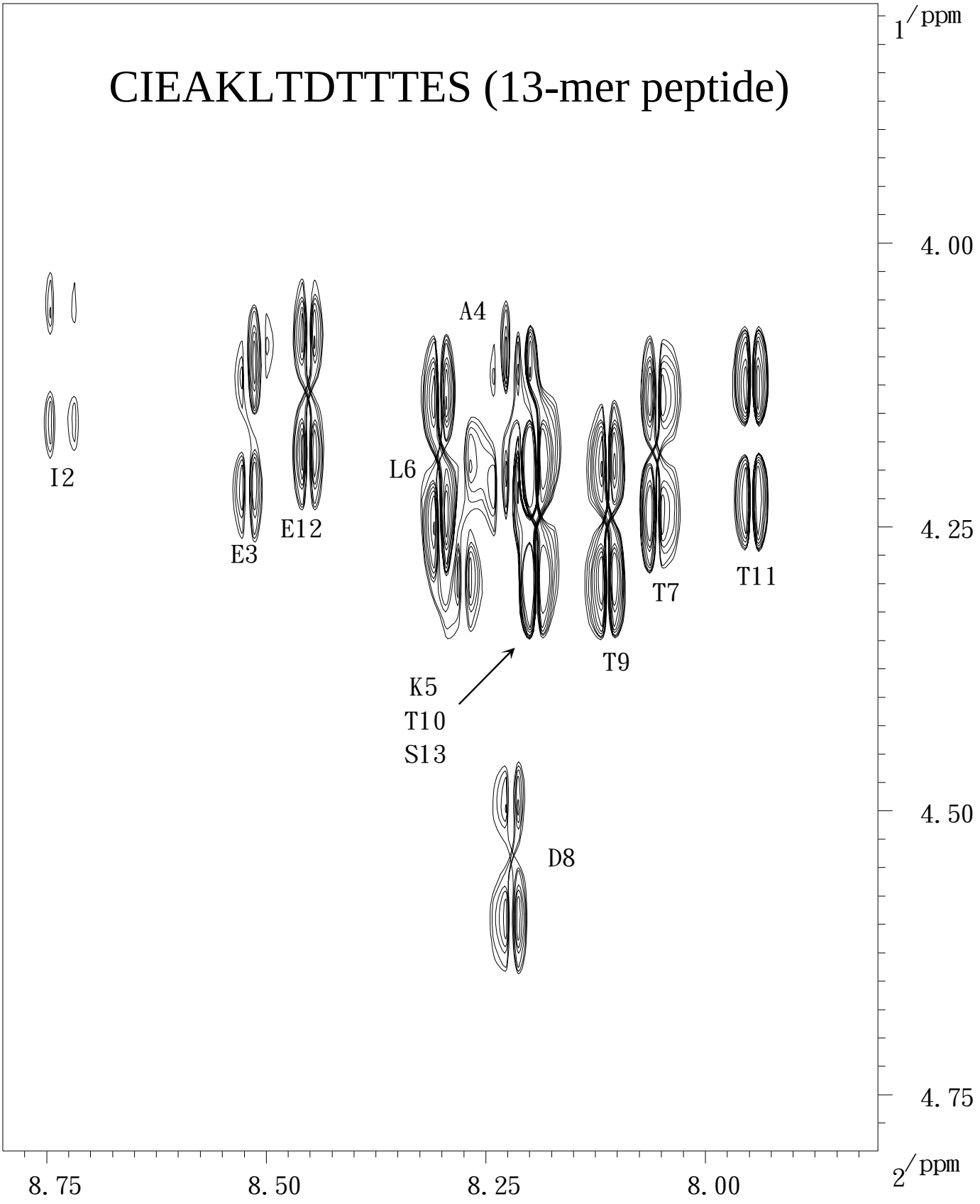

Fig 5-17 胜肽Den7 DQF-COSY光譜圖, pH 5.0的50mM phosphate buffer 300 μL及30 μL D2O,298K的條件下測得

CIEAKLTDTTTES (13-mer peptide)

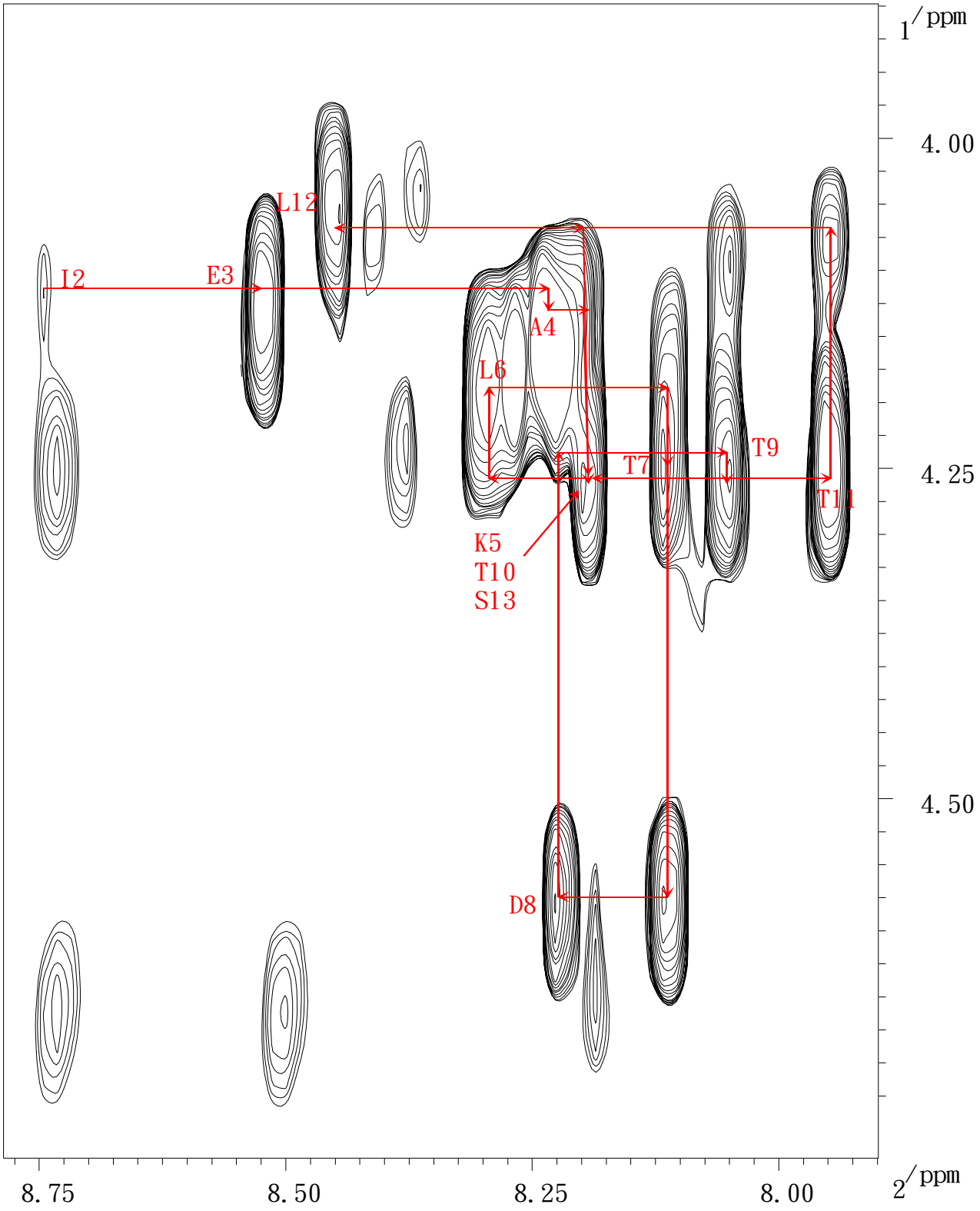

Fig 5-18 胜肽Den7 NOESY光譜圖, pH 5.0的50mM phosphate buffer 300 μL及30 μL D2O,298K,mixing time爲450ms的條件下測得

1D proton NMR spectra of I–2(1–172)

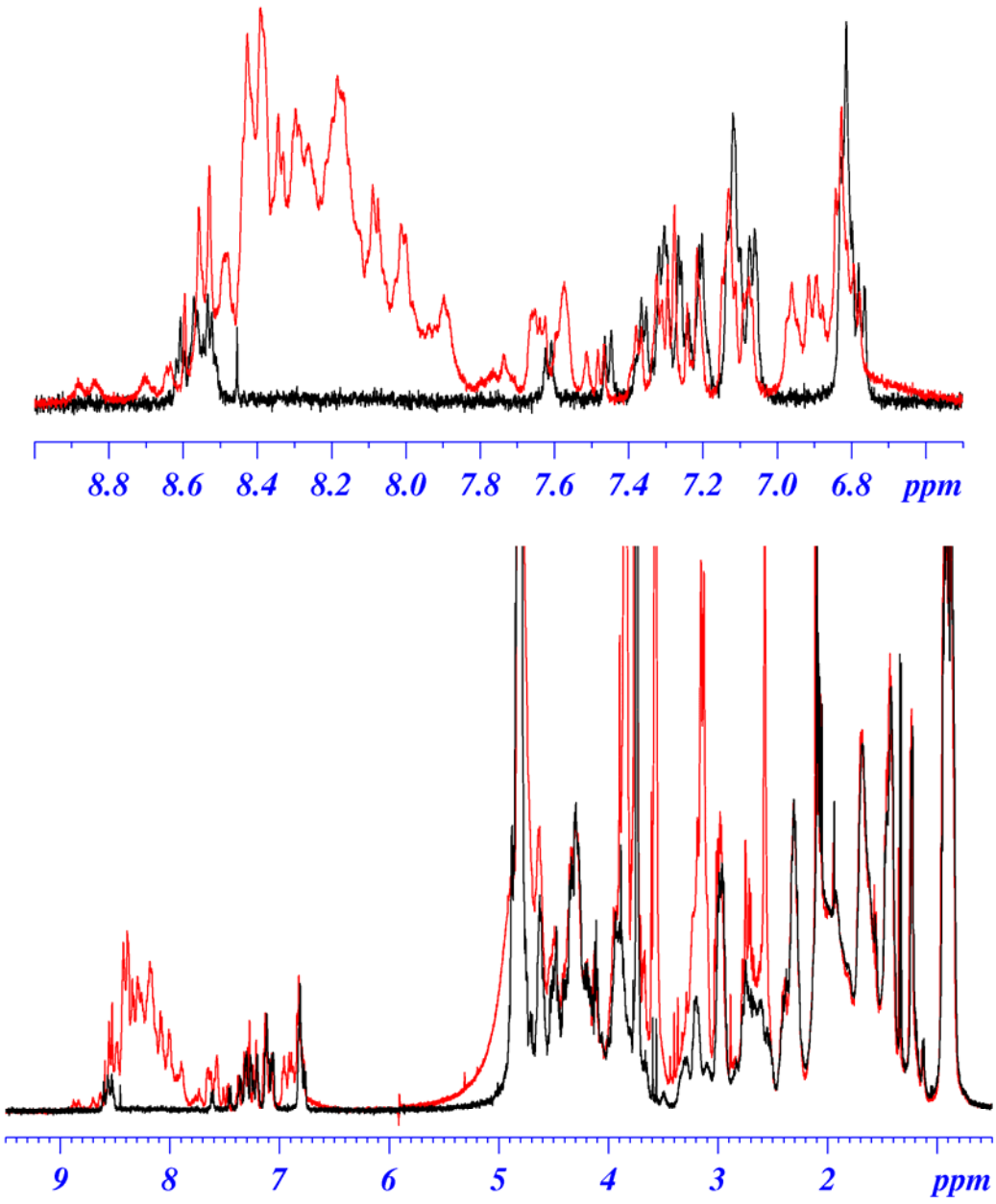

Determination of Macromolecular Structure by Multidimensional NMR Spectroscopy

Spin-spin coupling constants in peptides

Spin-spin coupling constants, like chemical shifts, depend on chemical environment and are therefore of great use in structure determination.

J-coupling constants

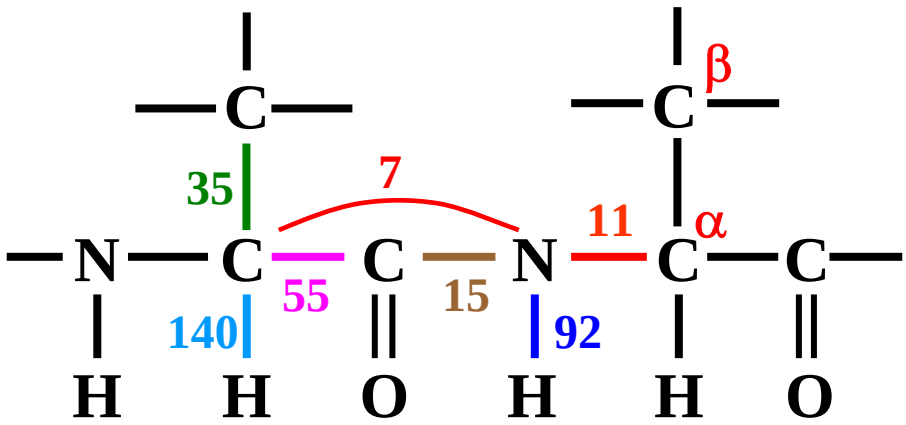

The flowchart of the protein structure determination from NMR data

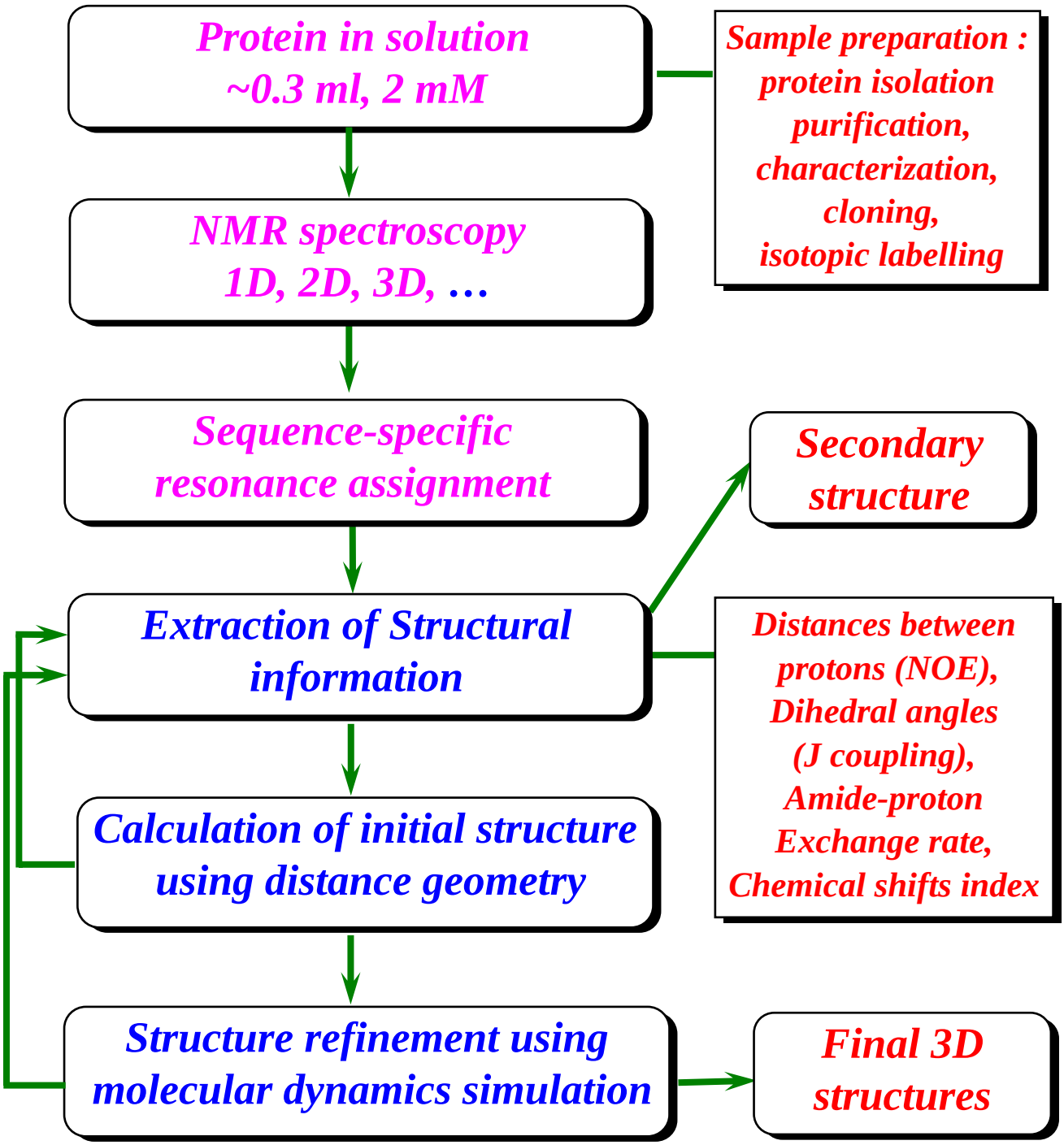

(a) HNCO : $H^N(i) \leftrightarrow N(i) \leftrightarrow C'(i-1)$

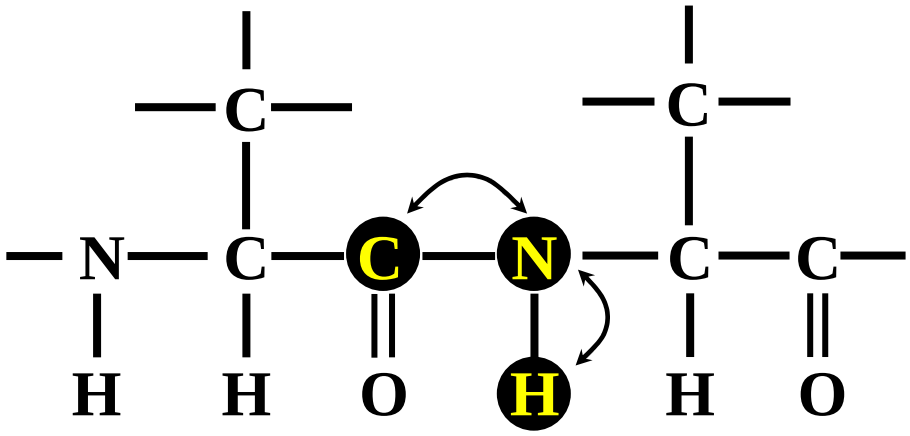

(b) HN(CA)CO : $H^N(i) \leftrightarrow N(i) \leftrightarrow C^{\alpha}(i) \leftrightarrow C'(i)$

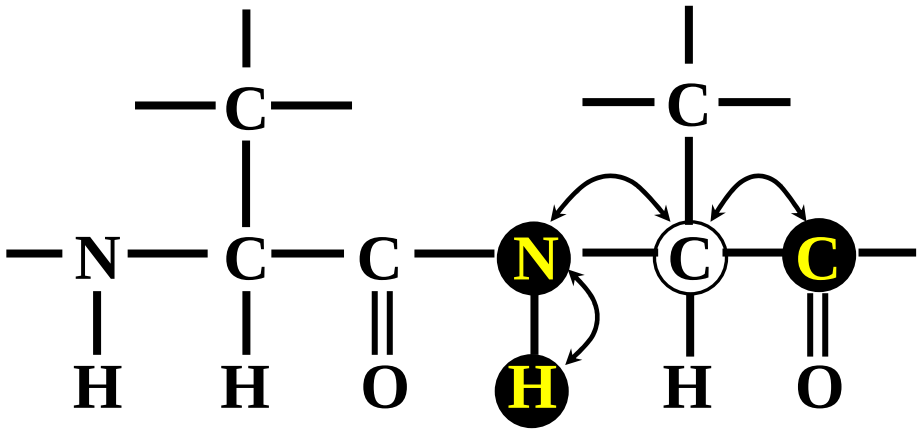

(c) HNCA : $H^N(i) \leftrightarrow N(i) \leftrightarrow C^\alpha(i-1)$, $C^\alpha(i)$

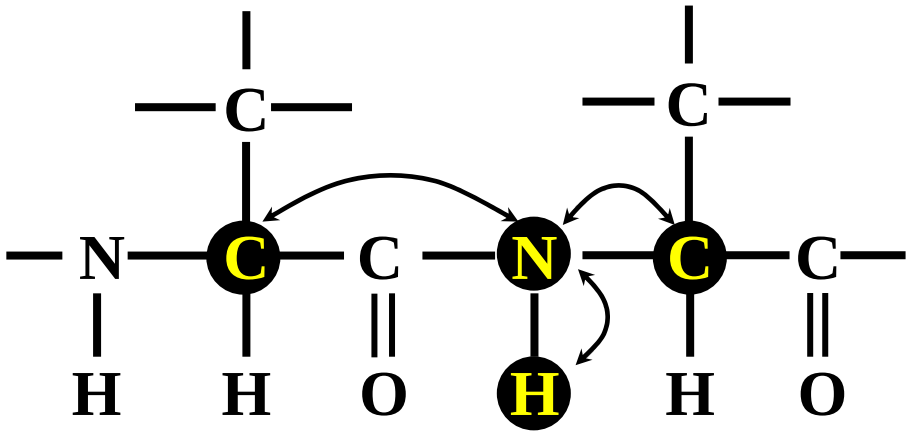

(d) HN(CO)CA : $H^N(i) \leftrightarrow N(i) \leftrightarrow C'(i-1) \leftrightarrow C^\alpha(i-1)$

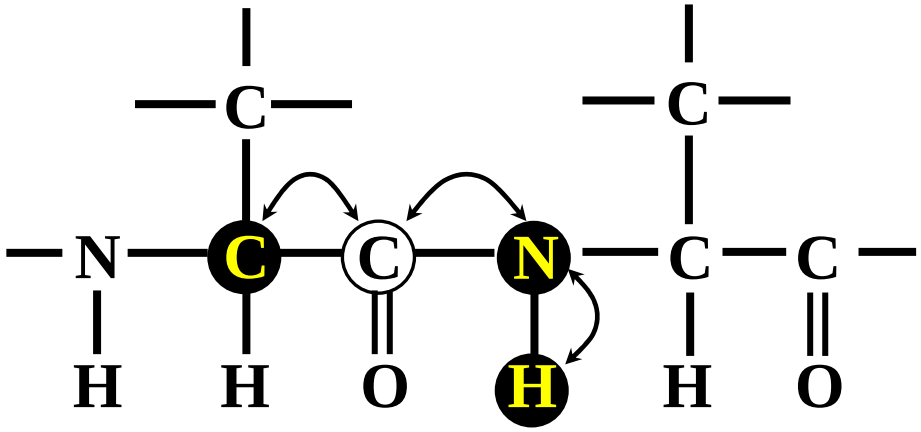

(e) HNCACB : $H^N(i) \leftrightarrow N(i)$ → $C^\alpha(i-1) \leftrightarrow C^\beta(i-1)$ and $C^\alpha(i) \leftrightarrow C^\beta(i)$

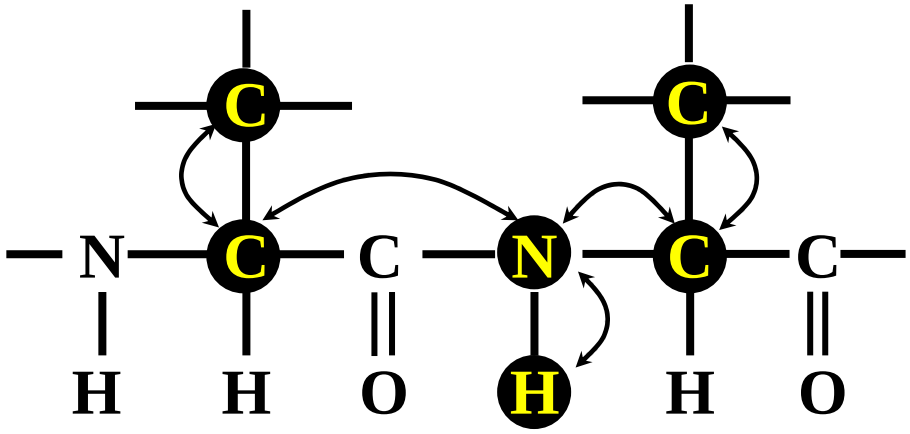

(f) CBCA(CO)NH :

$H^\alpha(i-1) \rightarrow C^\alpha(i-1) \rightarrow C'(i-1) \rightarrow N(i) \rightarrow H^N(i)$

$H^\beta(i-1) \rightarrow C^\beta(i-1)$

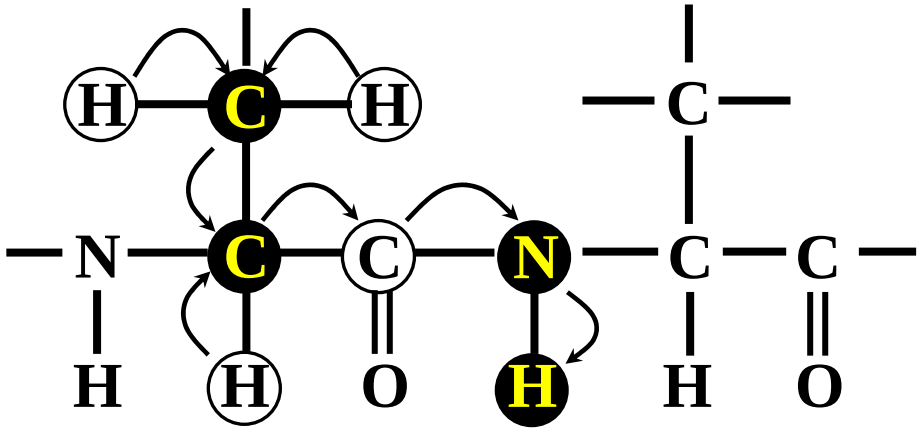

(g) HN(COCA)HA : $H^N(i) \longleftrightarrow N(i) \longleftrightarrow C'(i-1) \longleftrightarrow C^\alpha(i-1) \longleftrightarrow H^\alpha(i-1)$

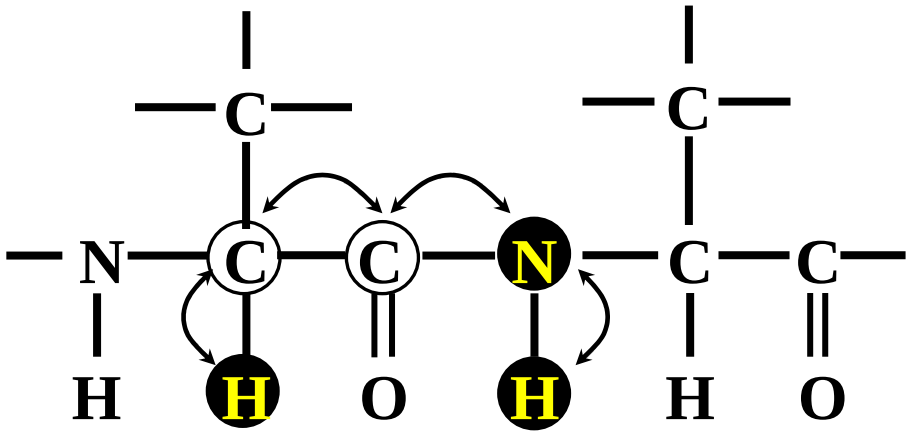

(h) HN(CA)HA : $H^N(i) \longleftrightarrow N(i) \longleftrightarrow C^\alpha(i) \longleftrightarrow H^\alpha(i)$

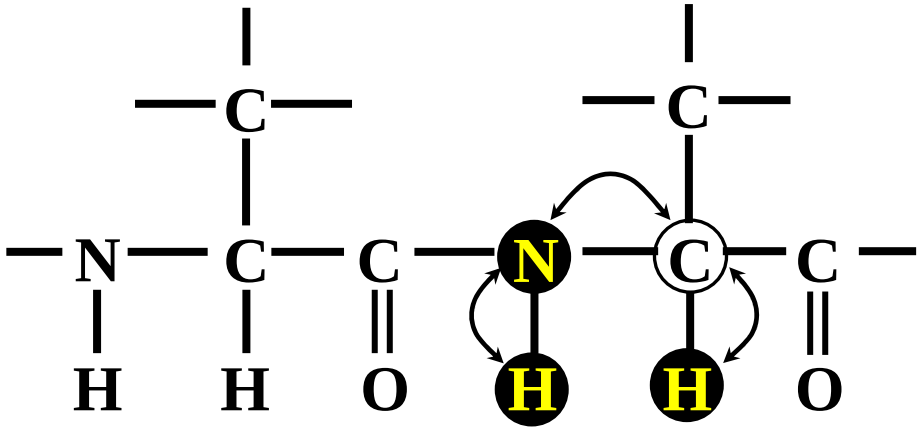

(i) TOCSY-HSQC : $H^{\gamma}(i) \longleftrightarrow H^{\beta}(i) \longleftrightarrow H^{\alpha}(i) \longleftrightarrow H^{N}(i) \longleftrightarrow N(i)$

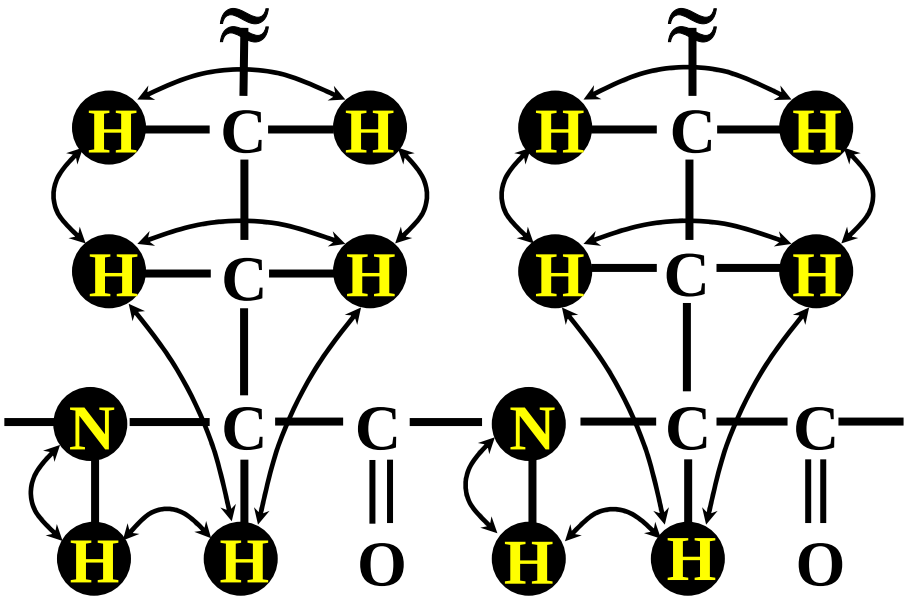

(j) HCCH-TOCSY : $H^{\alpha}(i) \longleftrightarrow C^{\alpha}(i)$, $H^{\beta}(i) \longleftrightarrow C^{\beta}(i)$, $H^{\gamma}(i) \longleftrightarrow C^{\gamma}(i)$

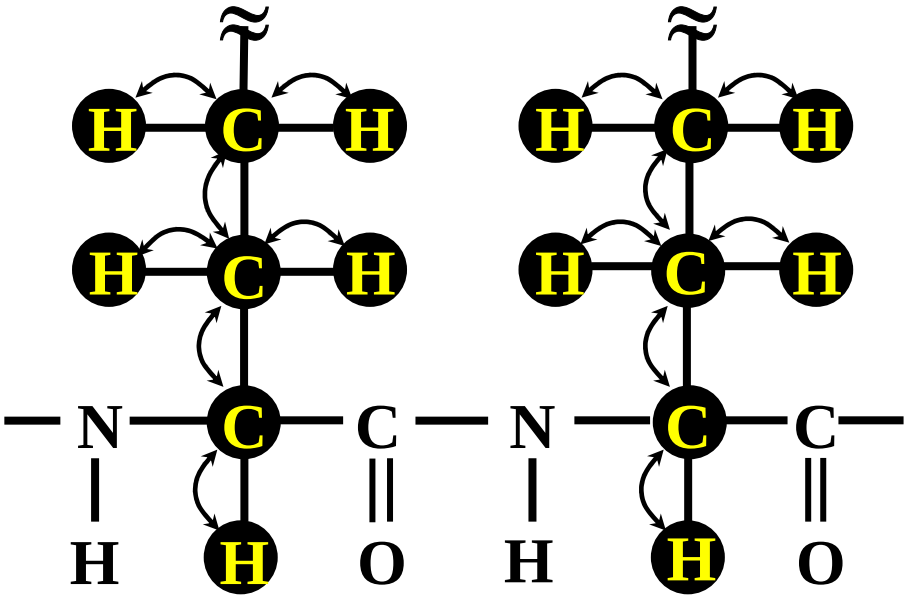

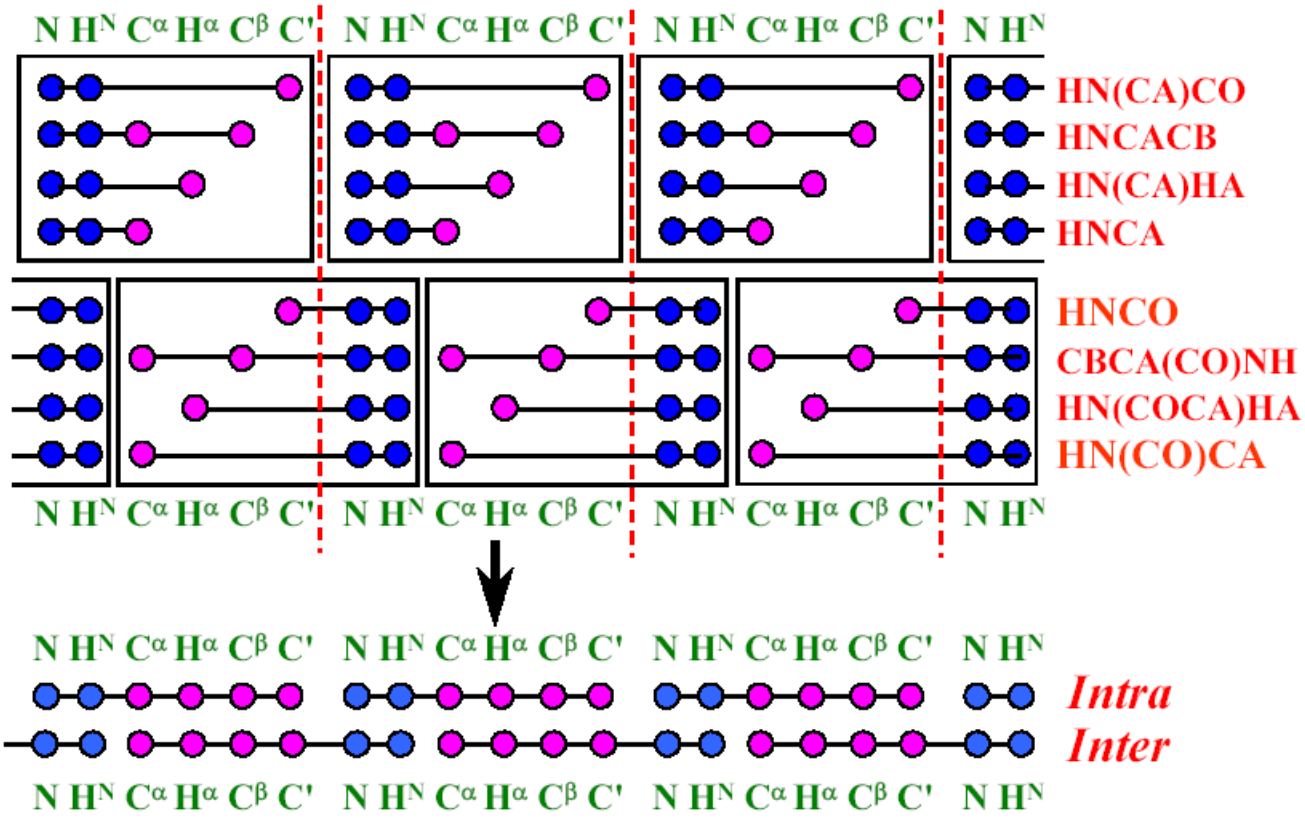
N H^N C^α H^α C^β C'
N H^N C^α H^α C^β C'
N H^N C^α H^α C^β C'
N H^N
HN(CA)CO
HNCACB
HN(CA)HA
HNCA
HNCO
CBCA(CO)NH
HN(COCA)HA
HN(CO)CA
N H^N C^α H^α C^β C'
N H^N C^α H^α C^β C'
N H^N C^α H^α C^β C'
N H^N
N H^N C^α H^α C^β C'
N H^N C^α H^α C^β C'
N H^N C^α H^α C^β C'
N H^N
Intra
Inter
N H^N C^α H^α C^β C'
N H^N C^α H^α C^β C'
N H^N C^α H^α C^β C'
N H^N

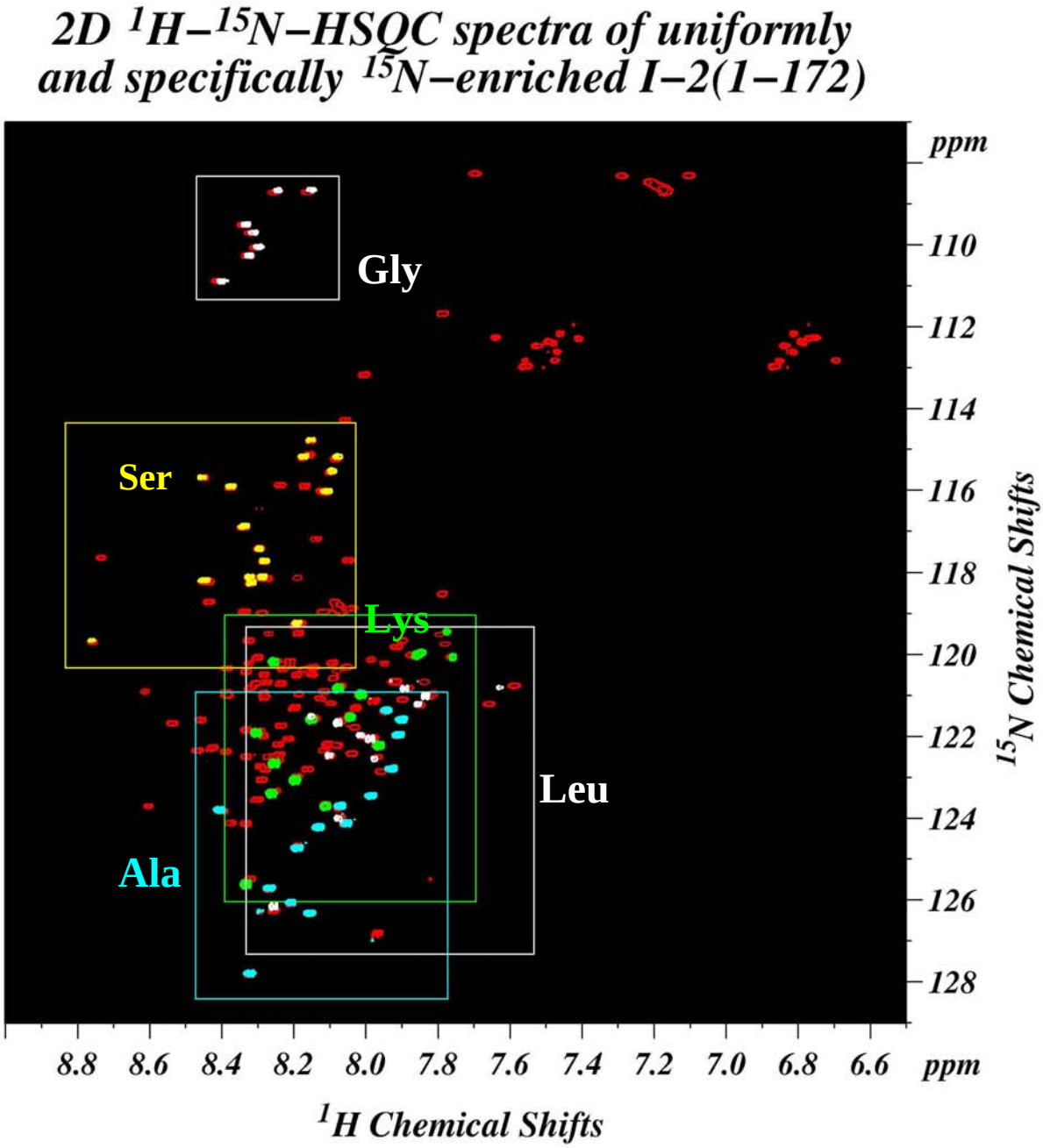
2D $^{1}H-^{15}N-HSQC$ spectra of uniformly and specifically $^{15}N-$enriched I–2(1–172)
Gly
Ser
Lys
Leu
Ala
ppm
110
112
114
116
118
120
122
124
126
128
^{15}N Chemical Shifts
8.8
8.6
8.4
8.2
8.0
7.8
7.6
7.4
7.2
7.0
6.8
6.6
ppm
^{1}H Chemical Shifts

Three-dimensional CBCA(CO)NH Spectrum

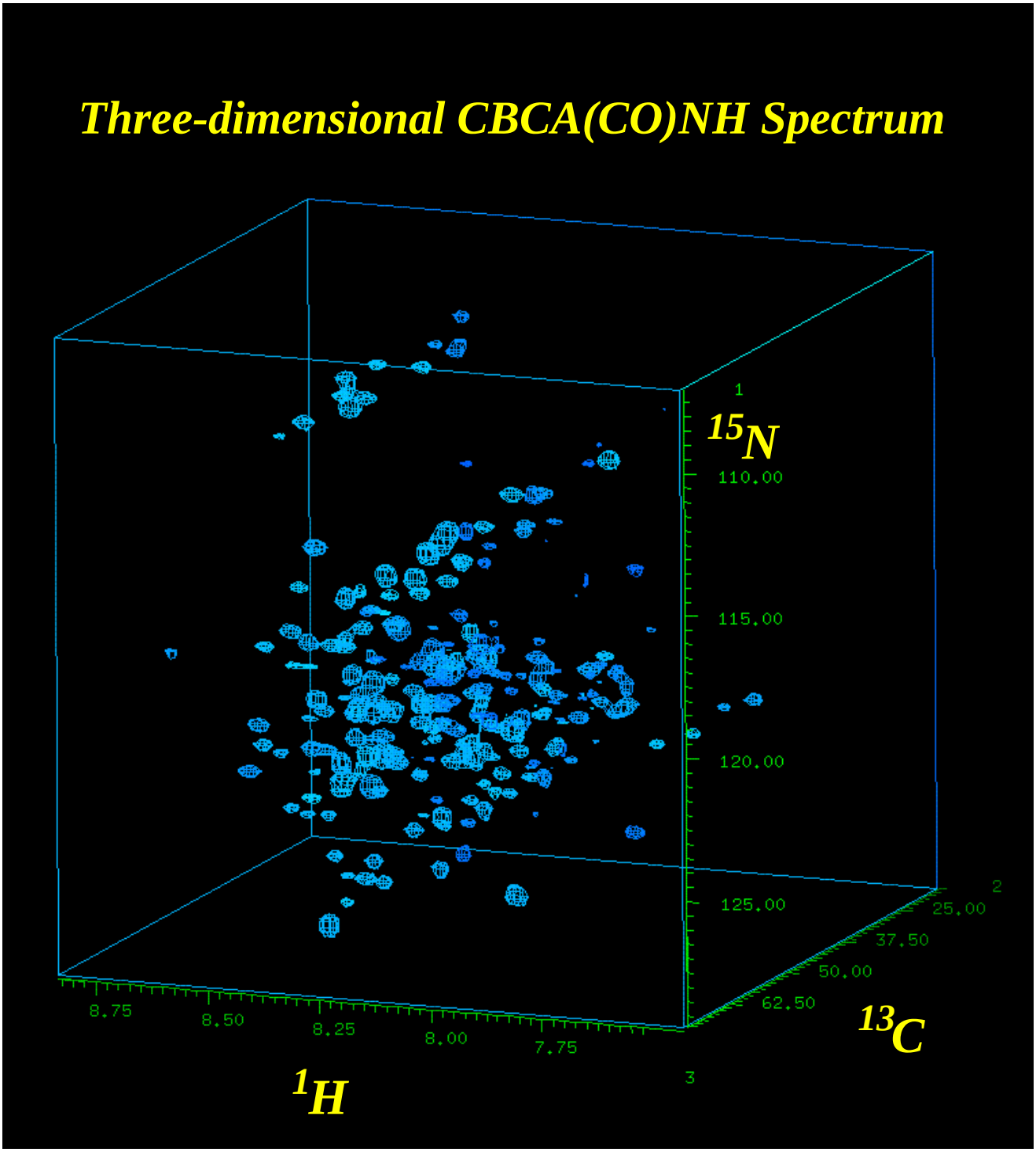

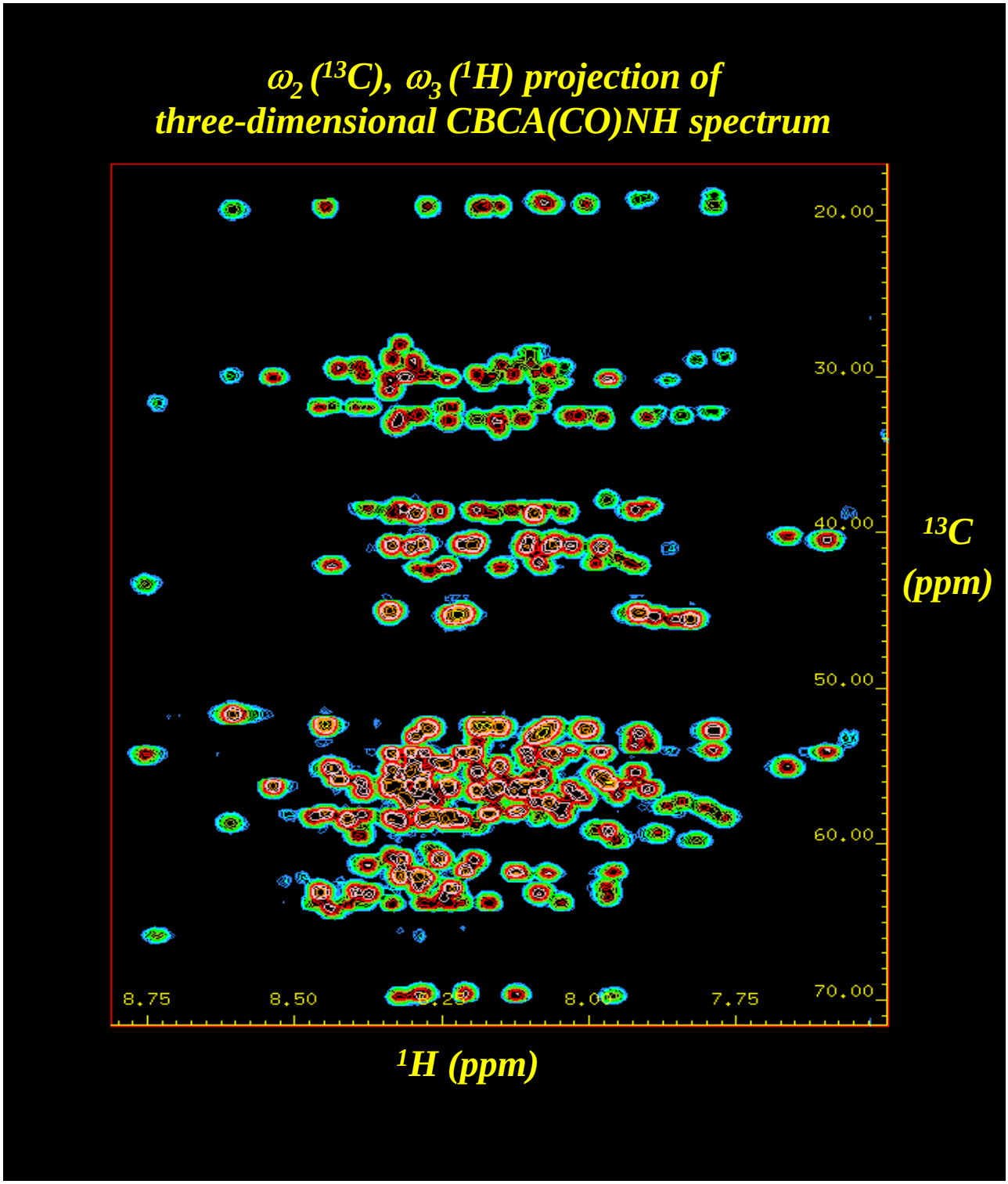
ω2 (13C), ω3 (1H) projection of
three-dimensional CBCA(CO)NH spectrum
20.00
30.00
40.00
50.00
60.00
70.00
13C
(ppm)
8.75
8.50
8.25
8.00
7.75
1H (ppm)

Strip plot of 3D CBCANH spectrum of inhibitor-2(1-172)

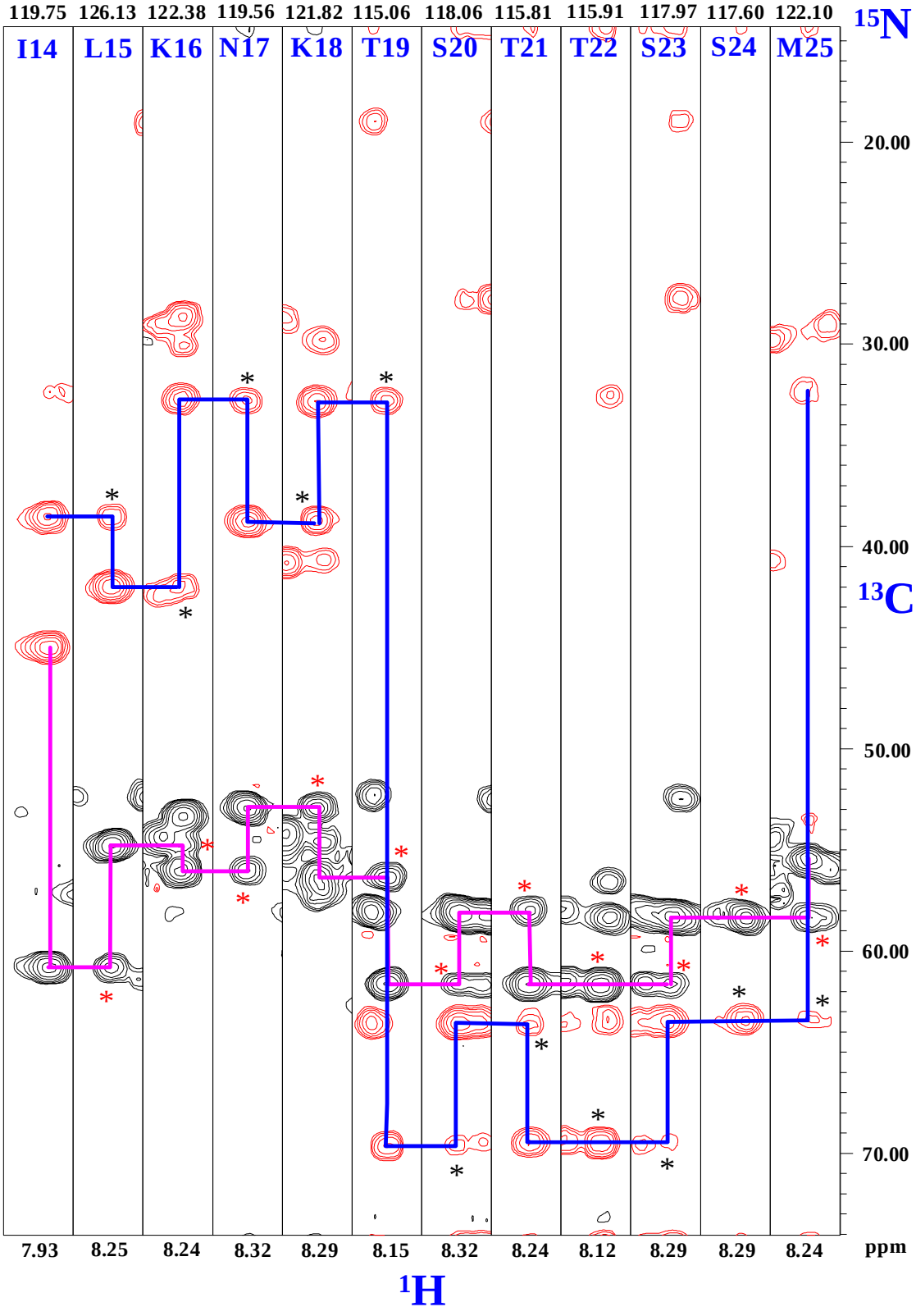

Strip plot of 3D HN(CA)CO spectrum of I-2(172)

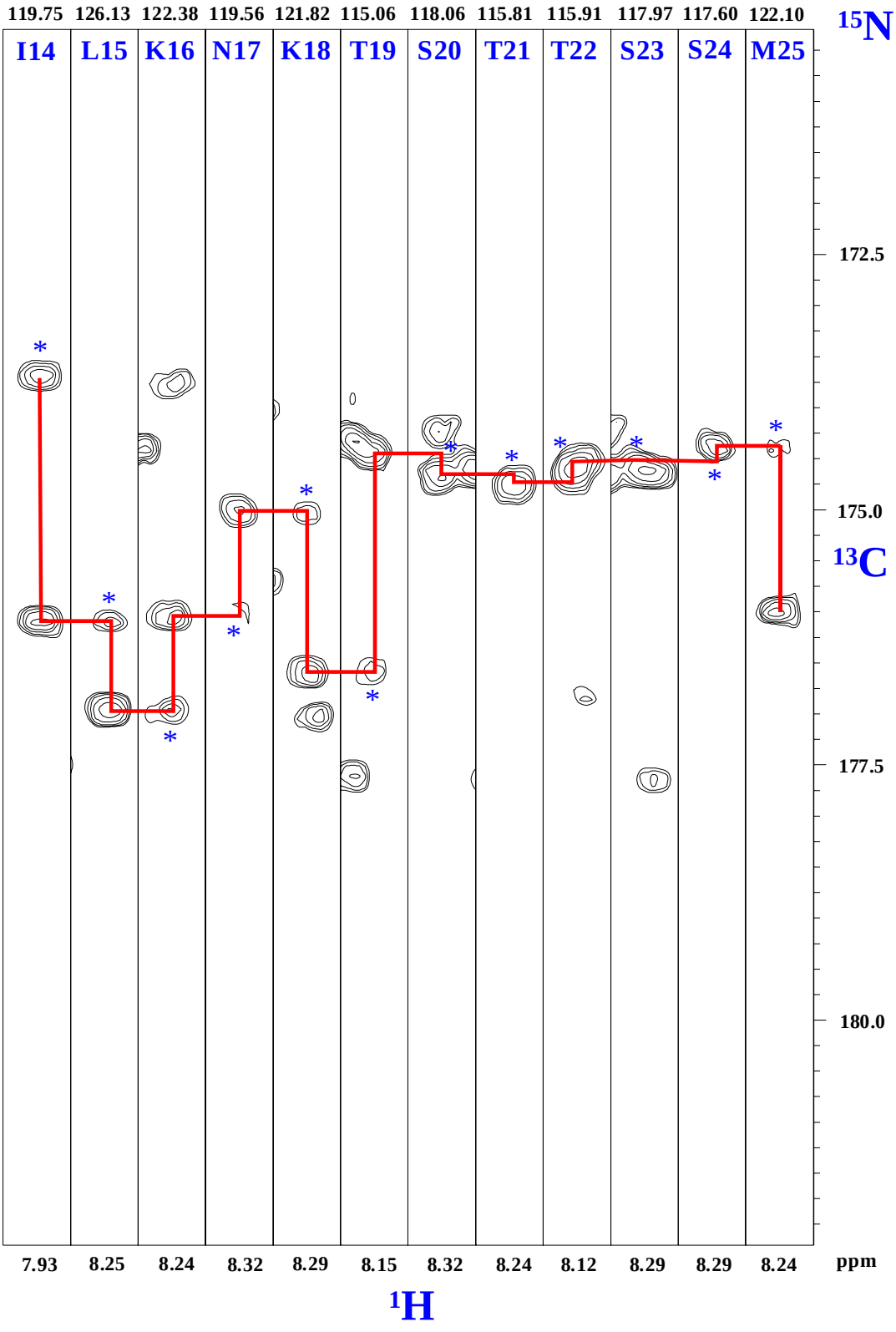

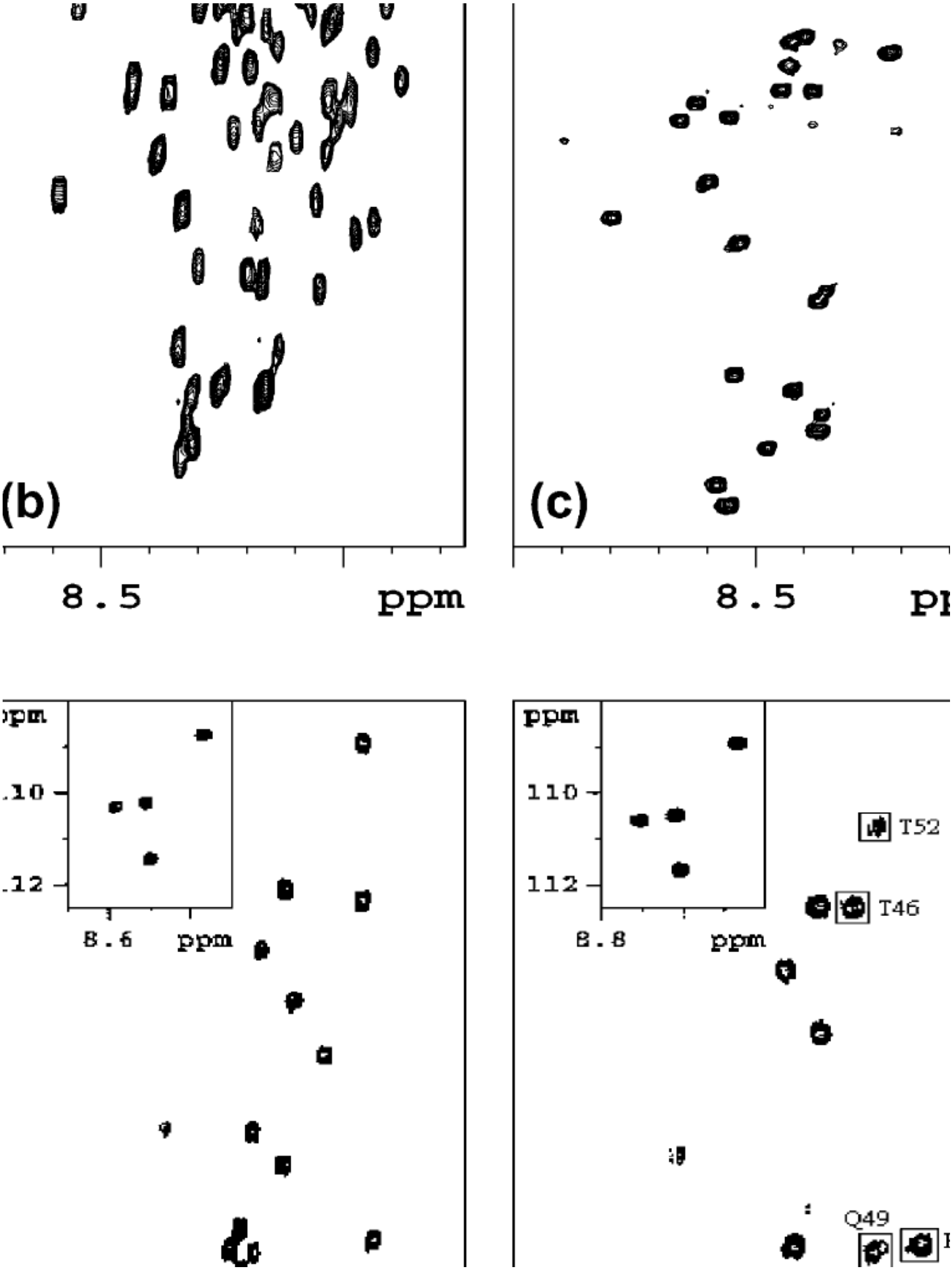
(b)
8.5
ppm
(c)
8.5
pp
.10
.12
8.6
ppm
ppm
110
112
8.8
ppm
T52
T46
Q49

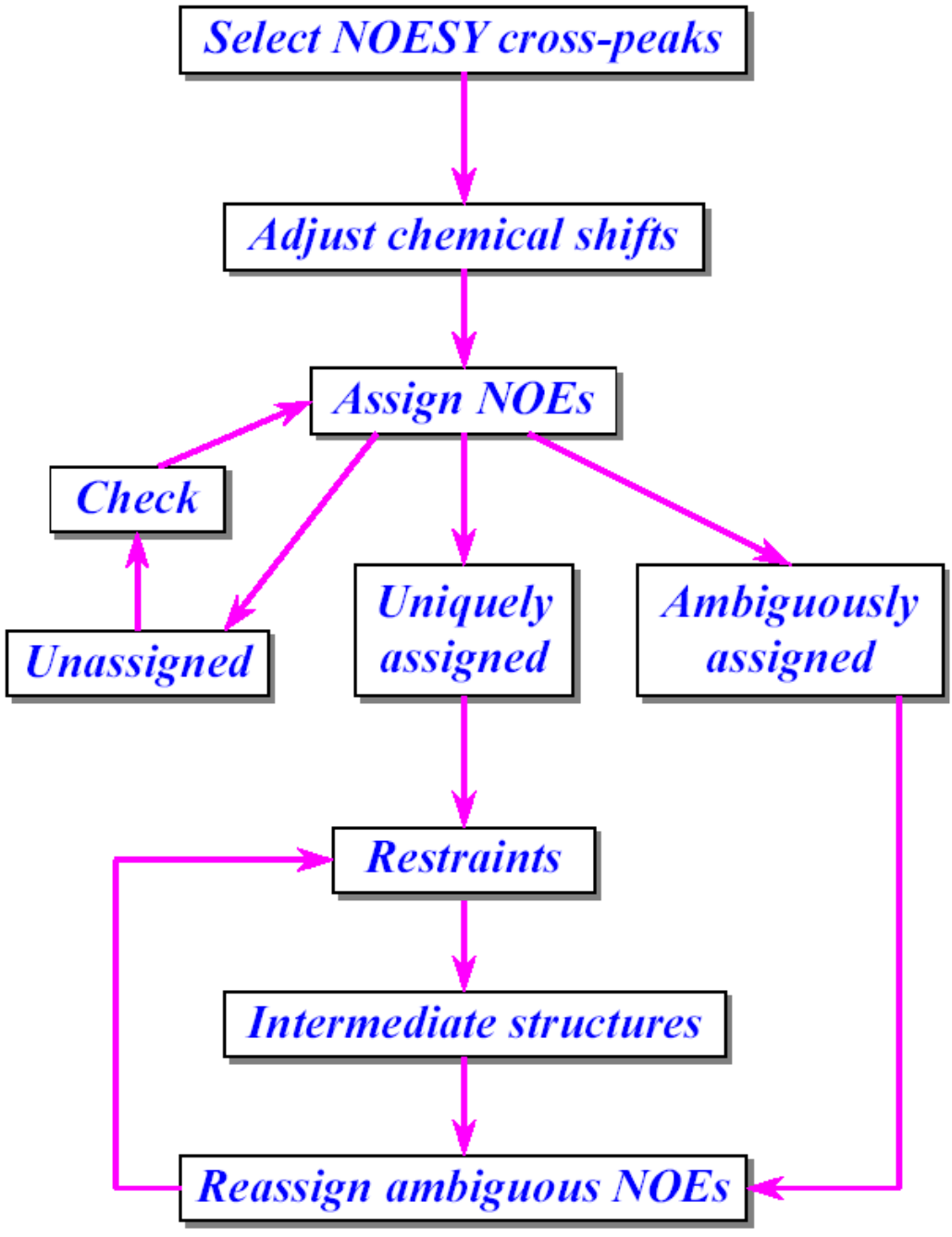
Select NOESY cross-peaks
Adjust chemical shifts
Assign NOEs
Check
Unassigned
Uniquely assigned
Ambiguously assigned
Restraints
Intermediate structures
Reassign ambiguous NOEs

Table 1. Structural statistics for the 20 final NMR structures of NRho

NMR constraints	
Distance constraints	
Total NOE	1830
Unambiguous	1469
Ambiguous	361
Intra-residue[a]	585
Inter-residue[a]	884
Sequential ($\|i–j\| = 1$)	344
Medium-range ($\|i–j\| \leq 4$)	305
Long-range ($\|i–j\| > 5$)	235
Hydrogen bonds[b]	54
Dihedral angles	
Φ	48
Ψ	48
Structure statistics[c]	
Violations	
NOE violations > 0.5 Å	0
Dihedral angle violations > 5°	0
Deviations from idealized geometry	
Bond lengths (Å)	$7.60 \times 10^{-3} \pm 2.38 \times 10^{-4}$
Bond angles (°)	0.96 ± 0.03
Impropers (°)	2.45 ± 0.09
Agreement with experimental restraints	
NOE	$5.46 \times 10^{-2} \pm 2.69 \times 10^{-3}$
Dihedral angles	0.81 ± 0.11
Average RMSD (Å)[d]	
Backbone[e]	0.45 ± 0.09 (0.25 ± 0.06)
Heavy atoms[e]	0.89 ± 0.08 (0.79 ± 0.13)
Ramachandran plot[f]	
Most favored (%)	69.8 (71.5)(92.9)
Additionally allowed (%)	22.0 (19.4)(7.1)
Generously allowed (%)	7.5 (9.1)(0.0)
Disallowed (%)	0.7 (0.0)(0.0)

[a] Splits shown only for unambiguous assignments.

[b] Hydrogen bond restraints were H^N–O distance of 1.8–2.3 Å and an N–O distance of 2.8–3.3 Å.

[c] Structural characteristics for the final ensemble of 20 water-refined structures.

[d] RMSD of the mean structure from individual structures in the ensemble.

[e] RMSD for residues 3–66 shown (these residues have $^1H^N$-{^{15}N}NOE at 800 MHz > 0.6). The numbers in the parentheses indicate the RMSD for regions with definite secondary structure.

[f] Ramachandran plot data shown for residues 3–66. The first set of numbers in parentheses indicates the statistics for the smaller subset after removal of residues (3, 5, 6, 7, 35, 36 and 42) shown to undergo a significant amount of conformational exchange. The second set indicates the characteristics for those residues in ordered regions of definite secondary structure.

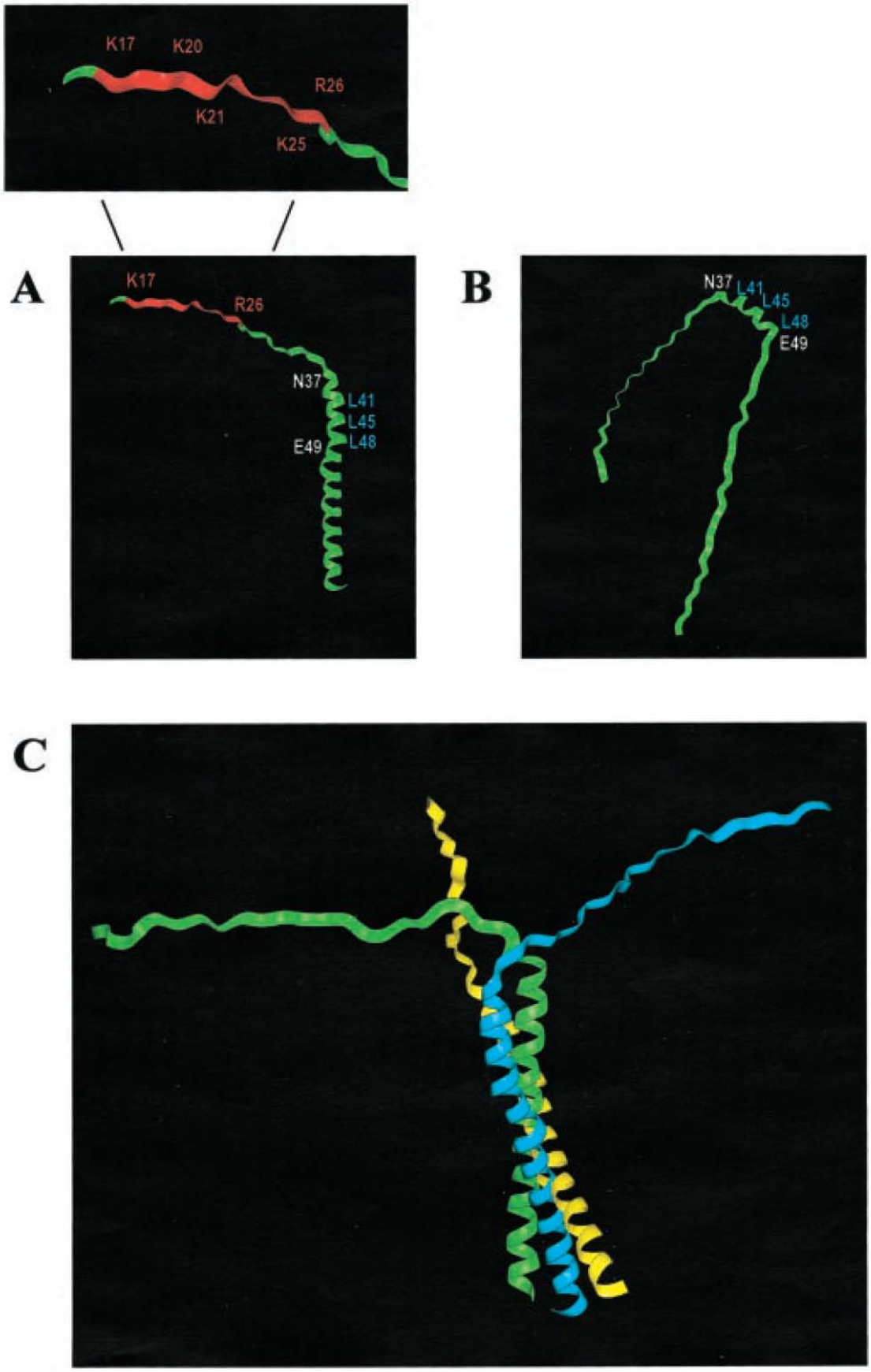
K17
K20
R26
K21
K25
A
K17
R26
N37
L41
L45
E49
L48
B
N37
L41
L45
L48
E49
C

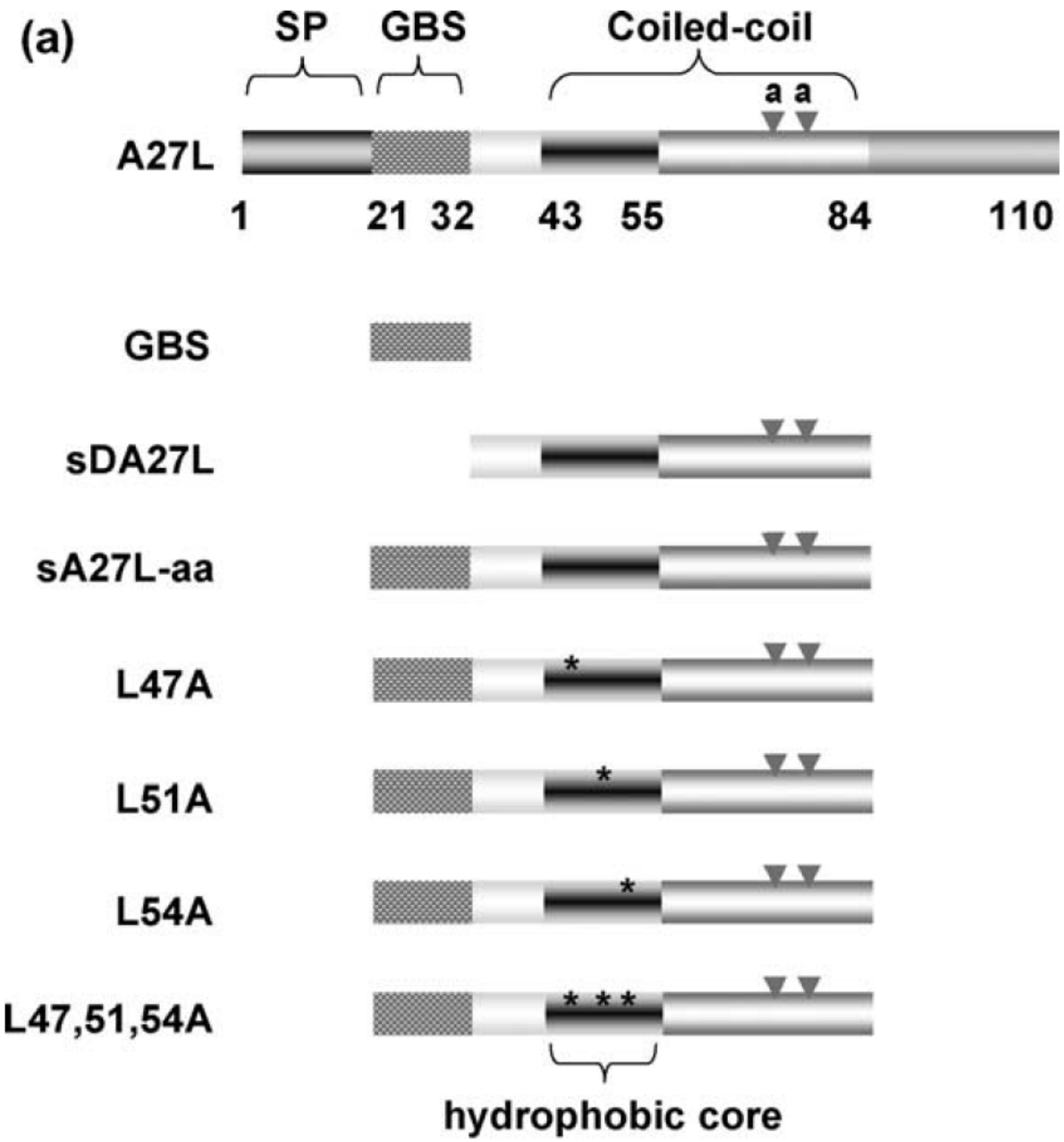
(a)
SP
GBS
Coiled-coil
a a
A27L
1
21
32
43
55
84
110
GBS
sDA27L
sA27L-aa
L47A
L51A
L54A
L47,51,54A
hydrophobic core

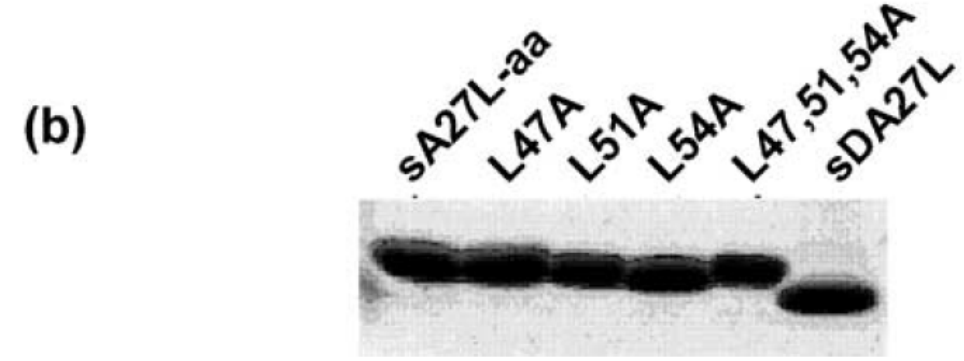
(b)
sA27L-aa
L47A
L51A
L54A
L47,51,54A
sDA27L

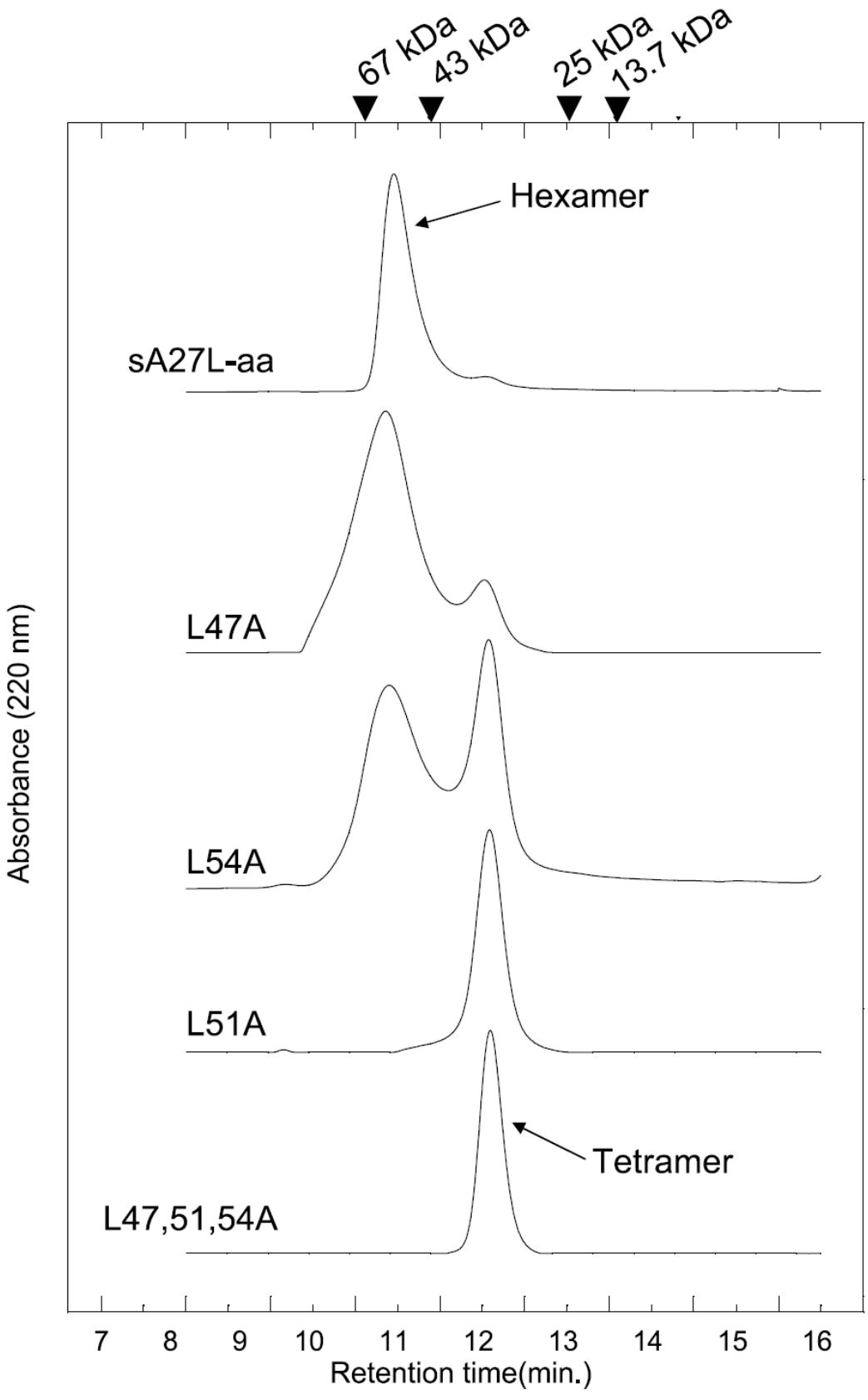
67 kDa
43 kDa
25 kDa
13.7 kDa
Hexamer
sA27L-aa
L47A
L54A
L51A
Tetramer
L47,51,54A
Absorbance (220 nm)
7
8
9
10
11
12
13
14
15
16
Retention time(min.)

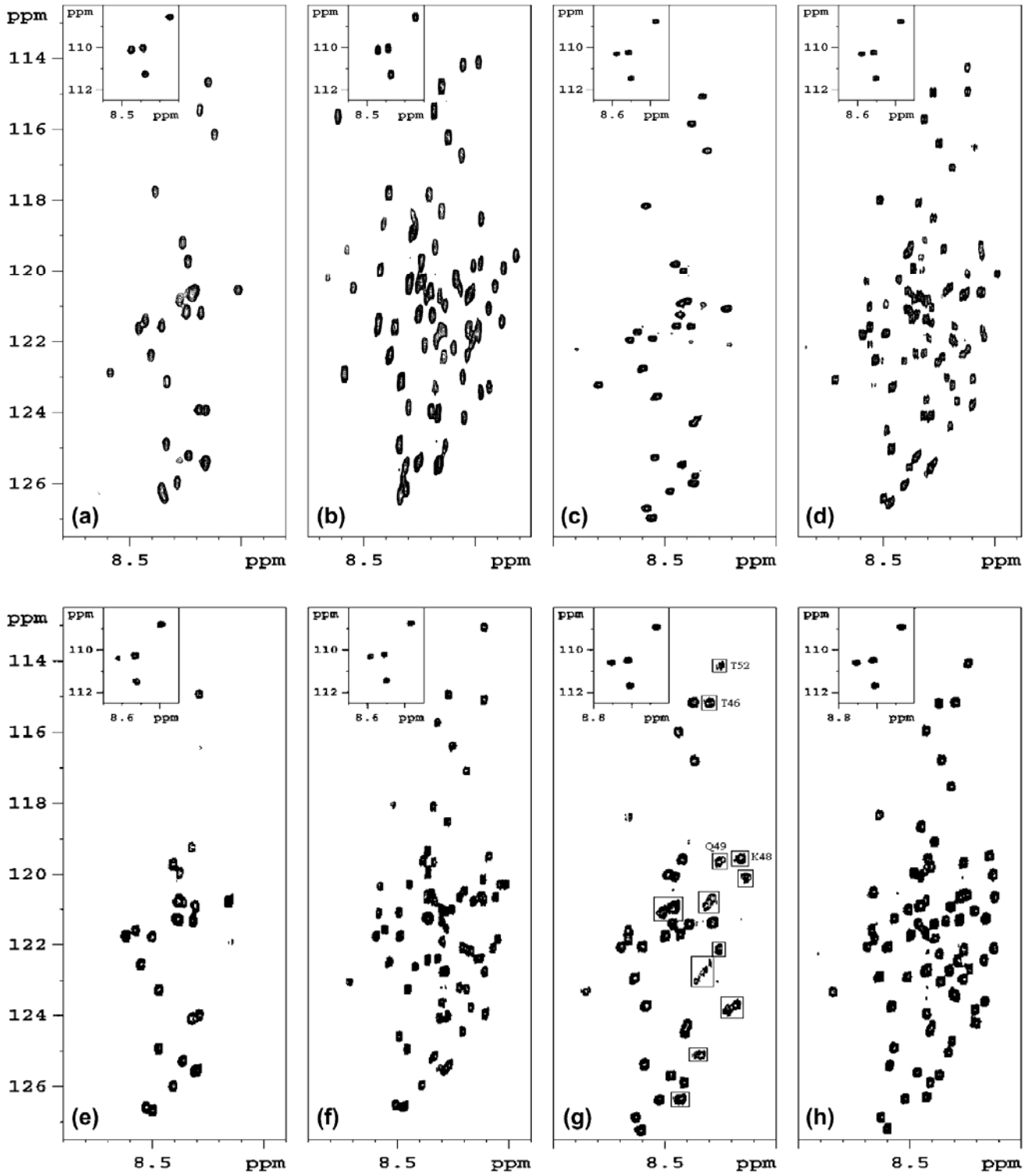
ppm
114
116
118
120
122
124
126
8.5
ppm
(a)
(b)
(c)
(d)
(e)
(f)
(g)
(h)
110
112
8.6
8.8
T52
T46
Q49
K48

Protein sequences of sA27-aa and its mutants

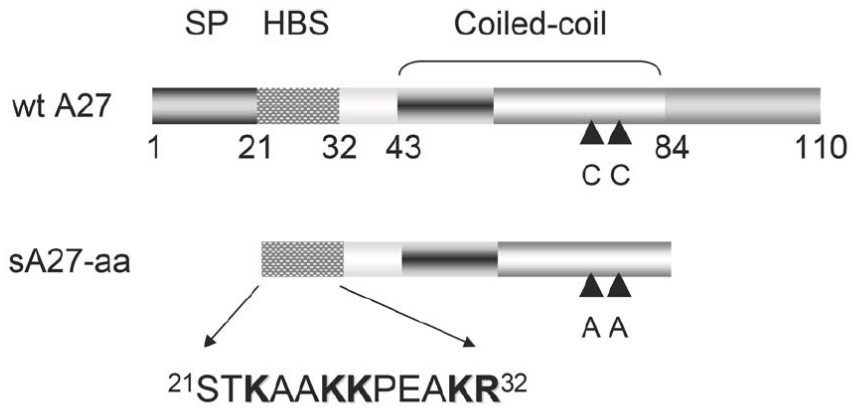

sA27-aa mutant	GAG binding sequence	
K23A	STAAAKKPEAKR	A series
K26A	STKAAAKPEAKR	
K27A	STKAAKAPEAKR	
K31A	STKAAKKPEAAR	
R32A	STKAAKKPEAKA	
K3A3	SKAAKAAKEAKR	
E29K	STKAAKKPKAKR	K series
A30K	STKAAKKPEKKR	
T22K	SKKAAKKPEAKR	
A25K	STKAKKKPEAKR	
T22K/A25K	SKKAKKKPEAKR	

BIAcore GAG binding assay of sA27-aa and its mutants

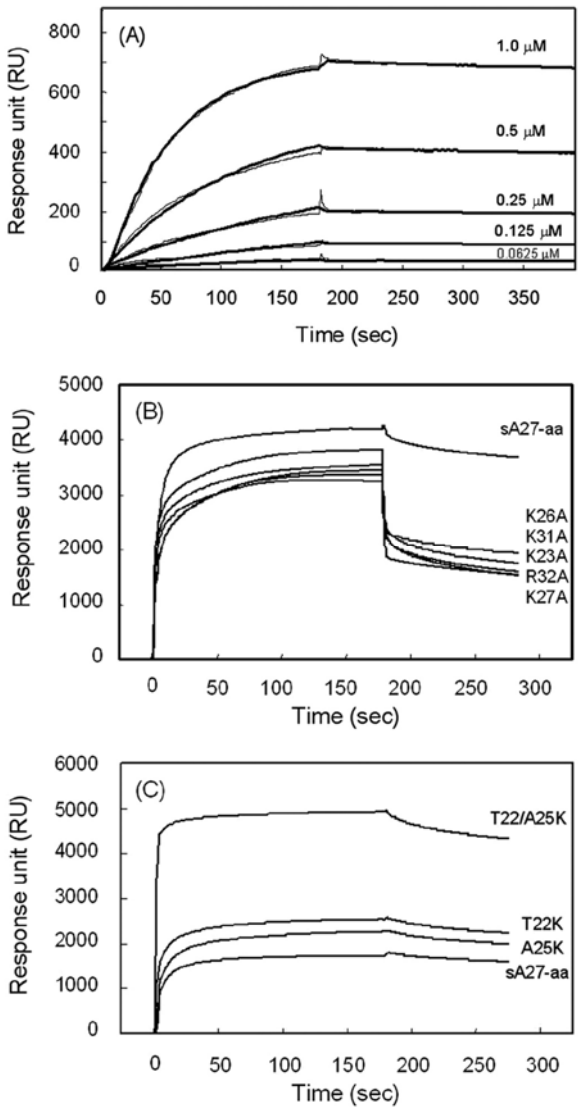

TABLE 1

Binding constants (K_A), association rate constant (k_{on}), and dissociation rate constant (k_{off}) of specific and nonspecific GAG binding affinity of vaccinia viral envelope proteins sA27-aa and D8

Binding constants (K_A) were calculated from the ratio k_{on}/k_{off}. Data represent the means ± S.D. of at least four independent experiments at five different protein concentrations.

Specific	k_{on} ($\times 10^3\ M^{-1}\ s^{-1}$)	k_{off} ($\times 10^{-6}\ s^{-1}$)	K_A ($\times 10^8\ M^{-1}$)
sA27-aa, HP	1.71 ± 0.42	13.7 ± 2.3	1.25 ± 0.80
D8, CS	11.9 ± 1.5	36.8 ± 26.6	3.23 ± 0.20
Nonspecific	k_{on} ($\times 10^3\ M^{-1}\ s^{-1}$)	k_{off} ($\times 10^{-3}\ s^{-1}$)	K_A ($\times 10^5\ M^{-1}$)
sA27-aa, CS	2.58 ± 0.04	15.6 ± 0.7	1.65 ± 0.40
D8, HP	1.45 ± 0.04	1.60 ± 0.35	9.06 ± 0.17
T22K/A25K, CS	3.57 ± 0.02	5.64 ± 0.18	6.33 ± 0.30

TABLE 2

Heparin binding constants (K_A), association rate constant (k_{on}), and dissociation rate constant (k_{off}) of sA27-aa mutants determined by SPR

Binding constants (K_A) were calculated from the ratio k_{on}/k_{off}. Data represent the means ± S.D. of at least four independent experiments at five different protein concentrations.

	k_{on} ($\times 10^3\ M^{-1}\ s^{-1}$)	k_{off} ($\times 10^{-3}\ s^{-1}$)	K_A ($\times 10^6\ M^{-1}$)
A series			
K23A	1.60 ± 0.22	2.20 ± 0.14	0.72 ± 0.07
K26A	2.00 ± 0.27	1.70 ± 0.71	1.18 ± 0.53
K27A	1.10 ± 0.19	1.90 ± 0.13	0.58 ± 0.05
K31A	1.20 ± 0.04	1.20 ± 0.15	1.00 ± 0.12
R32A	0.97 ± 0.03	1.40 ± 0.13	0.69 ± 0.07
Scrambled			
K3A3	2.56 ± 0.36	0.46 ± 0.03	5.57 ± 0.78
K series			
E29K	26.5 ± 16.0	1.92 ± 0.11	13.80 ± 1.80
A30K	12.8 ± 0.63	3.76 ± 0.10	3.40 ± 0.23
	k_{on} ($\times 10^3\ M^{-1}\ s^{-1}$)	k_{off} ($\times 10^{-6}\ s^{-1}$)	K_A ($\times 10^9\ M^{-1}$)
T22K	3.88 ± 0.15	2.21 ± 0.10	1.75 ± 0.50
A25K	2.55 ± 0.10	3.40 ± 0.12	0.75 ± 0.20
	k_{on} ($\times 10^3\ M^{-1}\ s^{-1}$)	k_{off} ($\times 10^{-7}\ s^{-1}$)	K_A ($\times 10^{11}\ M^{-1}$)
T22K/A25K	26.7 ± 2.3	1.39 ± 0.01	1.90 ± 0.40

2D NMR HSQC spectra of sA27-aa and K3A3 mutant

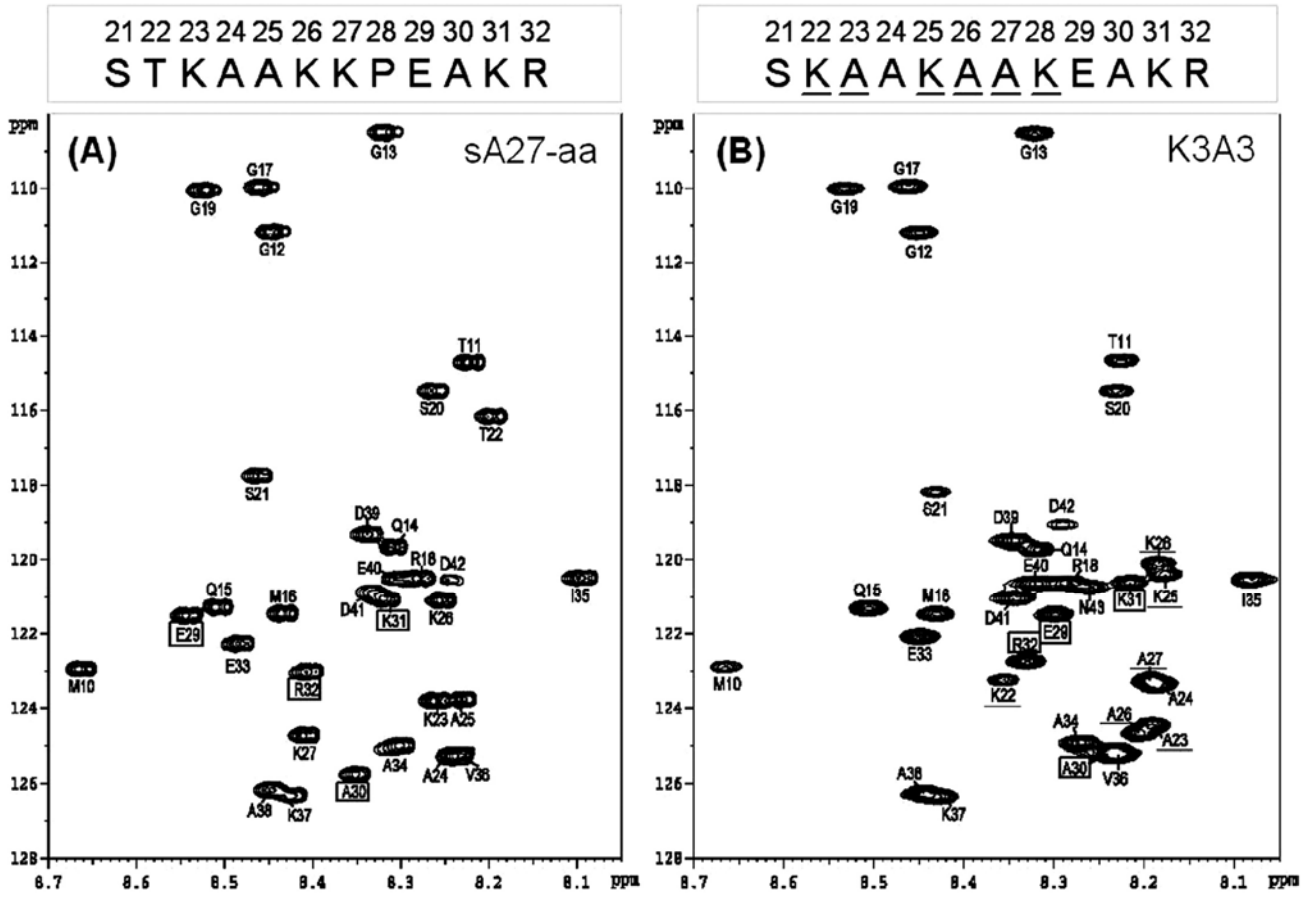

2D NMR HSQC spectra of sA27-aa and K3A3 mutant

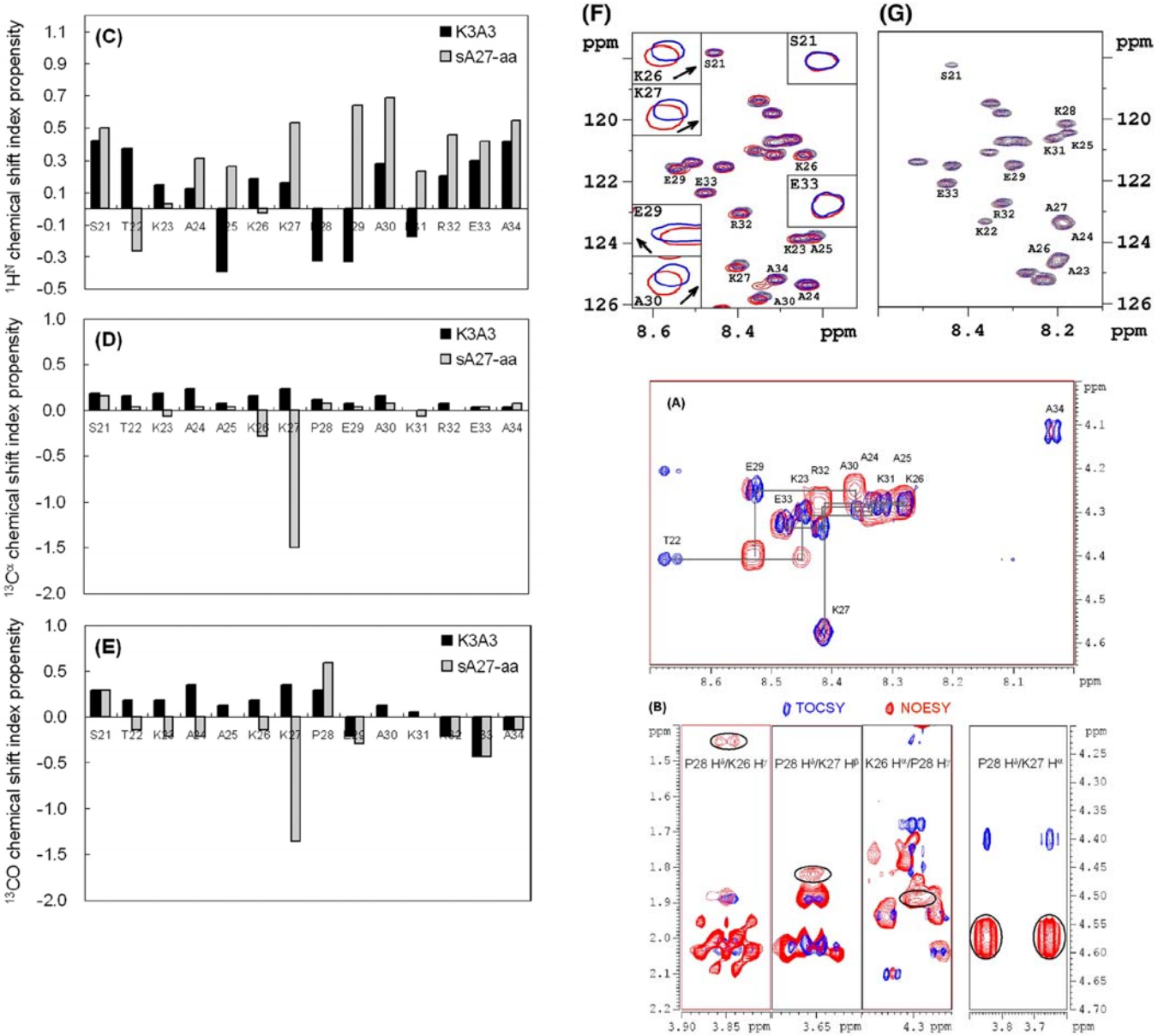

TABLE 3

^{1}H chemical shift assignments of synthesized 14-mer, a copy of HBS sequence STKAAKKPEAKREA, in the absence of HP

For comparison, the $^{1}H^{N}$ and $^{1}H^{\alpha}$ chemical shifts that extracted from recombinant sA27-aa protein are given in parentheses.

Residue	H^{N}	H^{α}	H^{β}	Others
Thr^{22}	8.666 (8.190)	4.408 (4.374)	4.204	H^{γ} 1.228
Lys^{23}	8.445 (8.262)	4.309 (4.336)	1.816, 1.750	H^{γ} 1.430, 1.430
				H^{δ} 1.690, 1.690
				H^{ϵ} 2.997, 2.997
				H^{ζ} 7.540
Ala^{24}	8.334 (8.234)	4.270 (4.306)	1.356	
Ala^{25}	8.280 (8.219)	4.280 (4.296)	1.375	
Lys^{26}	8.279 (8.253)	4.298 (4.325)	1.779, 1.742	H^{γ} 1.443, 1.443
				H^{δ} 1.690, 1.690
				H^{ϵ} 2.997, 2.997
				H^{ζ} 7.540
Lys^{27}	8.413 (8.404)	4.573 (4.608)	1.816, 1.740	H^{γ} 1.466, 1.483
				H^{δ} 1.706, 1.723
				H^{ϵ} 3.011
				H^{ζ} 7.540
Pro^{28}		4.399 (4.436)	2.296, 2.019	H^{γ} 1.889
				H^{δ} 3.837, 3.654
Glu^{29}	8.530 (8.546)	4.242 (4.276)	2.018, 1.944	H^{γ} 2.349, 2.331
Ala^{30}	8.357 (8.351)	4.299 (4.325)	1.374	
Lys^{31}	8.314 (8.311)	4.280 (4.318)	1.800, 1.760	H^{γ} 1.412, 1.412
				H^{δ} 1.685, 1.685
				H^{ϵ} 2.992, 3.008
				H^{ζ} 7.525
Arg^{32}	8.417 (8.404)	4.334 (4.354)	1.834, 1.779	H^{γ} 1.632, 1.632
				H^{δ} 3.213, 3.213
				H^{ϵ} 7.223
				H^{η} 6.670
Glu^{33}	8.477 (8.480)	4.316 (4.306)	2.073, 1.928	H^{γ} 2.349, 2.330
Ala^{34}	8.036 (8.318)	4.113 (4.346)	1.338	

TABLE 4

^{1}H chemical shift assignments of synthesized 14-mer, a copy of HBS sequence STKAAKKPEAKREA, in the presence of HP

Residue	H^N	$^1H^\alpha$	H^β	Others
Thr^{22}	8.635	4.420	4.239	H^γ 1.228
Lys^{23}	8.382	4.291	1.845, 1.773	H^γ 1.456, 1.448
				H^δ 1.701, 1.701
				H^ϵ 3.022, 3.022
				H^ζ 7.494
Ala^{24}	8.292	4.271	1.384	
Ala^{25}	8.190	4.280	1.384	
Lys^{26}	8.197	4.280	1.813, 1.753	H^γ 1.466, 1.466
				H^δ 1.701, 1.701
				H^ϵ 3.012, 3.012
				H^ζ 7.494
Lys^{27}	8.297	4.583	1.824, 1.793	H^γ 1.488, 1.488
				H^δ 1.713, 1.713
				H^ϵ 3.022, 3.022
				H^ζ 7.494
Pro^{28}		4.402	2.303, 1.965	H^γ 2.038
				H^δ 3.832, 3.656
Glu^{29}	8.488	4.258	2.050, 1.956	H^γ 2.380, 2.380
Ala^{30}	8.303	4.291	1.394	
Lys^{31}	8.256	4.290	1.824, 1.766	H^γ 1.436, 1.436
				H^δ 1.692, 1.692
				H^ϵ 3.022, 3.011
				H^ζ 7.494
Arg^{32}	8.333	4.331	1.854, 1.782	H^γ 1.641, 1.630
				H^δ 3.215, 3.215
				H^ϵ 7.207
				H^η 6.670
Glu^{33}	8.415	4.342	2.101, 1.947	H^γ 2.376, 2.376
Ala^{34}	8.036	4.127	1.344	

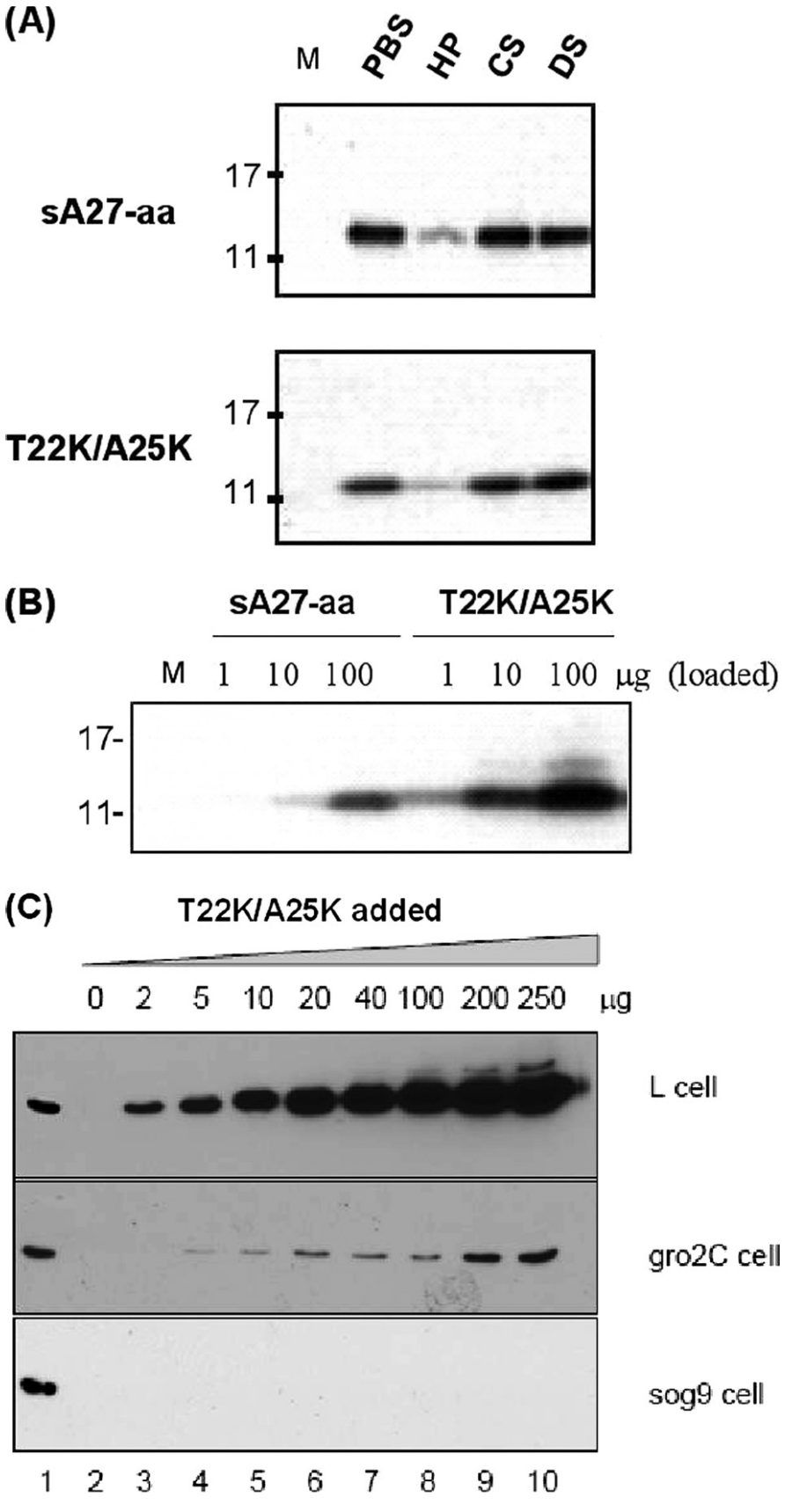
(A)
M
PBS
HP
CS
DS
sA27-aa
17
11
T22K/A25K
17
11
(B)
sA27-aa
T22K/A25K
M 1 10 100 1 10 100 μg (loaded)
17-
11-
(C)
T22K/A25K added
0 2 5 10 20 40 100 200 250 μg
L cell
gro2C cell
sog9 cell
1 2 3 4 5 6 7 8 9 10

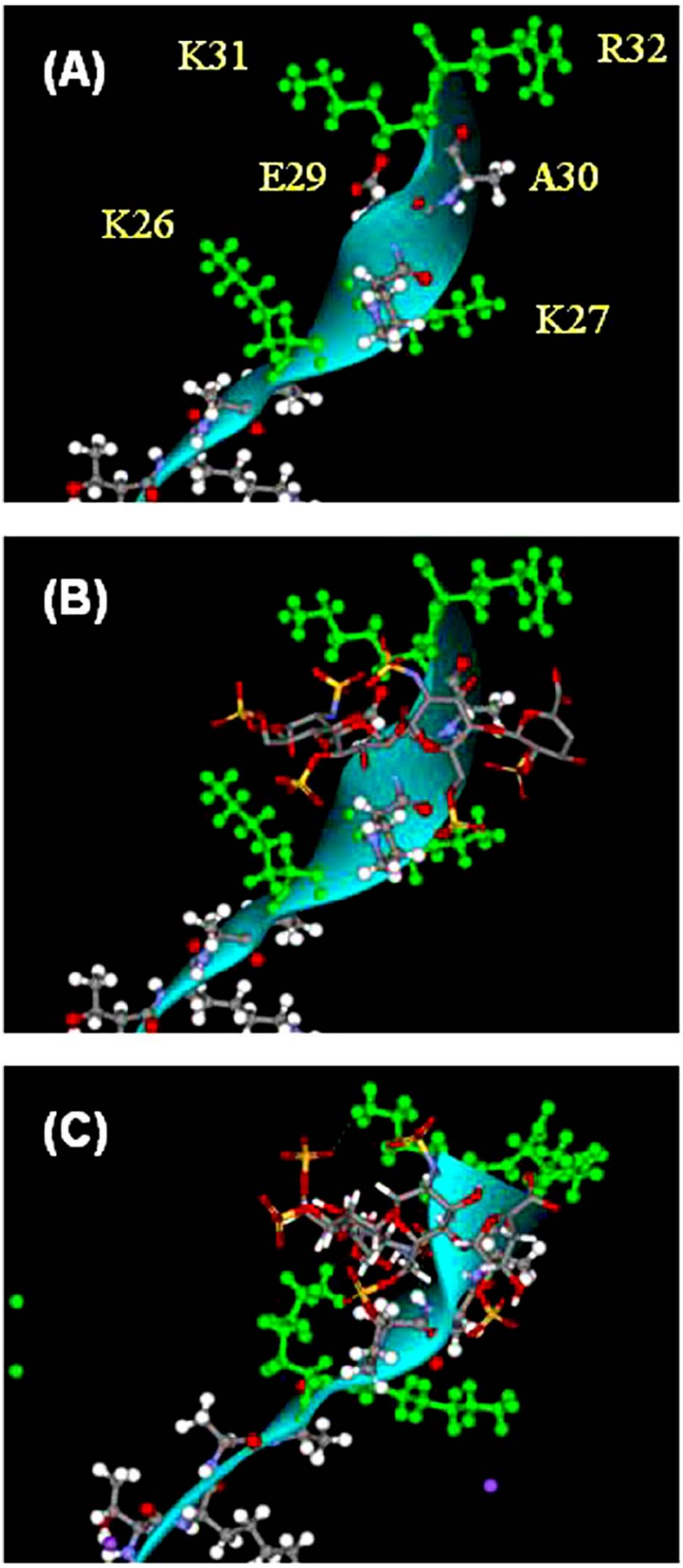
(A)
K31
R32
E29
A30
K26
K27
(B)
(C)